ARCHIVES OF ACOUSTICS
21, 2, 123–130 (1996)

INTELLIGIBILITY OF POLISH AND GERMAN SPEECH FOR THE POLISH AUDIENCE IN THE PRESENCE OF NOISE

E. HOJAN and H. FASTL

Institute of Acoustics
Adam Mickiewicz University, Poznań

Institute of Man-Machine Communication
Technical University, München, Germany

The ability of Polish listeners to understand Polish in the presence of two different noises, the Fastl noise and CCITT Rec. 227 noise was measured. The Speech Perception in Noise SPIN test was administered at 68 dB SPL to 10 normal listeners. The results are compared with those of similar experiments done for German. In the case of CCITT noise, most of the listeners have more difficulty to understand both Polish and German.

1. Introduction

The development of the hearing aids technique and new procedures of their fitting as well as the progress in acoustics and sound perception, have opened new opportunities in the field of aiding the hearing impaired people.

The hearing aids based on analog-digital converters can operate at a selection of programs, in many frequency bands, employing several regulating modules with variable parameters. Many of the technical features of these instruments have not been exploited yet due to the lack of knowledge about the nature of the hearing processes, particularly under pathological conditions and when the intelligibility of signal information is affected by noise [1, 8, 9, 10].

The results of tests of hearing aids conducted according to the recommendations of the standards IEC 118 or DIN 45605 differ from those of appraisal of the same devices in clinical tests [15, 17]. The necessity of applying natural signals while fitting a hearing aid arises from the attempts at simultaneous testing of most psychoacoustic characteristics of hearing which determine the quality of perception [15, 28]. Research focusing on allowing an optimal acoustic comfort for hearing-impaired people showed that the most stable attributes appeared to be the *sharpness* and *loudness* of a sound [11].

Basing on the *loudness* attribute with reference to natural sounds of time-variable amplitude, a new method (HGJ-standing for Hojan, Geers and Jezierska) is proposed for fitting hearing aids [13, 14].

The hearing aid chosen and subsequently fitted to the hearing impaired person will be accepted only when it satisfies the condition of a better intelligibility of speech [18].

Tests containing lists of monosyllabic words are used for this purpose [2, 3, 19, 20]. For the German language these lists are compiled into the so called Freiburger-Wörtertest [27], for Polish they are newly created by PRUSZEWICZ and DEMENKO [22, 23, 24].

Next, intelligibility of speech requires the hearing to be characterized by correct properties, particularly with regard to the following features:

a. temporal resolution
b. frequency resolution
c. frequency discrimination
d. intensity discrimination.

The effectiveness of all, or only some, of those properties are degraded among hearing impaired persons when compared to normally hearing people. The former frequently complain, for example, about environmental acoustic noise interfering with their listening to a speech [7, 28].

In many instances, a hearing aid optimally selected an fitted under laboratory conditions (isolated room) ceases to work satisfactorily when used in a loud acoustic environment, and its usage is frequently discontinued by the person with hearing problems. In a loud acoustic environment, people hearing normally can manage to concentrat on a unique speech signal and perceive it correctly [7, 17]. Very frequently, this skill vanishes with the heairng impaired people.

There is a common understanding of the need to design new procedures to be used in fitting the hearing aids, procedures based on natural sounds, under the conditions of an acoustic environment. First attempts towards the solution of this problem have been reported [12, 16, 25].

2. Masking noise

With the aim of examination hearing impaired people under condition of acoustic disturbances, FASTL [5, 6] has proposed to use the noise characterized in Fig. 1.

The spectrum and time evolution of this noise resembles the spectrum and time evolution of a speech signal representing fluent speech of many nationalities [26]. Parameters of this noise with regard to the form of its time envelope (with the same spectrum) differ from the parameters of noise employed in audiology according to CCITT Rec. G 227 specifications [5].

Fastl's noise was weated by modulating CCITT noise by a bandpass noise centered at 4-Hz. The disturbing noise proposed by Fastl allows among others, to

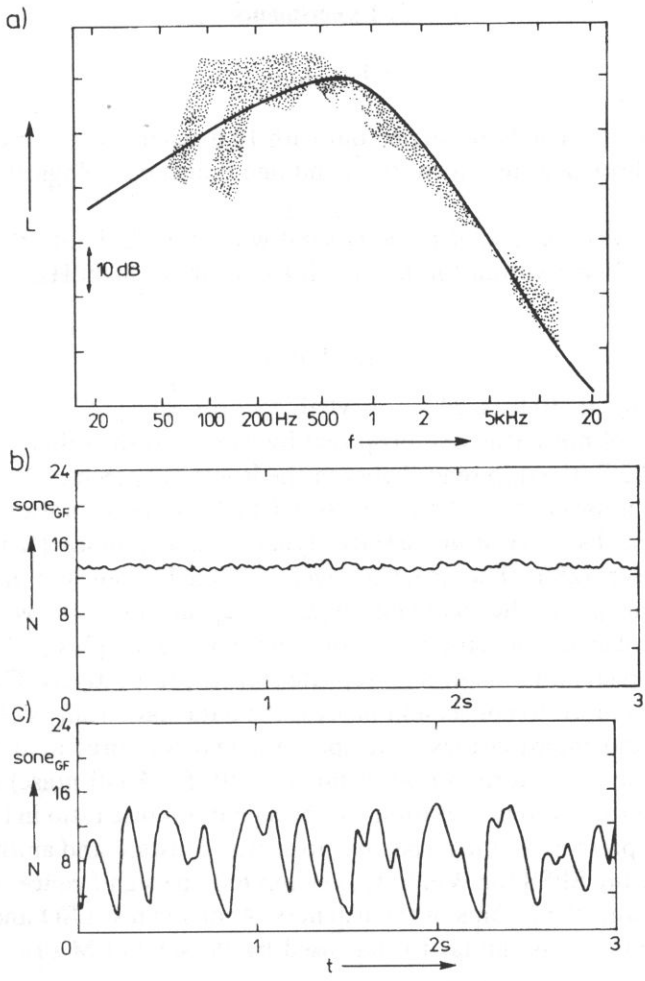

Fig. 1. Envelope in frequency a) and time domain of the CCITT Rec. G 227 noise b) and Fastl's noise c); From [6, 12].

simulate the effects like competing speech or cocktail party and helps to indicate the reduction of the effectiveness of the hearing properties listed above under **a**. through **d** in hearing impaired people.

In the present study, the intelligibility of Polish speech by a sample audience, made up of 10 Polish listeners of normal hearing and one Polish pathological listener, is investigated under the condition of Fastl's noise and next under that of CCITT Rec. G 227 noise. Next, the data for normal hearing people are compared with the results of intelligibility of the German speech by Polish and German listeners [12, 16, 25], in order to get information on the feasibility of the international normalization of this noise.

3. Experiments

3.1. Subjects

The experiments have been carried out with 10 listeners of Polish nationality aged from 36 to 55 whose hearing was normal and one Polish pathological listener aged 65 years.

The hearing was considered to be normal when the audibility threshold did not drop more than 20 dB within the bandwith from 100 to 8000 Hz.

3.2. Methods

The speech signal (10 lists, 24 monosyllabic words each [22, 23] in presence of one of the two kinds of noise (the one proposed by Fastl and the other one according to CCITT Re. G. 227), the difference between the levels of speech and noise being -18 to 0 dB (Fastl's noise) and -11 to $+3$ dB (CCITT Re, G227 noise), was applied to both ears of the listeners using electro-dynamic headphones (Beyer DT48 with freefield equalizer [28]). The listeners were isolated from the natural acoustic environment in a cabin. They were instructed to repeat loudly the words they heard. The instructor collected the data into a computer coding the plus (+) and minus (−) signs for the correctly and incorrectly repeated words, respectively. Custom designed software was employed to collect and process the data statistically yielding the values of the median and interquartiles. The speech signal was presented to the listeners using the successive lists form amongst no. 1 to 10 (for Fastl noise) and 1 to 8 (for CCITT noise) at the random variations of the signal to noise ratio in (2 dB steps); the level of acoustic pressure of the respective noise was constant and amounted to 68 dB. Subsequently, using SPSS for Windows, version 6.0, the significance of differences at 0.05 was tested with the groups of the listeners. Acoustic test LSD and Duncan were used. The procedure was similar to that used by PLOMP and MIMPEN [21].

4. Results

The results of the study of 10 listeners of Polish nationality, representing normal hearing, is presented in Fig. 2.

The circles in Fig. 2 refer to the first experimental data concerning the intelligibility of the Polish speech in the presence of Fastl's noise averaged over 10 listener sets whereas the squares refer to the noise pattern as specified by CCITT Rec. G. 227.

The medians for 50% of the data read as follows:

— in the presence of Fastl's noise, $\Delta L = -8.0$ dB

— in the presence of CCITT noise, $\Delta L = -5.0$ dB.

In Fig. 3 the results of the same experiment carried out with a Polish pathological listener are displayed, (circles — Fastl noise, squares — CCITT noise).

The medians for 50% of the date are as follows:

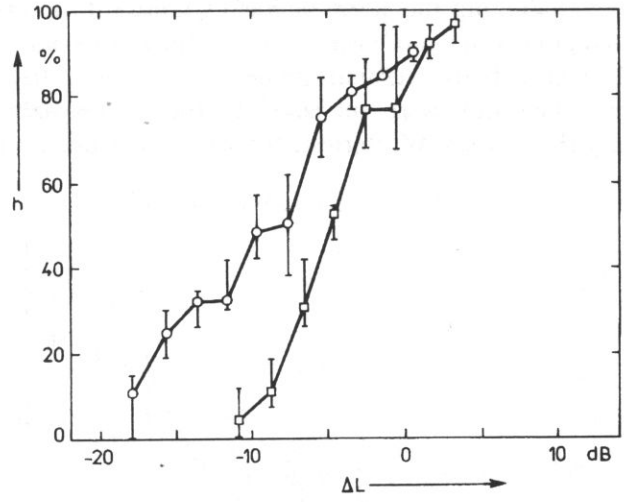

Fig. 2. Scores h for the monosyllables as a function of speech to noise ratio for 10 normal hearing Polish listeners in the presence of: — Fastl's noise circles, — CCITT noise squares.

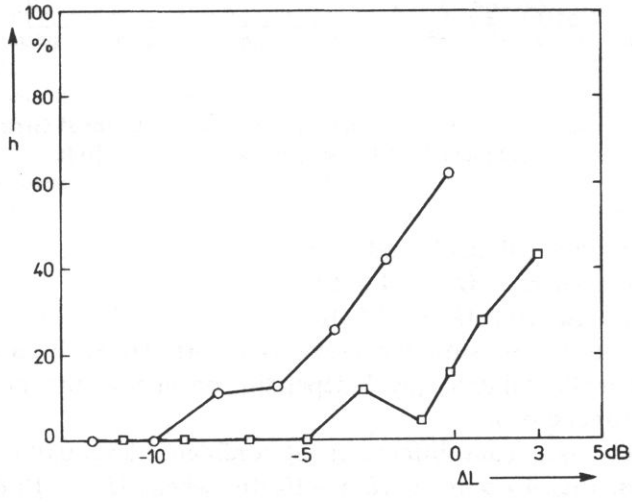

Fig. 3. Scores h for the monosyllables as a function of speech to noise ratio for pathology: — Fastl's noise circles, — CCITT noise squares.

— in the presence of Fastl's noise

$$\Delta L = -1.2 \text{ dB}$$

— in the presence of CCITT noise

$$\Delta L > +3.0 \text{ dB}.$$

With the aim of evaluating the effect of Fastl's noise on the process of speech perception and intelligibility in a more general sense, the results of a similar study are shown in Fig. 4, where both German (circles) and Polish (squares) speaking populations (normal hearing), were subjected to the monosyllabic tests built of German words only (Freiburger Wortertest, the words lists no. 1–17).

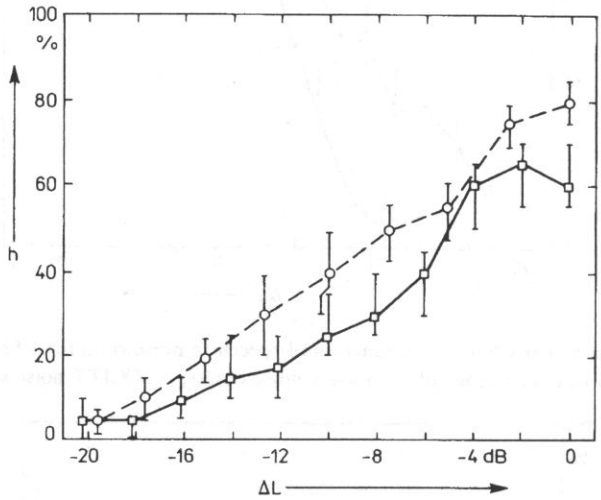

Fig. 4. Scores h for the monosyllables as a function of speech to noise ratio for 88 German subjects (circles — see [12]) and 40 Polish subjects (squares — see [16]).

The corresponding medians for 50% are:
— for Polish listeners $\Delta L = -4.0$ dB
— for German listeners $\Delta L = -7.5$ dB.

This result is in accord with the previous reports [1, 8, 9] and points to the differences in the intelligibility of speech depending on whether the speech is produced in one's mother tongue or not.

The statistically significant differences (at confidence level 0.05) relevant for the plotted data from Fig. 4 occur at $\Delta L \geqslant -10$ dB; when $\Delta L < -10$ dB all the data coincide within the statistical error.

5. Conclusions

1. The intelligibility of both the native and foreign speech is better in the presence of the Fastl's noise than in that of CCITT Rec. G. 227 noise.

2. Fastl's noise allows a better differentiation between the intelligibility of normal and pathological cases than the CCITT Rec. G. 227 noise does.

3. Similar medians of 50% of the intelligibility of the Polish speech by Polish listeners and the German one by German listeners, both affected by noise as designed

and specified by Fastl), evidence the equivalence of these two word tests: the Polish one and the German one.

4. The results indicate the universal character of Fastl's modulated noise normalized with respect to a multilingual speech.

Acknowledgements

This study was sponsored by the Deutsche Forschungsgemeinschaft under the project SFB 204 and by the Alexander von Humboldt Fund.

References

[1] S. Buus, M. Florentine, B. Scharf and G. Canevet, *Native, French listeners' perception of american-english noise*, Inter Noise'86, 895–898 (1986).

[2] W.B. Davenport, *A experimental study of speech-wave probability distributions*, J. Acoust. Soc. Amer., **24**, 4, 390–399 (1952).

[3] H.K. Dunn, and S.D. White, *Statistical measurements on conversational speech*, J. Acoust. Soc. Amer., **11**, 1, 278–288 (1940).

[4] *DIN 45 621 Wörter für Gehörprufung mit Sprache* (1973).

[5] H. Fastl, *A background noise for speech audiometry*, Audiological Acoustics, **26**, 1, 2–13, (1987).

[6] H. Fastl, *A masking noise for speech intelligibility tests*, Proc. TC Hearing Acoust. Soc. of Japan, H-93-70 (1993).

[7] H. Fletcher and R.H. Golt, *The perception of speech and its relation to telephony*, J. Acoust. Soc. Amer., **22**, 2, 89–151 (1950).

[8] M. Florentine, S. Buus, B. Scharf and G. Convert, *Speech perception thereshold in noise for native and non-native listeners*, J. Acoust. Soc. Amer. Supple., 1, 75, 84 (1984).

[9] M. Florentine, *Non-native listeners' perception of american-english in noise*, Inter Noise'85, 1021–1024 (1985).

[10] N. French and J. Steinberg, *Factors governing the intelligibility of speech sounds*, J. Acoust. Soc. Amer., **19**, 90–119 (1985).

[11] A. Furmann, E. Hojan, M. Niewiarowicz and P. Perz, *On the correlation between the subjective parameters for a selected source*, J. Acoust. Eng. Soc., **38**, 11, 837–844 (1990).

[12] I. Hautmann and H. Fastl, *Zur Verstandichkeit von Einsilbern und Dreinsilbern im Störgeräusch*, DAGA, 784–787 (1993).

[13] E. Hojan, W. Geers and D. Hojan-Jezierska, *Fitting hearing aids by using the scaling of categorical estimations of natural sounds*, (in Polish), 40th Open Seminar on Acoustics, Rzeszów 297–300 (1993).

[14] E. Hojan, *Fitting of hearing aids with loudness scaling of environmental sounds*, Inter-Noise-94, Yokohama, 851–856 (1994).

[15] E. Hojan, *Fitting of hearing aids*, III Conference of Electroacoustics, Poznań – Czerniejewo, 5–12 (1994).

[16] E. Hojan and H. Fastl, *Zur Verständlichkeit deutscher Sprache im Störgeräusch nach Fastl durch polnische Hörer mit verschiedenen Deutschkenntnissen*, Acta Acustica (1996).

[17] *ISO/DIS 1999, Acoustics-Determination of occupational noise exposures and estimation of noise-induced hearing impairment*, Genf, September 1980.

[18] K.D. Kryter, *Methods for the calculation and use of the articulation index*, J. Acoust. Soc. Amer., **34**, 1689 (1980).

[19] I. Kurcz, A. Lewicki, J. Sambor and K. Szafran, *Słownik frekwencyjny polszczyzny współczesnej* [in Polish], PAU, Inst. Jęz. Pol. Kraków (1990).

[20] P. Łobacz, *Psychometric classification of phones — Some methodological considerations*, Lingua Posnaniensis, 22–23 (1991).

[21] R. PLOMP and A.M. MIMPEN, *Speech reception threshold for sentences as a function of age*, J. Acoust. Soc. Amer., **66**, 5, 1333–1342 (1979).

[22] A. PRUSZEWICZ, G. DEMENKO, L. RICHTER and T. WIKA, *New articulation lists for speech audiometry*, Part I, Otolaryng. Pol. 1, 48, 50–55 (1994).

[23] A. PRUSZEWICZ, G. DEMENKO, L. RICHTER and T. WIKA, *New articulation lists for speech audiometry*, Part II, Otolaryng. Pol. **48**, 1, 56–62 (1994).

[24] A. PRUSZEWICZ, *Foniatria kliniczna*, PZWL, Warszawa (1992).

[25] I. STEMPLINGER, H. FASTL, K. SCHORN and F. BRÜGEL, *Zur Verständlichkeit von Einsilbern in unterschiedlichen Störgeräuschen*, DAGA, 1469–1472 (1994).

[26] T. TARNOCZY, *Das durchschnittliche Energie-Spektrum der Sprache für sechs Sprachen*, Acustica, **24**, 56–74 (1971).

[27] WESTRA, *Westra Audiometrie Disc. Nr. 11. Zahlen-Wörtertest nach DIN 45621 mit Störgeräusch Prof. Dr.-Ing. H. Fastl* (1992).

[28] E. ZWICKER and H. FASTL, *Psychoacoustics — Facts and Models*, Springer Verlag, Berlin (1990).

ARCHIVES OF ACOUSTICS
21, 2, 131–147 (1996)

SYNTHESIS OF ORGAN PIPE SOUND BASED ON SIMPLIFIED PHYSICAL MODELS

A. CZYŻEWSKI, B. KOSTEK and S. ZIELIŃSKI

Sound Engineering Department
Faculty of Electronics, Telecommunications and Informatics
Technical University of Gdańsk
890-952 Gdańsk, ul. Narutowicza 11/12

Problems related to the implementation of a physical model based synthesis of an organ pipe sound are discussed. A new approach to the physial modelling of an organ pipe sound, namely the waveguide synthesis is introduced. The results of some experiments with this kind of synthesis are presented. Specific features of presented methods and corresponding applications are quoted. Examples of a computer analysis of both synthesized and real musical sounds are presented and compared.

1. Introduction

The new generation of digital signal processors offers many possibilities to create synthesized sounds of classic-like instruments. On the basis of the new technology new synthesis algorithms created on the basis of the physics of instruments were proposed. One of the most modern methods that belongs to the category of physical modelling is the "digital waveguide" synthesis [23, 25, 26]. In this method the wave equation is first solved in a general way to obtain the travelling waves in the instrument body that are then simulated in the waveguide model. In the lossless case, a travelling wave between two points in the medium can be simulated using a digital delay line and frequency-dependent losses can be simulated by a FIR digital filter [8, 9, 23]. In the paper also a short review of widely-known traditional synthesis methods is included and their limitations, when applied to the organ pipe sound synthesis, are pointed out.

The tool used for the experiments was the NexTStep Operational System based workstation. This operational system available today with Sun, Hewlett-Packard and IBM Pentium computers is particularly suitable for the development of sound synthesis algorithms, especially because of the advanced software supporting this task.

The SynthBuilder system may serve as an example of such a software application. Within it, it is possible to create and test a new instrument. The unit generator panel

contains: an oscillator, buzz, random number generator, simple envelope with attack and decay, filter and mathematical operations. Since inputs and outputs are wired, it is possible to designate parameter fields. Moreover, some available analyzing software packages were designed for musical sounds [2]. The software enables various analyses, especially those more sophisticated, being very useful for the study of musical timbre through the examination of various graphic representations of the data.

Two methods of physical modelling of natural instruments were used in the study. The first one, proposed by Fletcher [11], is based on the numerical solution of the wave equation. The second one, known as the waveguide synthesis, is related to the simulation of travelling waves in the waveguide model of a natural instrument. A couple of experiments with these two methods were made in order to compare their output to results the obtained with some classical methods for digital synthesis and to the sounds of real organ pipes.

2. Traditional sound synthesis methods

Traditional synthesis methods fall into one of the four categories quoted below: additive synthesis, subractive synthesis, nonlinear distortion synthesis and sampling.

Generally, digital synthesis of sound is a function F described by the following equation:

$$s(n)=F(n,p_1,\ldots,p_m), \tag{2.1}$$

where: $s(n)$ — consecutive samples of synthesized sound,

$p_1,\ldots,p_m$ — set of synthesis control functions.

Depending on the selection of the synthesis control functions, one can discern many methods, such as additive synthesis, subtractive synthesis, frequency modulation (FM), phase distortion.

The additive synthesis belongs to the "classical" methods of digital synthesis of sound. It results from the reverse Discrete Fourier Transform of spectral components having variable amplitudes [13]. The additive synthesis demands a big number of stored data. It would be very difficult to relate these data providing input of this algorithm to the way of playing on a pipe organ instrument with regard to musical articulation.

The subtractive synthesis is based on filtration of a wide-band signal in the non-stationary linear circuit. Usually, the subtractive synthesis is used in digital technology as a tool for timbre formation of signals generated digitally in samplers, wavetable synthesizers and other ones. This method provides the most wide-spread technique for the synthesis of pipe organ sounds. However, it does not allow for musical articulation [14, 15] and is not suitable for modelling such phenomena as overtone generation, overblowing and other features accompanying the sound rise in a real pipe because it is technically difficult to obtain sufficiently fast and deep changes of filter parameters.

The frequency modulation (FM), waveshaping and phase distortion fall into the category of nonlinear distortion synthesis. Frequency modulation is well known in radio engineering. J. CHOWNING discovered [5] that by bringing the modulation rate down into the human hearing frequency range (20 Hz – 20 kHz) and controlling the relationship between the carrier frequency, the modulating frequency and the modulation index ratio, one can vary the timbre of the synthesized sound.

In practice, the spectrum shape of the synthesized sound is very difficult to predict and control (the equation may be solved using Bessel functions). Nevertheless, some modifications of this method, which solve the problem partially, were proposed lately [24], especially for the steady-state part of the signal. Independently of the method, the frequency modulation synthesis does not allow to control the spectrum behaviour during the transient states with sufficient, from the technological point of view, effectiveness. This drawback eliminates this method as a practical tool for an efficient synthesis of the pipe organ sound.

The phase distortion synthesis method is another kind of methods belonging to the category of nonlinear distortion synthesis. In this case, samples corresponding to a single period of the cosine wave are stored in the table of the phase distortion synthesizer. In the process of synthesis some samples are read out of the table at a rate different from those of others, which causes phase distortion. As a result various sound waveforms can be obtained.

The waveshaping synthesis is similar to the phase distortion method described above. The difference consists in the fact, that the sampled-data of one period of the cosine wave are read out at a constant rate and then processed according to the shaping functions [3]. As the last two methods are based on nonlinear equations, it is difficult to manage all parameters of such synthesis and to control all phases of the created sound.

Many electronic instruments, that allow for a plausible synthesis of natural sounds, utilize the sampling technique. In this method the musical sound is used as a sound source. Subsequently, it is converted into the digital domain, stored in the computer memory, processed according to the chosen algorithm and then converted back to the analogue domain. Although sampling allows for efficient synthesis of natural sounds, a large amount of data must be stored in the computer memory, especially when considering such a big instrument as a pipe organ. The last one of the methods described above is not a system of synthesis in the strict sense.

3. Sound production in an organ flue pipe

An open diapason and a flute pipe are typical organ flue pipes. They are shown schematically in Fig. 1. The main three parts of a flue pipe are: foot, languid, and body. The term "mouth" denotes respectively upper and lower lips, the languid and the ears in the case of a diapason pipe (ears are not shown in Fig. 1). The slit between the languid and the upper lip is called a "flue" or a "windway", therefore organ pipes of this kind of construction are often named "flue pipes".

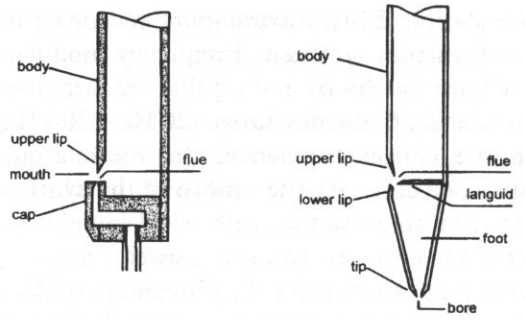

Fig. 1. a. Cross-section of the wooden organ pipe of a "flute" type, b. Cross-section of the open diapason pipe [19].

Fig. 2. Mechanism of "edge tone" production [21].

One of the first qualitative explanations of sound production in organ flue pipe was given by RICHARDSON [21, 22]. In his studies a flue pipe was treated as two compound systems in which an "edge-tone" is directly coupled to the column of air of fixed length. The mechanisms of "edge-tone" formation are illustrated in Fig. 2. In the simplest case, a vortex A leaves the outer wall of the orifice as the preceding one on the same side B strikes the edge. The frequency of the "edge-tone" is related to the frequency with which the vortices strike the edge. The wavelength of the "edge tone" equals, or is a small submultiple, of the distance between the vortices in the same row. There is a minimum distance l_0 of the distance l between the slit and the edge for any given velocity of efflux v at which a tone can be produced. In an organ pipe the distance between the slit and the edge of the upper lip is constant, but the velocity of the air-jet can be varied by changing the pressure in the pipe foot. When v is kept constant as l is increased beyond the minimum l_0, the pitch of this "edge-tone" is in accordance with the relation:

$$v/fl_0 = \text{constant} \tag{3.1}$$

until l reaches a value equal approximately to the double value of l_0; then the tone, which is now the sub-octave of the original, may suddenly rise an octave.

Richardson concluded that the "jump" of the frequency of the "edge tone" up to the higher frequency occurs when the pipe is supplied with relatively low pressure

and, as a consequence of this, the pipe can respond with some kind of overblowing [21]. The air, issuing from a slit in the mouthpiece and striking the upper lip, produces the "edge-tone", the pitch of which would rise continually in proportion to the wind velocity, i.e. to the square root of the pressure in the wind chest. Thus, the organ pipe can be considered as a resonator coupled to an "edge-tone" generator that amplifies its response. These possible modes of vibration in relation to the "edge-tone" are shown in Fig. 3 [20].

As already mentioned, the relation shown in Fig. 3 refers to the case when small power, at low pressure, is turned onto the pipe, before the normal pressure has been attained.

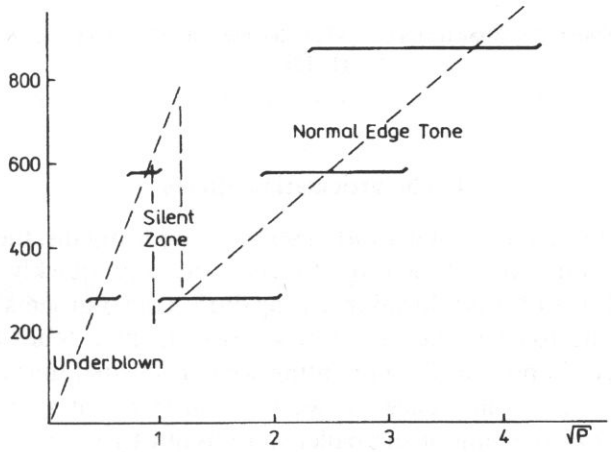

Fig. 3. Organ-pipe tones in relation to edge tones [19].

A systematic study of the sounding mechanism of the flute and organ pipe was undertaken by COLTMAN [7]. He pointed out that the picture of an organ pipe as a resonator that is coupled to the "edge-tone" generator and amplifies its response was oversimplified. He carried out detailed measurements of the acoustic impedance of the air jet. In this study, he measured the acoustic impedance at a given frequency as the function of a jet velocity [6]. A very important observation was made, namely that the interaction between normal resonance modes of the air column within the pipe and the air jet should be treated in terms of a nonlinear interaction [10]. The jet emerging from the narrow slit defined by the edge of the languid and the lower lip of the pipe mouth, is sensitive to the displacement by the fluid motion v through the mouth of the pipe. If the acoustic flow is out of the pipe mouth, the jet is deflected outside the upper lip and the pressure falls, while if the acoustic flow is inwards, the jet is deflected inside the upper lip and raises the pressure in the pipe near the mouth. For a steady velocity, v, in the pipe mouth, the driving force F produced by the jet had a form like that one shown in Fig. 4 [10, 11, 18].

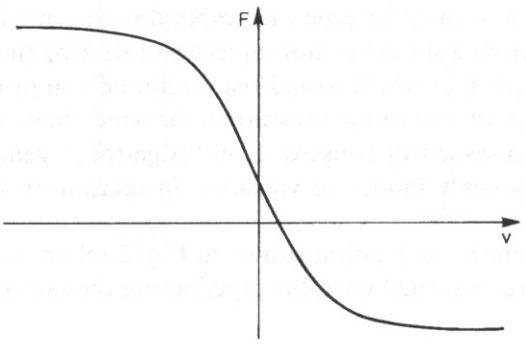

Fig. 4. An exemplary shape of nonlinearities caused by the interaction between the air jet and the pipe [10, 11, 18].

4. The articulation effects

LOTTERMOSER [17] reports that in most cases of baroque organs, the organist is able to influence the transients. When he touches the key quickly (staccato), the higher-frequency tones of short duration arising during the transients appear with full amplitude. When he touches the key slowly (legato), these tones disappear. This phenomenon is very important for presenting well-articulated music.

Significant qualitative differences between organ transient sounds obtained for fast and slow rates of opening of the pallet were found by CADDY and POLLARD [4]. NOLLE and FINCH [19] measured transients of flue organ pipes in relation to the pressure rise time. They found that in the case of short-time transients, an overshoot of the second mode harmonic occurred. In the "slow" regime, not only is there no large overshoot, but modes 2 and 1 can become phase locked well before the final pressure is reached. These effects were also observed by us in our previous studies [14, 15, 16].

5. Physical model based on the wave equation

The organ pipe can be considered as two subsystems, for example, the air column — a very, nearly linear, resonant system — and the jet system including a highly non-linear interaction with the pipe lip. The air column system of the pipe has a series of normal modes with (angular) frequencies n_i. The displacement x_i of the ith mode obeys the equation of the form [11]:

$$\ddot{x}_i + k_i \dot{x}_i + n_i^2 x_i = \lambda_i F(t), \tag{5.1}$$

where: $F(t)$ — external force, k_i — damping coefficients, λ_i — coupling coefficients between the pipe and the air stream.

As far as the air jet is concerned, the driving force F for the static case can be written as a power series expansion:

$$F=c_0+c_1v+c_2v^2+c_3v^3+... \tag{5.2}$$

where v is the acoustic velocity of the air stream and c_n are coefficients of the blowing pressure function. Considering the time delay, δ_i, related to the jet travelling across the mouth of the pipe and the dispersive character of the jet, Δ_i/ω_i, equation (5.2) can be written:

$$F(t)=\sum_{m=0}^{\infty} c_m\left[\sum_{i=1}^{\infty}\dot{x}_i\left(t-\delta_i-\frac{\Delta_i}{\omega_i}\right)\right]^m, \tag{5.3}$$

where: δ_i — time necessary for a single vortex to be displaced along the air stream leaving the organ pipe mouth, Δ_i — phase shift.
The set of equations (5.1) and (5.3) can be written in the following form:

$$\ddot{x}+n_i^2x_i=f_i(\dot{x}_i)\,, \tag{5.4}$$

where:

$$f_i(\dot{x}_j)=-k_i\dot{x}_i+\lambda_i\mathrm{F}(\dot{x}_1,\dot{x}_2,...)\,. \tag{5.5}$$

This equation can be solved using the method of slowly varying parameters. The delay δ for a jet of length l is:

$$\delta=8\times10^{-4}lp^{-1/2}\alpha^{-1} \tag{5.6}$$

where α — coefficient of air flow velocity.

As the attack transient is strictly related to the pressure rise time and has a crucial influence on the timbre of the resulting sound, the main attention has been paid to modelling the pressure changes in the pipe foot described by the following equation:

$$p(t)=p_0+(p_1-p_0)\exp(^-t/\tau) \tag{5.7}$$

where: p_1 specifies the pressure peak, p_0 is the steady pressure and τ is the decay time from the peak level. It is possible to discern between at least two possibilities. When $p_1\gg p_0$, the pressure peak is occurring and it may be referred to as the plosive transient attack. When $p_1\ll p_0$, the transient is slow. A more detailed description of the phenomena related to the sound rise in flue pipes can be found in the literature [1, 11, 15].

In the experiment studies carried out in the Sound Engineering Department of the Technical University of Gdańsk, the method proposed by Fletcher has been implemented in a personal computer [14]. In these studies the frequency dispersion was neglected.

6. Waveguide synthesis

The digital waveguide synthesis is based on a modified approach to the physical model: the wave equation is first solved in a general way to obtain travelling waves in

the medium interior. The travelling waves are explicitly simulated in the waveguide model, in contrast to computing a physical variable [12, 23, 26]. In the lossless case, a travelling wave between two points in the medium is simulated using a digital delay line. Frequency-dependent losses and dispersion can be modeled using digital filters.

The general class of solutions to the lossless, one-dimensional, second-order wave equation describing the air column system of the pipe can be expressed as:

$$x(l,t)=x_r(l-ct)+x_l(l+ct), \tag{6.1}$$

where: $x_r(l-ct)$ — right-going travelling waves, $x_l(l-ct)$ — left-going travelling waves, c — speed of propagation, l — position.

Fig. 5 shows the way of modelling such travelling waves using a pair of digital delay lines. The upper delay line simulates the right-going travelling waves, whereas the lower one is responsible for modelling the left-going waves. It is possible to compute the physical air column displacement in any sampling point by simply adding corresponding samples derived from delay lines, as illustrated in Fig. 5.

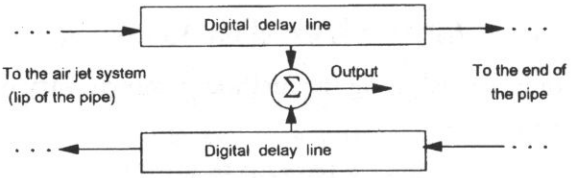

Fig. 5. Scheme of an elementary waveguide.

A more detailed schematic diagram of the semi-physical model of the flue organ pipe is illustrated in Fig. 6a. This model is based on a flute model developed in 1992 by VÄLIMÄKI *et al.* [26]. Experiments with this model were also performed by P.R. COOK [9] who proposed inaudible simplifications. A pair of digital delay lines (each of N/2 sample length) is used for modelling the vibrating air column inside the pipe. Linear filters at the ends of the pipe in this waveguide model simulate losses and the dispersive characteristics of the air column summed up together with the reflections. The lengths of the delay lines correspond to the effective length of the pipe. Since delay lines consist of an integer number of unit delays, the problem related to the proper tuning of the pipe, according to the musical scale, could appear. This problem can be solved using a fractional delay filter based on Lagrange interpolation [27, 28]. Filters F_A and F_B (see Fig. 6a) are responsible for modelling frequency-dependent damping and dispersion in the pipe and reflection properties of the corresponding ends. The oscillation in the pipe is produced by a nonlinear interaction of the air jet and the air column. This interaction can be described in terms of a nonlinear function and implemented by means of a look-up table [10, 11, 19]. Since the air jet has to travel a certain distance from the pipe foot to the lip, it is necessary to model it using an additional delay line (*dl1*). The whole system is excited with the noise shaped by the

envelope generator that models changes of pressure in the pipe foot. It is possible to simplify this model by lumping delay lines and the corresponding filters as illustrated in Fig. 6b. This simplification does not cause any audible effect.

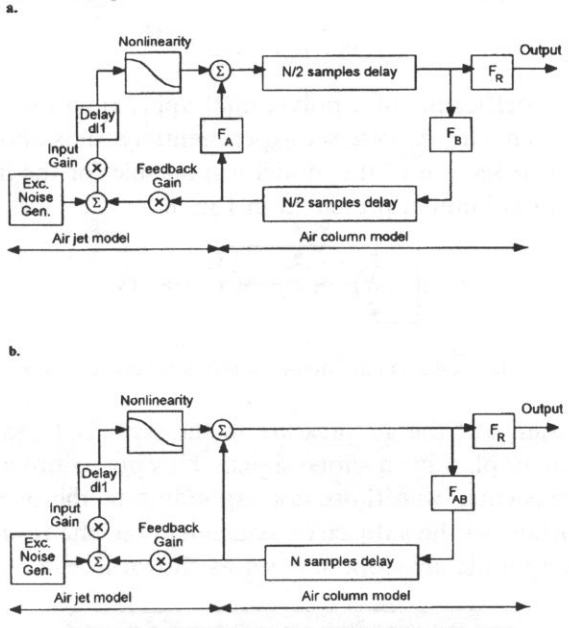

Fig. 6. Block diagram of a flue pipe model:
a. full lay-out,
b. simplified lay-out with elements lumped together.

In the experiments we have carried out, the waveguide model of a flute proposed by VÄLIMÄKI [26] was adopted. In order to simplify the model, the filter F_R was removed (see Fig. 7). This model consists of typical blocks such as delay lines, multipliers, one-pole filter and generators. The transfer function of the one-pole filter is as follows:

$$H(z)=\frac{b_0}{1-a_1 z^{-1}}, \tag{6.2}$$

where: b_0 — amplification and a_1 — pole coefficient. The one-pole filter and a delay line (*dl1*) are used to simulate the travelling wave in the air column of the pipe. The jet

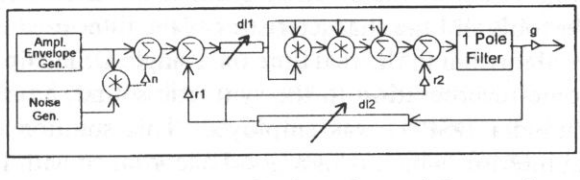

Fig. 7. Waveguide model of a flute pipe used for experiments.

delay is modeled using the second delay line (*dl2*). The amplitude envelope generator and the noise generator are used to model the changes of the air pressure in the pipe foot. In order to ensure efficient DSP calculations, non-linearities are modelled on the basis of a polynomial approximation. This function can be written in the form:

$$y(x) = a_0 x - a_3 x^3, \tag{6.3}$$

where: a_0 and a_3 — coefficients of a polynomial approximation of the 3-rd order. The values of coefficients a_0, a_3 were set experimentally, thus adopted as: $a_0 = 1$ and $a_3 = -1$. The nonlinear section of the model responsible for the interaction between the air jet and the air column is presented in Fig. 8.

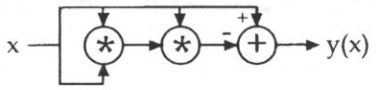

Fig. 8. Nonlinear section of the model simulating the interaction between the air jet and the air column.

The attack transients of the air pressure in the pipe foot can be modeled using various shapes of an amplitude envelope signal. This procedure allows to synthesize various types of transients, even those corresponding to the overblow of the pipe, which is very important to the subjective assessments of the resulting organ sound. The shape of the amplitude envelope was set as shown in Fig. 9.

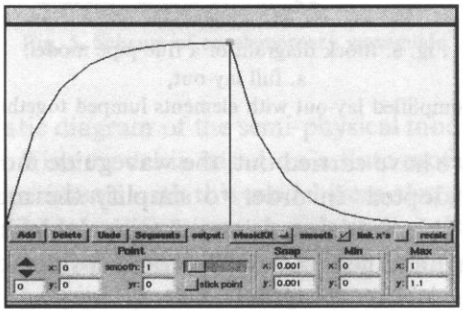

Fig. 9. Shape of an attack transient generated in the amplitude envelope generator.

In the experiments with waveguide synthesis, the SynthBuilder system written for the NeXT computer was used (Software elaborated by Nick Porcaro et al., Stanford University). This application allowed to model the pipe according to the algorithm described before. Fig. 10 shows the block diagram of this model constructed with the use of SynthBuilder tools and the characteristics of the filter used in the model. It was possible to run this algorithm in the real time on a single DSP chip (Motorola 56001). In order to add some reverberation to the synthetic sound, an external sound field processor unit (Yamaha DSP-1) was employed. This solution enables simulating conditions of a big interior, which is in a good accordance with the listeners' habits accustomed to perceiving organ sounds in the acoustical conditions of a church.

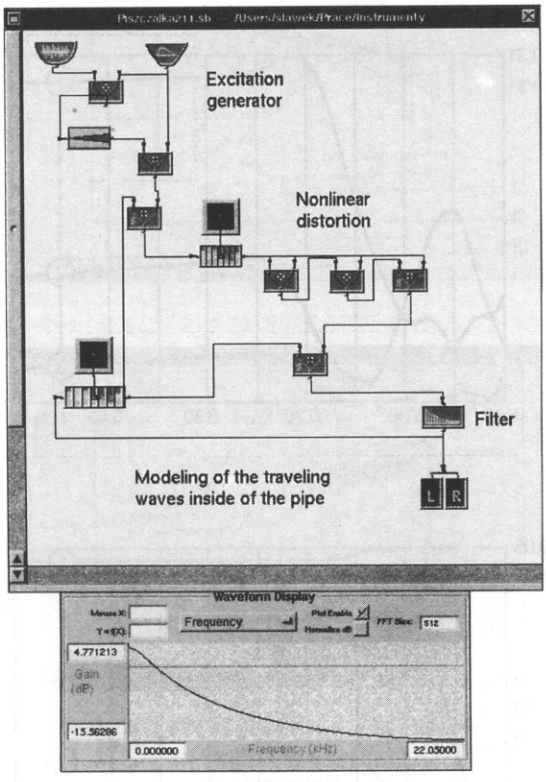

Fig. 10. Waveguide model of the organ pipe implemented using the SynthBuilder software tool and response of the applied low pass filter.

7. Experiments and results

As a result of the carried out experiments, sound of an organ flue pipe were synthesized using the two methods described above, namely the method based on solving differential equations and the waveguide modeling, both describing physical phenomena related to sound bore in organ pipes. Synthetic sounds were then analysed in time- and frequency-domains and compared to the corresponding analyses of natural sounds. Preliminary listening tests were also made in order to compare synthetic and natural sound patterns.

Calculations based on the method proposed by Fletcher have been performed for a wide variety of cases from which only two examples, shown in Fig. 11, have been selected. The plosive attack produces a speech transient in which the second pipe mode is dominant within the first 0.1 s (Fig. 11.a). For the slow attack the speech is delayed, with the fundamental being always predominant (Fig. 11.b). These effects are closely related to musical articulation distinctive features that appear in the sound of a real organ pipe, namely a flue pipe [15]. The harmonic analyses of the corresponding natural sounds are presented in Fig. 12.

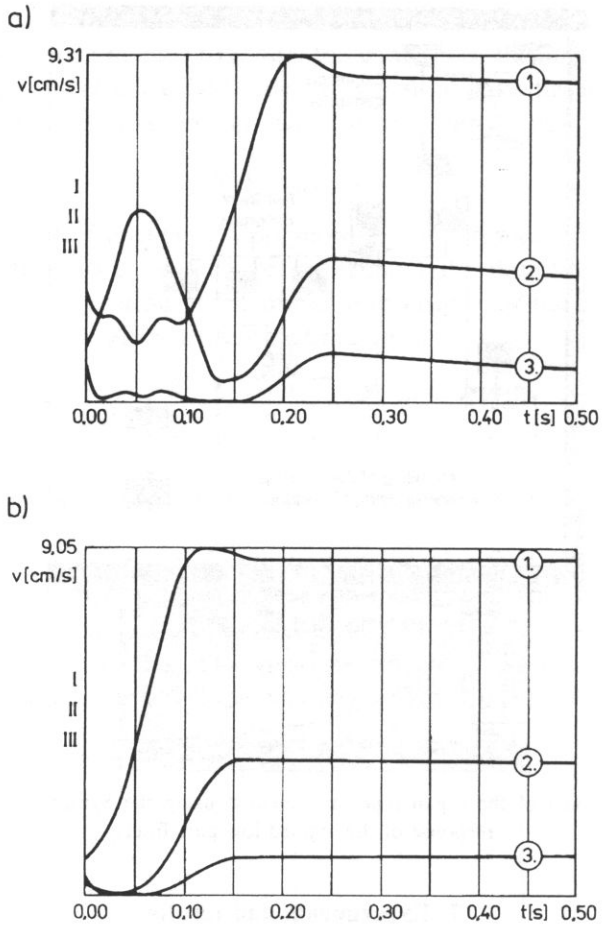

Fig. 11. Calculated pipe transients. In both figures, curves no. 1, 2, 3 refer to the first, second and third pipe modes, respectively:
a. fast attack (p_0=2 mbar, p_1=6 mbar),
b. slow attack (p_0=2 mbar, p_1=0.5 mbar).

Similar frequency analyses were made with sounds obtained using the waveguide synthesis [16]. Spectrum plots of the synthetic and natural (steady state) sounds of an organ flue pipe are presented in Fig. 13. There is a good qualitative accordance between them. The content of harmonic components is relatively small. There are only 6 harmonics of significant importance, whereas the higher ones are hidden under the noise components. It is important to note, that the amplitude of the second harmonic is in both cases less than the amplitude of the first and the third ones. Apart from this, the amplitude of the sixth harmonic in the natural sound is greater than the amplitude of the same harmonic in the synthetic one (Fig. 13).

a.

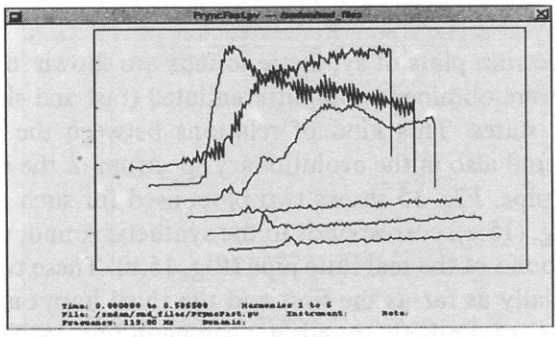

b.

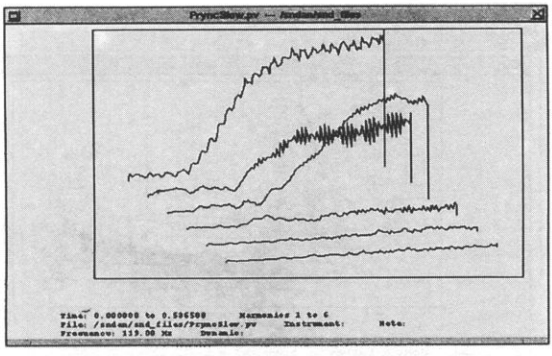

Fig. 12. Evolutionary plot of a spectrum of a Principal organ pipe:
a. fast attack,
—
b. slow attack
(Analyzing tool: *AnView* — program elaborated by C. Gennaula, C. Goudeseune, J. Beauchamp).

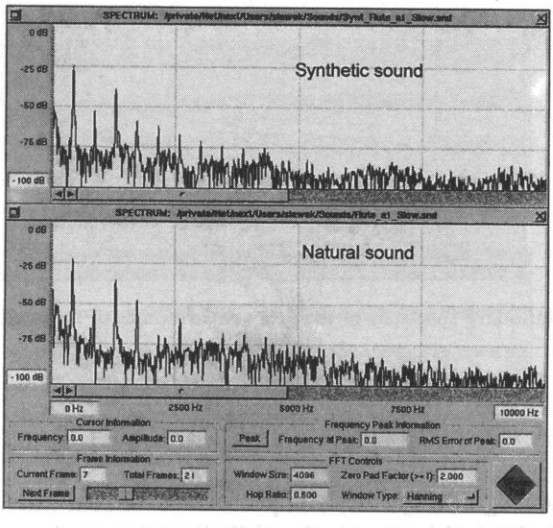

Fig. 13. Spectrum plots of the synthetic and natural sounds (of the flute type).

Evolutionary spectrum plots of synthetic sounds are shown in Fig. 14.a and Fig. 14.b. These sounds were obtained using differentiated (fast and slow) articulation of the attack transient states. This kind of relations between the fundamentals and harmonics can be found also in the evolutionary spectrum of the sound produced by the real organ flute pipe. Fig. 15 shows two plots used for such a comparison. The upper part of this Fig. (15.a), corresponds to the synthetic sound, while the lower one corresponds to the sound of the real flute pipe (Fig. 15.b). These two plots are similar to each other, especially as far as the first and the third harmonics are considered. Time-domain analyses of synthetic sounds are shown in Fig. 16. The fast attack gives a shorter amplitude envelope rise time than in the case of a slow attack.

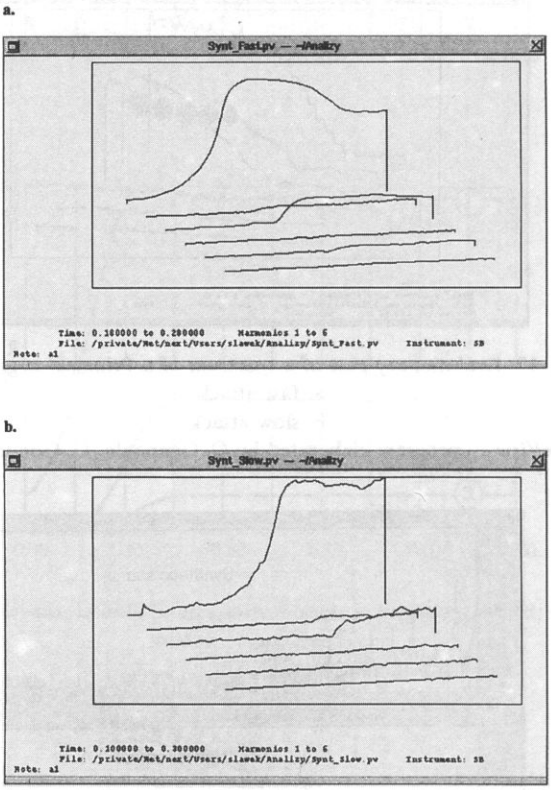

Fig. 14. Evolutionary spectrum of the first six harmonics of the synthetic sound:
a. fast attack,
b. slow attack.

The process of waveguide synthesis is performed in real time. Parameters of the synthesis have been adjusted interactively while listening to the synthetic sound. The parameters specified in Table 1 were found to be optimal for the synthesis of an organ

a.

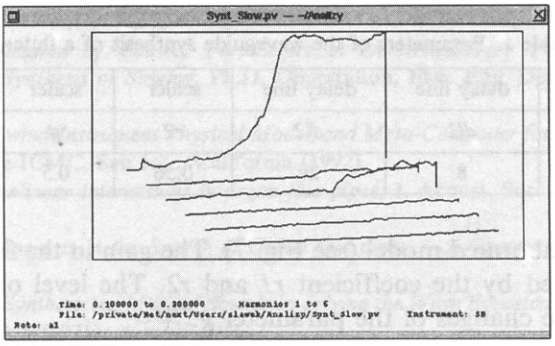

b.

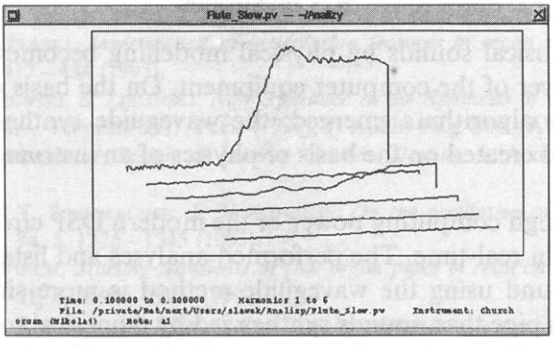

Fig. 15. Evolutionary spectrum of the first six harmonics of the synthetic and natural sound:
(a) synthetic sound,
(b) natural sound.

a.

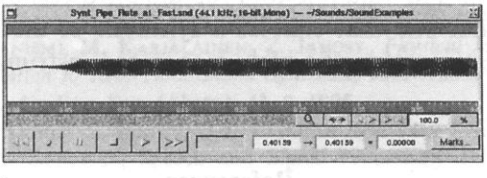

b.

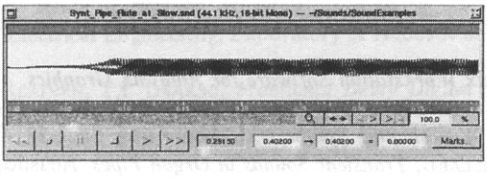

Fig. 16. Time-domain analyses of synthetic sound patterns:
a. fast attack,
b. slow attack.

Table 1. Parameters of the waveguide synthesis of a flute pipe.

scaler	scaler	delay line	delay line	scaler	scaler	filter	filter
n	*r1*	*dl1*	*dl2*	*r2*	*g*	b_0	a_1
1	0.1	8	29	0.56	0.5	−0.3	−0.8

flute pipe in the elaborated model (see Fig. 7). The gain in the feed-back loop in the model is determined by the coefficient *r1* and *r2*. The level of the input signal is proportional to the changes of the parameter *g*.

8. Conclusions

Synthesis of musical sounds by physical modelling becomes feasible due to the increase in the power of the computer equipment. On the basis of a new technology also new synthesis algorithms emerged; the waveguide synthesis that starts to be known as a method created on the basis of physics of an instrument or an instrument family.

The relatively high computing power of the modern DSP circuitry allows such an instrument to run in real-time. The performed analyses and listening tests show that the synthesized sound using the waveguide method is more similar to the natural sound of the organ pipe than sounds synthesized by numerical solution of "classical" equations describing the acoustical behaviour of pipes. What is most important, this observation concerns also the initial stage of a sound rise being critical to the subjective assessment of naturalness of the organ sound produced by pipes excited with various types of air blow. Taking into account that the waveguide method is applicable in real time with the use of popular digital signal processors, it can be considered to be a new and valuable tool for the synthesis of the organ pipe sound. This method is the first one that enables a synthesis of the organ pipe sound with a quality comparable to sounds of widely recognized instruments with a mechanical tracker action.

References

[1] A.H. Benade, *Equivalent Circuits for Conical Waveguides*, J. Acoust. Soc. Amer., **83**, 5, 1764–1769 (1988).

[2] J.W. Beauchamp, *Unix Workstation Software for Analysis, Graphics, Modification, and Synthesis of Musical Sounds*, 94th Audio Eng. Soc. Conv., Preprint 3479, Berlin (1993).

[3] M. Le Brun, *Digital Waveshaping Synthesis*, J. Audio Eng. Soc., **27**, 4, 250–266 (1979).

[4] R.S. Caddy, H.F. Pollard, *Transient Sounds in Organ Pipes*, Acustica, **7**, 277–280 (1957).

[5] J.M. Chowning, *The Synthesis of Complex Audio Spectra by Means of Frequency Modulation*, J. Audio Eng. Soc., **21**, 7, 526–534 (1973).

[6] J.W. Coltman, *Sounding Mechanism of the Flute and Organ Pipe*, J. Acoust. Soc. Amer., **44**, 4, 983–992 (1968).

[7] J.W. Coltman, *Jet drive mechanisms in edge tones and organ pipes*, J. Acoust. Soc. Amer., **60**, 3, 725–733 (1976).

[8] P.R. Cook, *Identification of Control Parameters in an Articulatory Vocal Tract Model with Applications to the Synthesis of Singing*. Ph.D. Dissertation, Elec. Eng. Dept., Stanford University (1990).

[9] P.R. Cook, *A Meta-wind-Instrument Physical Model, and Meta-Controller for Real Time Performance Control*, Proc. of the ICMC, San Jose, California (1992).

[10] N.H. Fletcher, *Nonlinear interactions in organ flue pipes*, J. Acoust. Soc. Amer., **56**, 2, 645–652 (1974).

[11] N.H. Fletcher, *Transients in the Speech of Organ flue pipes — A Theoretical Study*, Acustica, **34**, 224–233 (1976).

[12] L. Hiller, P. Ruiz, *Synthesizing Musical Sounds by solving the Wave Equation for Vibrating Objects*, J. Audio Eng. Soc., **19**, 6 (1971).

[13] P. Kleczkowski, *Group Additive Synthesis*, Computer Music J., **13**, 1, 12–20 (1989).

[14] B. Kostek, A. Czyżewski, *Computer Modelling of the Pipe Organ Valve Action*, 92nd Audio Eng. Soc. Conv., Preprint 3266, Vienna (1992), J. Audio Eng. Soc. (Abstr.), **40**, 5 (1992).

[15] B. Kostek, A. Czyżewski, *Investigation of articulation features in organ pipe sound*, Archives of Acoustics, **18**, 2, 3, 417–434 (1993).

[16] B. Kostek, A. Czyżewski, S. Zieliński, *New Approach to the Synthesis of Organ Pipe Sound*, 98th Audio Eng. Soc. Conv., Preprint 3957, Paris (1995), J. Audio Eng. Soc. (Abstr.), **41**, 5, (1995).

[17] W. Lottermoser, *Acoustical Design of Modern German Organs*, J. Acoust. Soc. Amer., **29**, 6, 682–689, (1957).

[18] M.E. McIntyre, R.T. Schumacher, J. Woodhouse, *On the oscillation of musical instruments*, J. Acoust. Soc. Amer., **74**, 5, 1325–1345 (1983).

[19] A.W. Nolle, T.L. Finch, *Starting transients of flue organ pipes in relation to pressure rise time*, J. Acoust. Soc. Amer., **91**, 4, 2190–2202, (1992).

[20] A. Rakowski, E.G. Richardson, *Eine Analyse des Intonierungsvorganges bei Orgeln*, Gravesaner Blätter, 15, 16, 46–58 (1960).

[21] E.G. Richardson, *Technical Aspects of Sound*, Elsevier Publishing Company, New York, (1953).

[22] E.G. Richardson, *The Transient Tones of Wind Instruments*, J. Acoust. Soc. Amer., **26**, 6, 960–962, (1954).

[23] J.O. Smith III, *Physical Modeling using Digital Waveguides*, Computer Music Journal, special issue on *Physical Modeling of Musical Instruments*, Part I, **16**, 4, 74–91, Winter, (1992).

[24] B.T.G. Tan, S.L. Gan, S.M. Lim, S.H. Tang, *Real-Time Implementation of Double Frequency Modulation (DFM) Synthesis*, J. Audio Eng. Soc., **42**, 11, 918–926 (1994).

[25] V. Välimäki, J. Huopaniemi, M. Karjalainen, Z. Janosy, *Physical Modeling of Plucked String Instruments with Application to Real-Time Sound Synthesis*, 98th Audio Eng. Soc. Conv., Preprint 3956, Paris (1995), J. Audio Eng. Soc. (Abstr.), **41**, 5, 1995.

[26] V. Välimäki, M. Karjalainen, Z. Janosy, U.K. Laine, *A Real-Time DSP Implementation of a Flute model*, Proc. Int. Conf. Acoustics, Speech and Signal Processing (ICASSP'92), San Francisco, California, USA (1992).

[27] V. Välimäki, *Fractional Delay Waveguide Modeling of Acoustic Tubes*, Helsinki University of Technology, Faculty of Electrical Engineering, Laboratory of Acoustic and Audio Signal Processing, Report 34 (1994).

[28] V. Välimäki, M. Karjalainen, T.I. Laakso, *Fractional Delay Digital Filters*, Proc. IEEE Intern. Symposium on Circuits and Systems, Chicago, Illinois (1993).

ARCHIVES OF ACOUSTICS
21, 2, 149–157 (1996)

THE PERCEPTIBILITY OF THE FREQUENCY DROP CAUSED BY THE DOPPLER EFFECT FOR SIMULATED SOUND SOURCE MOTION IN THE MEDIAN PLANE

U. JORASZ* and G.J. DOOLEY**

* Institute of Acoustics
Adam Mickiewicz University
(60-769 Poznań, Matejki 48/49)

** Dept. of Otolaryngology
University of Melbourne
(Parkville, Victoria 3052, Australia)

Simulations of constant velocity (10 m/s and 20 m/s), pure-tone (1 kHz and 2 kHz) sound source moving in the median plane relative to a stationary observer were set up. The simulations were either simulations of approaching sources which stopped at the point of closest passing or of retreating source which began at the point of closest passing. The durations required for the detection of the Doppler-induced frequency drop were determined in a two-alternative, forced-choice task. One interval contained the Doppler-induced frequency drop and in the other the frequency was kept constant. Two types of signals were used: One simulated frequency and level changes which would occur for a moving source. The other simulated only the frequency changes, with the level steady at 65 dB SPL. Threshold durations were determined for simulations of both approaching and retreating source. The pattern of results was similar for all three subjects. In general, the faster the source the smaller the duration needed to detect the frequency drop. Source frequency had little effect on the duration thresholds indicating that a constant percentage frequency change may be required.

1. Introduction

A sound source moving with constant velocity in the median plane relative to a stationary observer results in a change in intensity and frequency of the sound wave that reaches that observer. The extent of these changes is determined by the emission characteristics of the sound source, its velocity and the distance of closest passing with respect to the observer. The frequency drop induced by the Doppler effect is most marked in the region where the source passes closest to the observer irrespective of its velocity or emmission characteristics. This region was called the "passage zone" by RYFFERT *et al.* [7]. It is possible to derive equations for the level and frequency of the

sound field at the observer at any time t. The most convenient mathematical representation is obtained by letting the time $t=0$ represent the time at the point of closest passing of the source relative to the observer; this means that negative time represents an approaching object and positive time a retreating object. For example $t=-5$ s is the time 5 seconds before the object reaches its point of closest passing and $t=5$ s is the time 5 seconds after the object has passed through its point of closest passing. The sound level generated at the observer by such a source is given by the relationship:

$$L(t)=I+10\log\left\{\frac{d^2}{d^2+v^2t^2}\left(1-\frac{4v^2t}{c\cdot(d^2+v^2t^2)^{1/2}}\right)\right\}, \tag{1.1}$$

where $L(t)$ is the level in dB at the observer at time t; I is the level at the moment when the source passes closest to the observer, v is velocity of the source; d is the distance from the observer at the point of closest passing; and c is the propagation velocity of the tonal signal in the medium [4]. This relationship is valid under the assumption that $v \ll c$.

A simulation of sound source movement based on this equation assumes a point observer who remains stationary with respect to the plane of movement of the source; consequently, alterations of the sound field produced by the head and by the pinnae are not taken into account. Thus, sound fields of this type are spatially ambiguous; when presented diotically they could represent approach followed by retreat of the sound source either from in front of, or from behind and either over the head of, or underneath the observer. In this experiment symmetry of the head is also assumed so that any sound in the median plane is assumed to result in identical signals reaching both ears.

Because the source velocity component in the direction of the observer changes during the sound motion there is a corresponding frequency change at the observation point due to the Doppler effect. This change in frequency can be represented by the function:

$$f(t)=f_0\left[1-\frac{v^2t}{c\cdot(d^2+v^2t^2)^{1/2}}\right], \tag{1.2}$$

where $f(t)$ is the frequency at the observer at any time t and f_0 is the frequency of the tone emitted by the moving source. The parameters c, d and v are as described above.

The first purpose of this experiment was to determine the duration necessary for detection of the frequency drop induced by constant-velocity sound source motion in the median plane. Sound sources of different velocities passing through different points with respect to a stationary observer were used. Another aim was to determine whether the presence of the intensity change induced by these motions in any way 'masked' the detection of the frequency drop in the manner described by RYFFERT *et al.* [7] and called 'automasking'. In order to test this some of the simulations that we used were accurate simulations of both frequency and level changes and others simulated the frequency change alone with the level kept constant.

The results obtained correspond only approximately to the real conditions of a specific physical effect: the Doppler effect. They rather correspond to an explanation of some general phenomena in a simultaneous perception of frequency and intensity changes in simple sounds.

2. Stimuli

All stimuli were sinusoids derived from a Farnell DSG 1 signal generator controlled by a Texas Instruments 990/4 computer. The frequency was digitally controlled and was changed every 10 ms.

The desired amplitude envelope was achieved by multiplying the output from the signal generator by a voltage produced by a digital-to-analogue converter (DAC). The level was changed every 10 ms, the changes occurring midway between frequency changes. The DAC output was low-pass filtered through both halves of a Kemo VBF 8/03 filter (96 dB per octave slope, cut-off frequency 400 Hz); this resulted in a smooth sounding overall change.

Each signal had an envelope with 10-ms linear rise-fall times generated by updating the DAC output 10 times per ms. The signals were band-pass filtered through a Kemo VBF 8/03 filter (48 dB per octave slope, bandpass with cut-off frequencies 0.5 f and 1.5 f) to smooth frequency and level changes and to attenuate unwanted distortion products. The signal was then fed through a Hatfield 2125 manual attenuator.

3. Procedure

Thresholds were determined using an adaptive two-alternative forced-choice (2AFC) procedure that estimates the 70.7% correct point on the psychometric function [3]. In this experiment the values of the distance of closest approach (d) and the velocity (v) were chosen so that, for long duration signals, the frequency drop was clearly audible and the steepest part of the frequency drop covered a time period of between one and two seconds. To this end, velocities of 10 m/s and 20 m/s were chosen along with a distance of closest passing of 10 m. The experiment was run with two different emission frequencies (1 kHz and 2 kHz). Figures 1 and 2 show the level and frequency profiles, respectively.

Two conditions were run:

1) *Changing Level Condition* — in this condition one interval always contained a simulation of the frequency and intensity change and the other interval had the same intensity change but with the frequency fixed at the median frequency of the first interval.

2) *Fixed Level Condition* — in this condition the level was always set at 65 dB SPL in both intervals. In one interval the frequency drop associated with the simulation was present and in the other interval the frequency was fixed at the median frequency of the first interval.

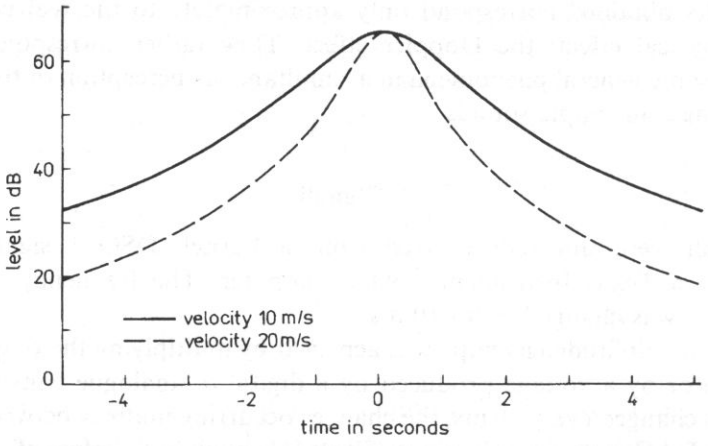

Fig. 1. The level change profiles for two different values of source velocity. The duration of source motion is 10 s.

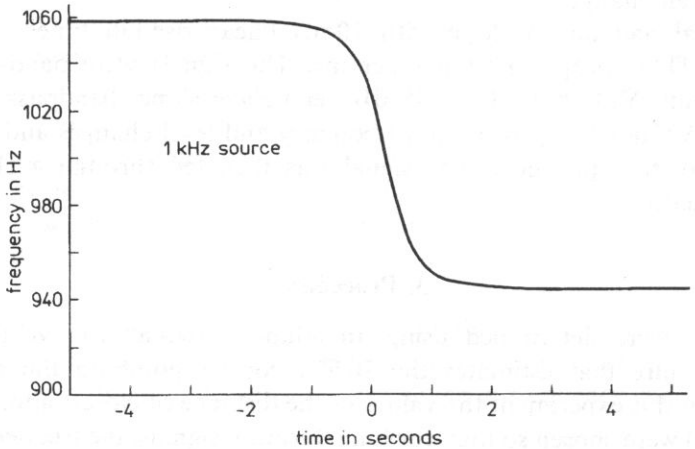

Fig. 2. The frequency change profile for source frequency 1 kHz.

Subjects were instructed to indicate which of the two signals contained the frequency drop by pressing the appropriate button on a response box in front of them. The stimuli were presented to the subject diotically over a Sennheiser HD414 headset and feedback was provided by means of lights. A run always started with a duration fixed such that the frequency drop was clearly audible (This was usually about 1 second). The duration was decreased after two consecutive correct responses and increased after one incorrect response. For both approaching and retreating stimuli the point of closest passing was the fixed point for all intervals. This means that for approaching stimuli the signals were made shorter by subtracting from the beginning of the signal and for retreating stimuli they were made shorter by subtracting from the end of the stimuli. All duration changes were accurate to the nearest millisecond.

The transition from increasing to decreasing duraton or vice-versa defines a turnaround. For each threshold determination testing continued until 12 turnarounds had been obtained, and threshold was taken as the geometric mean of the last 8 turnarounds. The step size was 50 ms for the first four turnarounds and was reduced to 10 ms thereafter. Each threshold reported is the geometric mean of five runs. The order of presentation of runs was randomised across all sessions.

4. Subjects

Three subjects were used: all received at least four hours of practice on frequency discrimination tasks before data collection began. Two subjects were the authors; the other was a male (aged 27 years) and was paid for his participation. None of the subjects had any known hearing defects. All had absolute thresholds within 10 dB of the 1969 ISO standard at all audiometric frequencies.

5. Results and discussion

Mean threshold values and standard deviations for individual subjects in all conditions are shown in Table 1. We conducted an ANOVA, which showed the following:

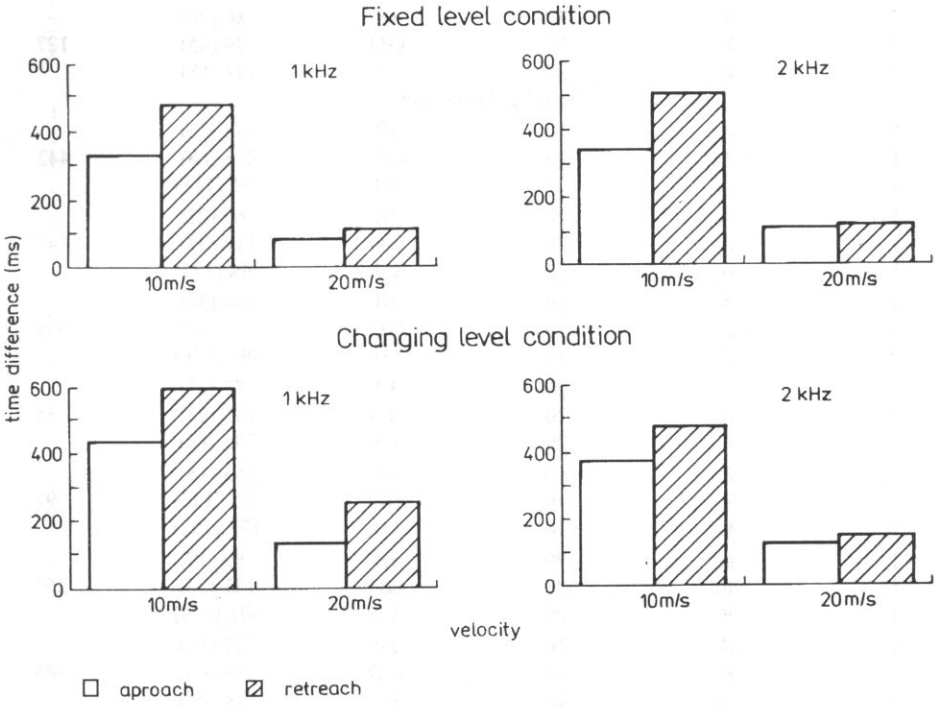

Fig. 3. The time thresholds collapsed across subjects in all experimental conditions

Table 1. Individual mean duration thresholds and standard deviations for detection of the frequency drop in moving source simulations.

FREQUENCY (1/2 kHz)	APPROACH RETREAT	VELOCITY (10/20 m/s)	SUBJECT	THRESHOLD & S.D. (ms)	MEAN (ms)
		Fixed Level Condition			
1	A	10	JB	258 (51)	
1	A	10	GD	387 (42)	342
1	A	10	UJ	381 (87)	
1	A	20	JB	58 (17)	
1	A	20	GD	106 (15)	93
1	A	20	UJ	115 (35)	
2	A	10	JB	331 (59)	
2	A	10	GD	315 (91)	350
2	A	10	UJ	405 (114)	
2	A	20	JB	94 (33)	
2	A	20	GD	95 (25)	118
2	A	20	UJ	164 (50)	
1	R	10	JB	287 (58)	
1	R	10	GD	606 (88)	486
1	R	10	UJ	564 (134)	
1	R	20	JB	88 (45)	
1	R	20	GD	120 (35)	118
1	R	20	UJ	147 (62)	
2	R	10	JB	314 (90)	
2	R	10	GD	378 (83)	510
2	R	10	UJ	838 (123)	
2	R	20	JB	86 (26)	
2	R	20	GD	99 (45)	127
2	R	20	UJ	197 (68)	
		Changing Level Condition			
1	A	10	JB	288 (73)	
1	A	10	GD	453 (68)	442
1	A	10	UJ	585 (111)	
1	A	20	JB	60 (22)	
1	A	20	GD	119 (31)	141
1	A	20	UJ	244 (124)	
2	A	10	JB	290 (36)	
2	A	10	GD	353 (31)	378
2	A	10	UJ	492 (136)	
2	A	20	JB	77 (27)	
2	A	20	GD	131 (23)	138
2	A	20	UJ	205 (82)	
1	R	10	JB	263 (18)	
1	R	10	GD	755 (125)	597
1	R	10	UJ	773 (201)	
1	R	20	JB	69 (19)	
1	R	20	GD	131 (33)	267
1	R	20	UJ	601 (254)	
2	R	10	JB	229 (53)	
2	R	10	GD	316 (66)	486
2	R	10	UJ	914 (55)	
2	R	20	JB	78 (23)	
2	R	20	GD	111 (27)	162
2	R	20	UJ	298 (198)	

Table 2. Individual mean thresholds expressed as percentage frequency drop in Hz for detection of the frequency changes in moving source simulations.

FREQUENCY (1/2 kHz)	APPROACH RETREAT	VELOCITY (10/20 m/s)	SUBJECT	%FREQ. DROP	MEAN (Hz)
		Fixed Level Condition			
1	A	10	JB	0.73	
1	A	10	GD	1.05	0.94
1	A	10	UJ	1.04	
1	A	20	JB	0.67	
1	A	20	GD	1.21	1.06
1	A	20	UJ	1.31	
2	A	10	JB	0.92	
2	A	10	GD	0.89	0.97
2	A	10	UJ	1.09	
2	A	20	JB	1.08	
2	A	20	GD	1.09	1.33
2	A	20	UJ	1.82	
1	R	10	JB	0.80	
1	R	10	GD	1.51	1.25
1	R	10	UJ	1.43	
1	R	20	JB	1.01	
1	R	20	GD	1.36	1.34
1	R	20	UJ	1.64	
2	R	10	JB	0.88	
2	R	10	GD	1.03	1.26
2	R	10	UJ	1.88	
2	R	20	JB	0.99	
2	R	20	GD	1.14	1.43
2	R	20	UJ	2.14	
		Changing Level Condition			
1	A	10	JB	0.81	
1	A	10	GD	1.20	1.16
1	A	10	UJ	1.47	
1	A	20	JB	0.69	
1	A	20	GD	1.35	1.53
1	A	20	UJ	2.56	
2	A	10	JB	0.81	
2	A	10	GD	0.97	1.02
2	A	10	UJ	1.29	
2	A	20	JB	0.89	
2	A	20	GD	1.48	1.53
2	A	20	UJ	2.21	
1	R	10	JB	0.74	
1	R	10	GD	1.76	1.43
1	R	10	UJ	1.78	
1	R	20	JB	0.80	
1	R	20	GD	1.48	2.25
1	R	20	UJ	4.48	
2	R	10	JB	0.65	
2	R	10	GD	0.88	1.16
2	R	10	UJ	1.96	
2	R	20	JB	0.90	
2	R	20	GD	1.27	1.72
2	R	20	UJ	2.99	

1) Source frequency has no significant effect on the thresholds. This indicates that subjects require a fixed amount of frequency change as a proportion of center frequency for correct detection. We can test this by looking at the thresholds for the different velocities and seeing whether they are consistent with a fixed change being required. Table 2 shows the mean thresholds expressed as percentage frequency drop for detection of the frequency changes.

2) The duration data collapsed across subjects are shown in Fig. 3. From this we see that thresholds for approach are lower than those for retreat. This is consistent with DOOLEY [1] who found that for simulations of median plane motion outside of the passage zone (where intensity change provides the cue for detection) subjects required a longer presentation to discriminate a retreating source from a stationary source than they did for discriminating an approaching source from a stationary source.

3) The thresholds for the fixed level condition — which are comparable with the absolute frequency difference limen [5] — are generally lower than those for the changing level condition. This implies that the presence of the additional intensity change makes the detection of the frequency drop more difficult. It is unclear whether this is due merely to increasing the difficulty of the task by having the extra change present, in other words a sort of confusion effect, or whether it is actually due to some real acoustic masking effect as reported by RYFFER *et al.* [7] and JORASZ [2].

4) ZWICKER [8, 6] attempted to account for the size of the frequency and intensity discrimination limens in terms of changes in the excitation pattern evoked by the stimulus. According to Zwicker's model, a change in frequency or intensity will be detected whenever the excitation on the steeply sloping, low frequency side of the excitation pattern changes by 1 dB or more. This model would predict that increasing the level of the tone would facilitate the detection of frequency drops compared with decreasing the level of a tone during a presentation. Our data are consistent with this model as approaching objects required a shorter duration for detection than retreating objects and approaching sources are associated with rising level and falling frequency and retreating sources are associated with falling level and falling frequency.

5) We should remember that — as it follows from the nature of this particular signal — the duration thresholds are strictly connected with the frequency discrimination thresholds [2] and intensity discrimination thresholds.

6. Conclusions

1. A fixed amount of frequency change as a proportion of center frequency is required for correct detection of the frequency changes in moving source. This is comparable with the absolute frequency difference limen if there is no level change (fixed level condition).

2. The presence of the intensity change elevates the thresholds. It may be like the masking effect inside the same sound sensation ('automasking').

Acknowledgments

We wish to thank Brian C.J. MOORE and Brian GLASBERG (Cambridge, U.K.) for their contributions to statistical verification.

The first author was partly sponsored by Cambridge Hospitality Scheme.

References

[1] G.J. DOOLEY, *Scientific report*, Cambridge University, unpublished (1985).

[2] U. JORASZ, *Perceptibility of pitch changes in a tonal signal emitted by a moving source*, Arch. Acoust. **7**, 1, 3–12 (1982).

[3] H. LEVITT, *Transformed up-down methods in psychoacoustics*, J. Acoust. Soc. Am., **49**, 467–477 (1971).

[4] R. MAKAREWICZ, *Intensity of a sound field generated by a moving source*, Acustica, **41**, 267–273 (1979).

[5] B.C.J. MOORE, *An introduction to the psychology of hearing*, Academic Press, 3rd edition, 1989, p. 160.

[6] B.C.J. MOORE [Ed.], *Frequency selectivity in hearing*, Academic Press, 1986, p. 158.

[7] H. RYFFERT, A. CZAJKOWSKA, U. JORASZ, R. MAKAREWICZ, *Dynamic approach to sound pitch*, Arch. Acoust. **4**, 3–9 (1979).

[8] E. ZWICKER, *Masking and psychological excitation as consequences of the ear's frequency analysis*, [In:] R. Plomp and G.F. Smoorenburg, Frequency Analysis and Periodicity Detection in Hearing, Sijthoff, Leiden 1970.

ARCHIVES OF ACOUSTICS
21, 2, 159–178 (1996)

AM SIGNALS WITH RANDOM MODULATION PARAMETERS AND THEIR DETECTION

E. OZIMEK and J. KONIECZNY

Institute of Acoustics Adam Mickiewicz University
(60-769 Poznań, ul. Matejki 48/49)

In this article a method of generating AM signals with randomly changing parameters was discussed. This method involves a modulation process in which some selected parameters of the modulation waveform (amplitude or frequency) are subjected to random variation. The result of this process are random changes (independent or simultaneous) in the depth or frequency of the modulation of AM signals. Using this method, it is possible to study the detection and discrimination of signals with parameters varying in time. This paper also presents the results of preliminary psychoacoustic studies related to the random amplitude modulation.

1. Introduction

Sounds perceived by humans vary in their amplitude-frequency structure. This particularly applies to the sounds of speech and music. The main feature of this variability is the irregular (pseudorandom) character of the amplitude and frequency changes.

In literature much attention has been devoted to the description of the mechanisms of perception of simple sounds, such as pure tones, multitones or more complex sounds like band-noise [3, 4, 16, 17]. Pure sounds can be described using relatively simple analytic expressions. The band noises cannot be described using such simple analytic relations, however the basic statistical moments describing the waveforms of these signals remain constant with time. Most complex to perceive are the real sounds of speech and music for which those moments may change with time. A first approximation of those sounds might be modulated signals with randomly changing parameters.

The hitherto studies on the perception of modulated sounds have focused on different aspects of the modulation process. For example, the similarity of the perception of AM and FM signals has been investigated [1, 3, 17]. The modulation transfer function MTF has been related to the perception of modulated signals [16]. Some masking effects, characteristics of the modulated sounds, have also been examined, e.g. the MDI effect [8]. In all these studies, however, the signals were usually subjected to a sinusoidal amplitude modulation (SAM).

It is worth noticing that random waveforms have very rarely been used so far as modulation sounds [8, 12, 15]. The results of psychoacoustic studies are not always univocal. For example, Sęk has proved that there is no significant difference in the AM detection thresholds between the regular and random modulation signals. MENDOZA *et al.* [8] showed that the AM detection thresholds for the random modulation signals are greater than those for the regular ones. It would be interesting to study the influence of random changes in signal parameters on the specific synchronous effect, i.e. the "phase locking" which clearly takes place in a simple tone [2]. One can expect that a complex envelope of the modulation waveform should cause a slightly different perception of the modulated signals than that of signals modulated with a tone parameters of constant.

The perception of AM signals can be affected if the frequency of the modulation tone changes with time. This effect may be also responsible for the differences in the ability to perceive modulation depending on the shape of the modulation waveform envelope.

Much attention has also been devoted to the psychophysiological aspect of these studies [2, 6, 7, 10, 14]. Some of the neurophysiological studies [6] have indicated the possibility to reproduce (provided the signal parameters have been properly selected) on the peripheral level a component of frequency equal to the modulation frequency. This effect might be responsible for the fact that the perception of modulation improves with the increase of the signal intensity [17].

JAVEL [6] proved the sensitivity of neurons to the temporal form of the waveforms of the signals stimulating them. He studied, among others, the dependence of the neurons' response on the level of the modulated signal intensity as well as on the depth and frequency of modulation. REES and PALMER [14] continued these studies and showed that the distributions of neuron firings in response to the amplitude-modulated stimuli depend on the modulation frequency.

For further studies concerning this problem it is necessary to develop a methodology of generating signals for which it would be possible to control the following features: random variation of their basic parameters, the independence or coherence of this variation for particular parameters, and the degree of their mutual correlation. This condition is not fulfilled by the narrowband noise applied so far as a modulation signal. With the above in mind, a study was undertaken aimed at the development of a method of generating random signals which would satisfy the above conditions. Moreover, a preliminary investigation of the detection thresholds of AM signals generated by this method was conducted.

2. Algorithm of the generating a modulation signal with parameters randomly changing in time

To generate a random AM signal, a modulation of a sinusoidal carrier by waveforms with discrete random changes in amplitude and frequency was applied. In the duration corresponding to the half-period of the modulation signal the amplitude and frequency. However, at the transition from one half-period to another, those parameters were subjected to random changes. Such a generating procedure required

a drawing of the "n" random numbers of a given distribution, where "n" is the number of half-periods of the modulation tone (dependent both on the frequency of this tone and its duration). These numbers were then used for the change in either the amplitude or frequency of the modulation waveform. This yielded random changes in the modulation or frequency of the AM signal. When only the amplitude was subjected to a random change, the zero-crossings of the modulation signal remained constant.

A crucial aspect of this method was the definiton of a coefficient describing the range of randomness of the changes of the parameter under investigation.

In the case of a classical AM modulation, in which the carrier and modulation signals are sinusoidal, this coefficient should correspond to that of the modulation depth m reported in literature. To satisfy this condition, for the modulation and carrier signal the value of RMS was at first determined according to equation (2.1):

$$V_{\mathrm{RMS}}=\sqrt{\frac{1}{n}\sum_{1}^{n}V_i^2(t)}, \tag{2.1}$$

where $V_i(t)$ is the temporal value of the modulation signal.

The modulation depth coefficient was defined in the logarithm scale as a product of two RMS values, one for the modulation signal and another one for the carrier signal, according to (2.2):

$$m=20\log\frac{V_{\mathrm{RMS}}}{V_{\mathrm{RMS}}(\mathrm{car})} \tag{2.2}$$

where $V_{\mathrm{RMS}}(\mathrm{mod})$ — RMS of the modulation signal, while $V_{\mathrm{RMS}}(\mathrm{car})$ — RMS of the carrier signal.

In the literature [13] one can encounter another measure which has the meaning of the variance of the signal power or intensity:

$$v_p=\frac{1}{n}\sum_{1}^{n}(V_i^2(t)-V_s^2)^2, \tag{2.3}$$

where "v_p" stands for the variance of the signal power, $v_i^2(t)$ is the square of the temporal value, while V_s^2 is the power of a signal corresponding to the mean value of the acoustic pressure.

This value also characterizes in a way the degree of irregularity of a modulation signal. It can be proved that for a sinusoidal signal, i.e. when the discrete values $V_i(t)$ are assigned to successive half-periods, this measure should be equal to zero irrespective of the amplitude because the $V_{(i)}(t)$ values are equal to the mean value V_s.

To estimate the degree of irregularity, sometimes a coefficient called "crest factor" [5] is used that is defined as the ratio of the peak value to the rms value of the waveform:

$$\mathrm{cf}=\frac{X_p}{X_{\mathrm{RMS}}}, \tag{2.4}$$

where "cf" is the "crest factor" coefficient, while X_p means the maximum value of the waveform and X_{RMS} its rms value.

3. Hardware and software of the signal generating

The signals (the modulation, carrier, and random ones) were generated using a special card equipped with a DSP made by Tucker Davis Technology (Gainsville, USA). This card has its own operational memory.

The operation buffer of this card may be filled with samples via APOS library functions and procedures. Upon the generation of a random signal, the working buffer of the memory of the card was filled with Gaussian distribution samples collected from the APOS library. When the program was running, this buffer was treated as a program array of random numbers. Then from the file as many numbers as there were the half-periods of modulation oscillations (at a given frequency) were drawn out.

The process of preparation of a random amplitude signal is shown in Fig. 1.

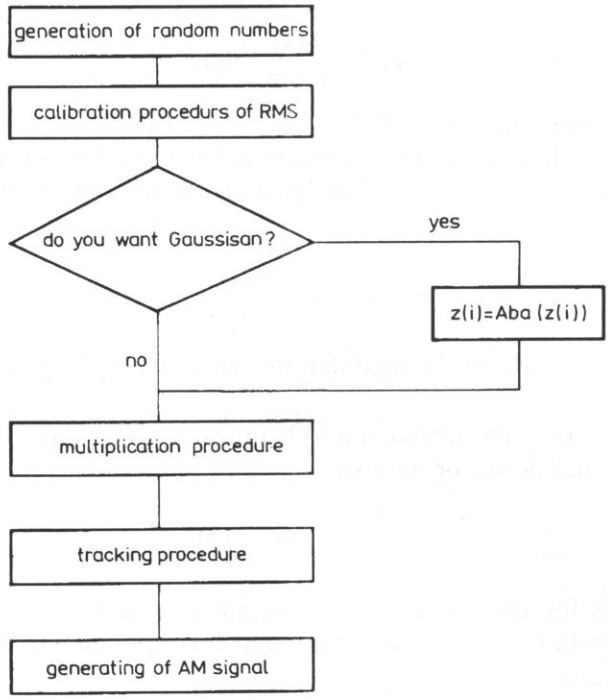

Fig. 1. Algorithm for preparation of a random amplitude signal.

The drawn out sequences of numbers were subjected to the so-called calibration procedure.

The first calibration stage consisted in the so-called centralization of the generated sequence of random numbers. The centralization procedure was carried out according to the following formula:

$$z(i)=x(i)-\frac{1}{n}\sum x(i), \tag{3.1}$$

where $x(i)$ denotes the primarily drawn out sequence of numbers, while $z(i)$ stands for a sequence of random numbers subjected to the centralization procedure. The centralization then consisted in the subtraction from the drawn out random variable its average value and it assured the clearing of the average value of realization $z(i)$. The subsequent calibration stage involved standardization, i.e. multiplication of the realization by such a scaling factor that the RMS of the resultant modulation waveform was equal to the RMS of the carrier waveform. Therefore, the initial modulation depth was always equal to 100%. During the detection or discrimination experiment, it was possible to reduce this value by rescaling the modulation waveform.

Further steps taken within this study depended on what kind of random variation was selected: the pseudorandom or Gaussian. In the case of the former one, the values of the amplitudes in each of the half-periods were multiplied by the drawn out, centralized and standardized numbers. Such an operation yielded a distribution of temporal values of the modulation signal which was a certain combination of the sinusoidal and Gaussian distribution. An important feature of this distribution values, further referred to as pseudorandom distribution, was the appearance of two characteristic maxima which made the distribution more similar to a bimodal distribution. The reason for the appearance of these two maxima is the multiplication of the positive and negative values of the amplitudes in the half-periods of the modulation signal by positive and negative random numbers of the prepared realization. Thus, to obtain a distribution with one maximum, which would be closer to the standard distribution, it was necessary to replace the negative numbers of equal value. This operation is illustrated by the right side branch of the algorithm presented in Fig. 1.

After that the values of the amplitudes for subsequent half-periods of the modulation tone were multiplied by the already drawn-out random numbers (just as in the case of the previously discussed distribution).

The prepared sequence of random numbers could be saved on a disc as the so-called "frozen realizations". This permitted a multiple application of this realization at different stages of the psychoacoustic studies.

Due to the options offered by a computer program it was possible to select the random changes either in the amplitude or the frequency of the modulation tone.

There was also a third option of combined (simultaneous) random changes in both amplitude and modulation frequency.

In the case when the option of combined random changes in amplitude and frequency was selected, it was also possible to choose the combination of the realization according to which these changes were to proceed, i.e.:

- to select simultaneous, random changes in amplitude and frequency taking place according to two different realizations;
- to select simultaneous, random changes in amplitude and frequency taking place according to the same realization.

Figures 2 and 5 present some modulation waveforms (first column), the probability distributions of the temporal values corresponding to them (second column), and the resultant modulated waveforms (third column) for different types of

random changes of the modulation parameters (for the carrier frequency equal to 250 Hz and a modulation depth of 50%). Figures 2b and 2c illustrate pseudosinusoidal changes of the modulation signal amplitude. Figures 3b and 3c refer to the Gaussian changes of the amplitude of the same signal. Figure 4b and 4c show random changes in the modulation frequency, while Figs. 5b and 5c present a simultaneous random changes in both amplitude and frequency of the modulation signal. The first line in these figures, marked with the letter "a", shows oscillograms, histograms and modulated signals for a sinusoidal (the so-called regular) modulation with no elements of randomness. The second line in these figures, marked with letter "b", encompasses oscillograms, histograms and modulated signals corresponding to a random variation of the selected parameter according to realization R1. The third line in the discussed figures marked with letter C, presents oscillograms histograms and modulated signals histograms, for realization marked as R2.

Comparing the side-most columns (both the left and right ones) of Fig. 2, one can see that for the modulation of a pseudorandom distribution waveform the distance between subsequent zero-crossings of the signal is constant. The amplitude, on the other hand, oscillates within a limited range at the transfer from one half-period to the next one.

A very different shape of oscillograms is obtained for the Gaussian distribution.

For this distribution, few fluctuations with maximum values of amplitude and numerous temporal values closer to zero can be observed.

Those close-to-zero values correspond to the temporal segments presented in the right column of Fig. 3, in which the resultant signal is not modulated.

For the modulation signals that temporal values change randomly (Gaussian change) it was tested whether the distribution of probability was normal. For this purpose, a test consisting in calculating statistical moments of higher orders was used, i.e. moments of the third order, m_3, and the fourth order, m_4, were calculated. These moments were then used to determine the so-called asymmetry coefficient "asym" and a value of excess "exc" according to the following formulae:

$$\text{asym} = m_3/s^3, \tag{3.2}$$

where "s" is the standard deviation of a random variable contained in the generated sequence of random numbers,

$$\text{exc} = m_4/v^2 - 3, \tag{3.3}$$

where "v" is the variance of a random variable contained in the generated sequence of random numbers.

Results of the test are presented in Table 1.

The calculated values of the asymmetry coefficient and of the excess given in this Table are always lower than 3 that made us to consider the tested distributions as normal.

Both for the sinusoidal signal used as a modulation waveform and for the signal generated using the R1 or R2 realizations, the calculation of the "crest factor" coefficient gave the following values:

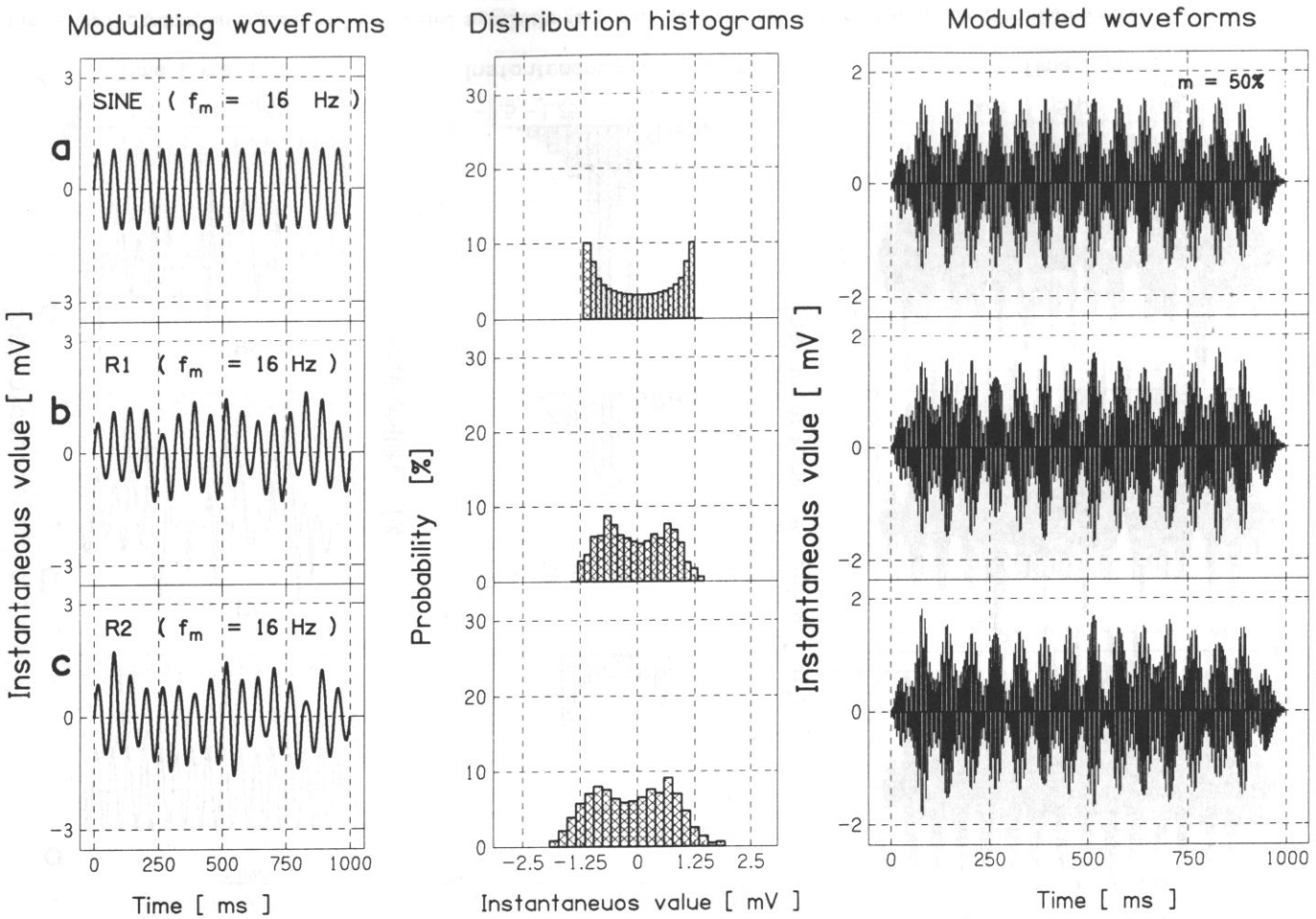

Fig. 2. Oscillograms, histograms and modulated signals for pseudorandom changes in the modulation signal (carrier frequency 250 Hz, modulation frequency — 16 Hz, modulation depth 50%).

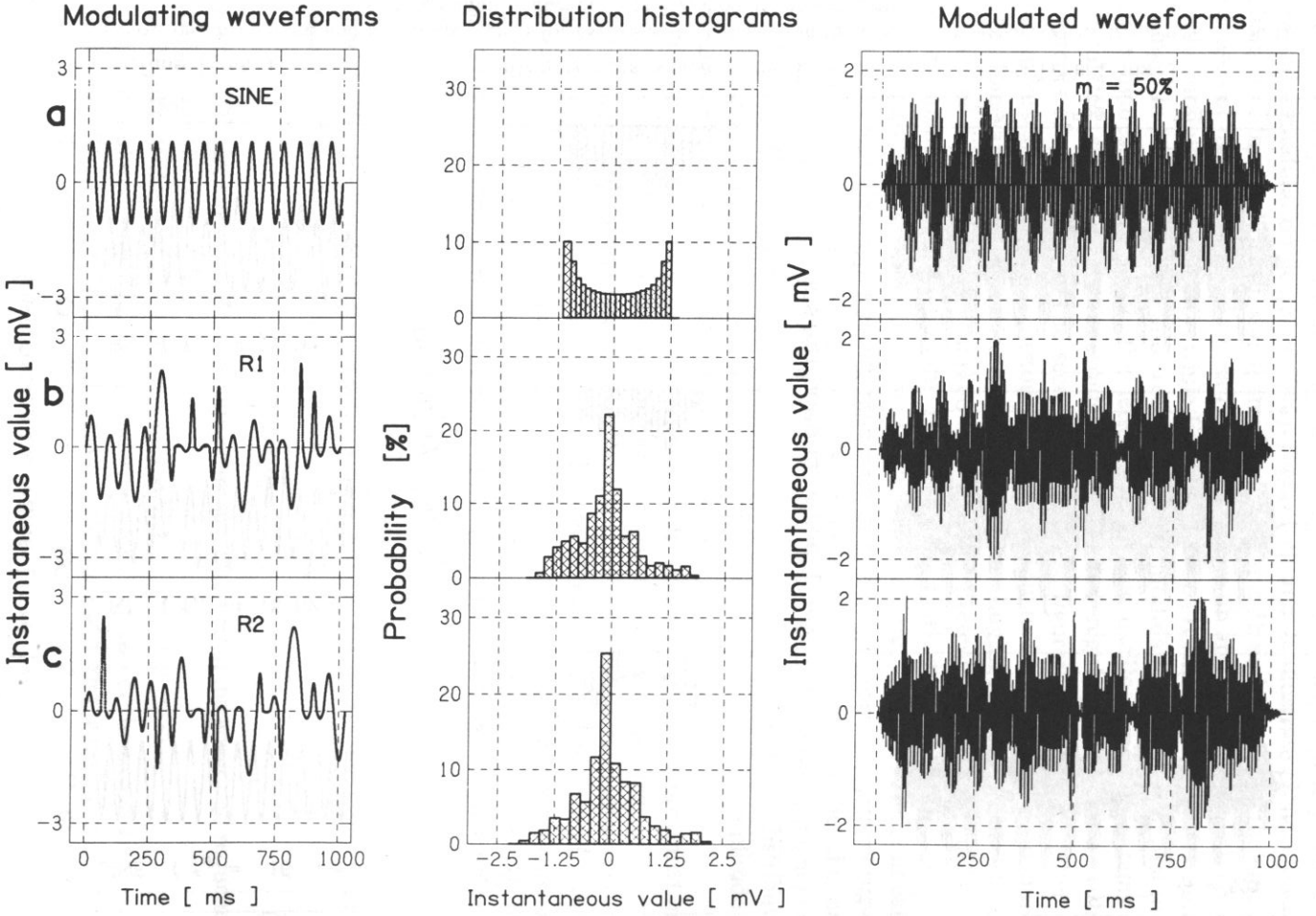

Fig. 3. Oscillograms, histograms and modulated signals for random, Gaussian amplitude changes in the modulation signal.

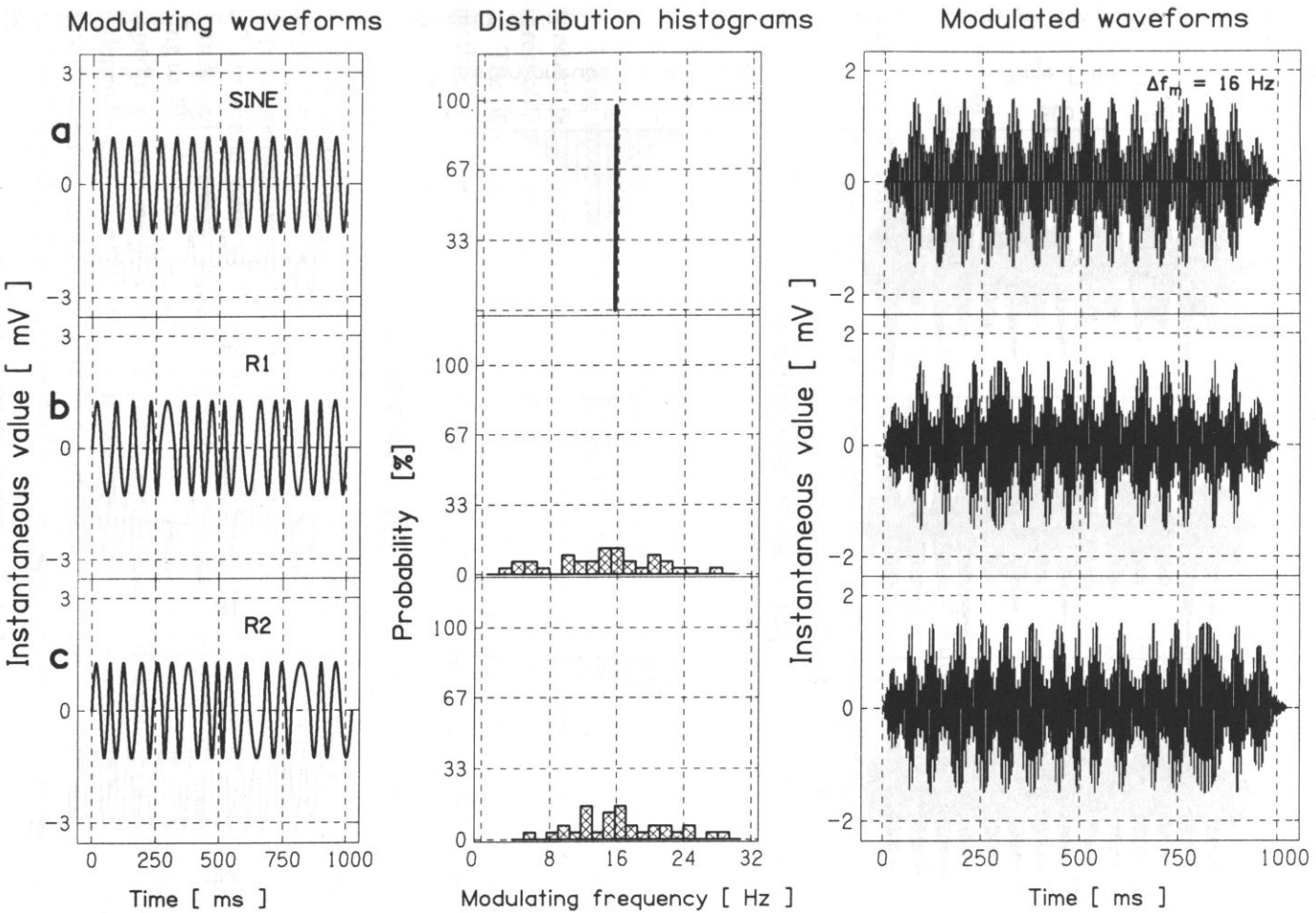

Fig. 4. Oscillograms, histograms and modulated signals for random frequency changes in the modulation signal.

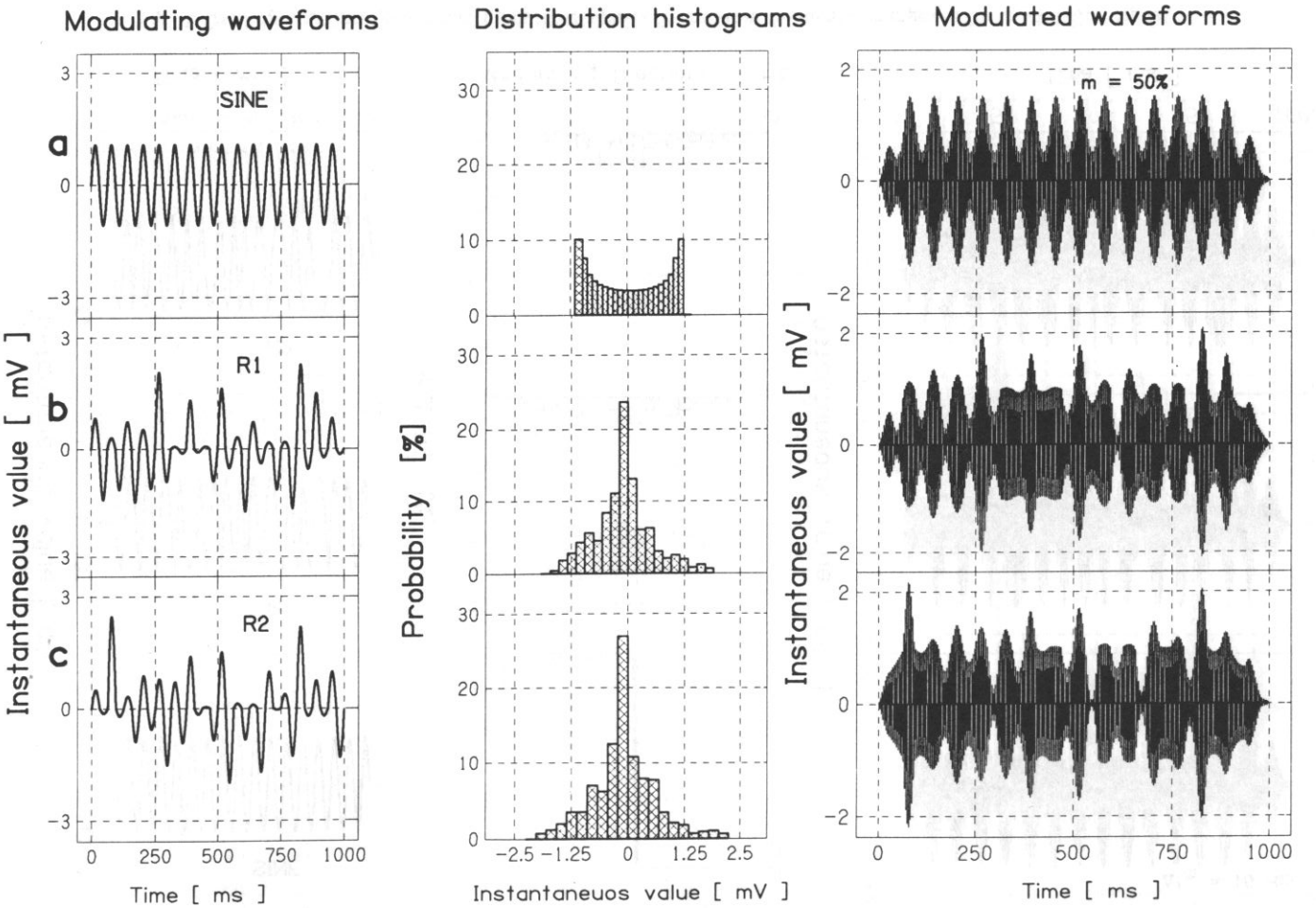

Fig. 5. Oscillograms, histograms and modulated signals for simultaneous, random amplitude and frequency changes in the modulation signal.

Table 1. Statistical coefficients of excess and skewness.

Fmod	asym	exc
4 Hz	1.62018	0.00543
16 Hz	1.76279	0.56968
64 Hz	1.78148	0.75914
128 Hz	2.02359	2.02076
256 Hz	2.02359	2.02076

— for the sinus: 1.41438;
— for the realization R1 and the pseudosinusoidal distribution: 2.13066;
— for the realization R2 and the pseudosinusoidal distribution: 2.9866;
— for the realization R1 and the Gaussian distribution: 3.02418;
— for the realization R2 and the Gaussian distribution: 3.29662.

As one can see, the crest factor coefficient assumes the highest values for the Gaussian distribution and slightly smaller ones for the pseudosinusoidal distribution.

Thus the coefficient may account for the differences observed between Fig. 2 and Fig. 3.

4. Methodology of psychoacoustic studies

Using the method of random signals generation described in 3, it was possible to conduct preliminary psychoacoustic studies that aim was to determine the detection thresholds of AM signals with random changes in amplitude.

The psychoacoustic studies were performed according to the Levitt's "up-down" method following the 2AFC paradigm and at the feedback between the listener and the experimental program. On each trial a pair of stimuli was presented to the listener: a standard stimulus (as an unmodulated sound — sinusoidal) and signal (AM modulated sound). The depth of the signal modulation changed throughout the experiment depending on the manner the listener responded. Two successive correct responses led to a decrease in the depth of signal modulation, while one wrong response caused an increase of this depth.

The initial value of the depth of signal modulation was always higher than the anticipated threshold value. The threshold value was assumed to be that corresponding to 70.7% of correct points (on the psychometric function). The parameters of the experiment were recorded in a special text file, the so-called condition file (Annex 1). Independent of this file, there was also an additional interface which enabled the experimenter to modify currently most of the parameters.

For the series of experiments under discussion, the following parameters were selected:

- carrier frequencies: 250 Hz and 1000 Hz;
- modulation frequencies: 4, 16, 64 and 128 Hz;

- stimulus duration (either standard or signal): 1000 ms;
- intensity level: 70 dB SPL.

An appropriate quality of signals within the whole range of variation of the selected parameters was guaranteed by the cooperation of the software with the Tucker-Davis Technology hardware. The signal was generated by a 16-bit DA converter at a sampling rate of 44 kHz was low-pass filtered at 8 kHz.

A program-controlled PA4 attenuator was placed in the channel of the analogue signal. The generated analogue signal was supplied to a HB5 headphone amplifier (which was a component of the TDT set) with DT-48A Beyer headphones. Each trial consisted of 5 runs, each consisting of 40 pairs of stimuli: standard-signal.

The averaged results of five such runs, as well as the particular results, were written into the file (Annex 2). It was also possible to plot the curve of the listener's responses (Annex 3). Additionally, a preliminary statistical processing of the currently obtained results was done by calculating the basic statistical moments and performing a one factor variance analysis involving the calculation of the Snedecor F coefficient for the results of five runs.

Three subjects whose audiograms did not reveal any hearing loss took part in the experiment (the auditory sensitivity of each subject was within 0–5 dB).

Each subject went through a control stage where the so-called classical AM detection threshold for sinusoidal modulation was measured. Then, the AM detection thresholds were determined for the modulation waveform with pseudorandom changes in amplitude.

5. Discussion of the obtained results

The results for three subjects plotted in Figs. 6 and 7 show the AM detection thresholds as function of the modulation frequency at the carrier frequencies of 250 Hz and 1000 Hz, respectively. The dashed-line curve illustrates the detection thresholds for sinusoidal changes in amplitude, while the solid one those for random changes.

As follows from the results presented, detection thresholds for the sinusoidal and pseudorandom changes in amplitude nearly overlap within the limits of SD. For the modulation frequency below f_m, the detection thresholds are almost constant and then, above that frequency, they clearly decrease in the function of f_m.

The above regularity was observed for the detection threshold both for the sinusoidal and pseudosinusoidal modulation which is particularly apparent for the carrier frequency of 100 Hz.

The results obtained for the carrier of 250 Hz seem to imply that there is a slight difference between the two types of thresholds for the modulation frequencies of 4 Hz and 128 Hz. In order to resolve this problem an additional testing for these data was performed applying the t-Student test. The calculated value of the t-Student coefficient were equal to 1.606 and 2.421 at the modulation frequencies of 4 Hz and 128 Hz, respectively. The critical value of the t-Student coefficient amounted to 2.775 at four degrees of freedom and at the level of significance equal to 0.75. The results of

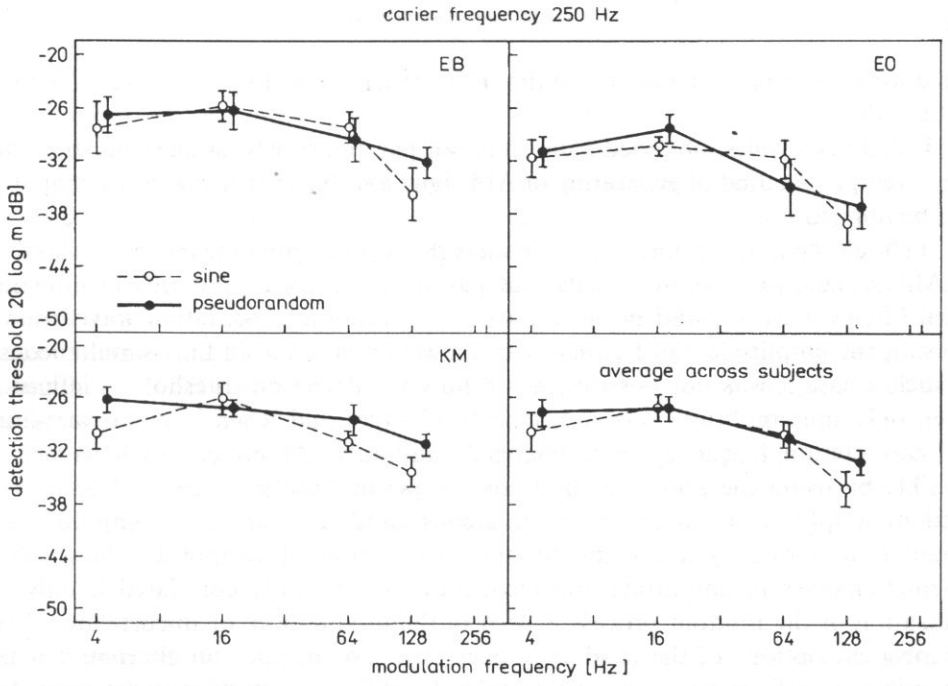

Fig. 6. Detection thresholds of pseudorandom changes in amplitude for the carrier frequency of 250 Hz.

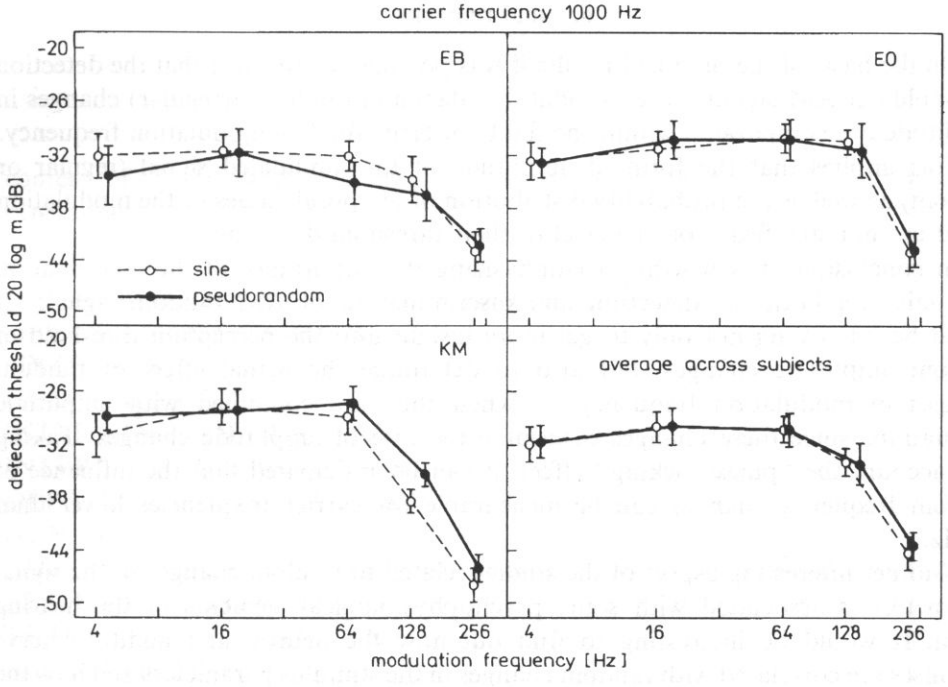

Fig. 7. Detection thresholds of pseudorandom in signal amplitude for the carrier frequency of 1000 Hz.

the testing have proved that the differences observed in Fig. 6 are not significant statistically.

The above results, obtained from the pilot psychoacoustic studies, illustrate how the developed method of generating of AM signals with random changes in amplitude can be applied.

It should be noticed that in some papers [8, 9] concerning the detection threshold of AM signals, to generate signals that parameters change randomly in time most often filtered narrow-band noise was used as a random modulation waveform. As a result, the amplitude and frequency of the signal changed in time simultaneously. In such a case it was not possible to see how the detection threshold is influenced when only the amplitude was subjected to changes and when both the amplitude and modulation frequency were changed randomly. At present such studies are possible by using the above method since it permits the generating of either only random amplitude changes or simultaneous random changes in amplitude and modulation frequency according to any distribution of temporal values. Simultaneous changes in amplitude and frequency may be fully correlated if only one realization of the random process is used in the modulation, or uncorrelated if two independent options of the random process are chosen. Such an alternative makes it possible to perform psychoacoustic studies for different detection or discrimination purposes.

6. Final remarks

On the basis of the obtained results it was possible to conclude that the detection thresholds of AM signal for sinusoidal (regular) and random (irregular) changes in amplitude are comparable within the limits of error for low modulation frequency.

This implies that the form of amplitude of the modulated signal (regular or random) as well as the probability distribution of temporal values of the modulation signal are not significant on the level of their threshold detection.

In conclusion, it is worthy of emphasizing the importance of the continuation of studies on both the detection and discrimination of AM random signals. It would be interesting not only to get more insight into the perception threshold of random amplitude changes, but also to determine the actual effect of random changes in modulation frequency — when they are combined with amplitude fluctuations since these changes determine the rate of amplitude changes. Taking into account the "phase locking" effect, it can be anticipated that the influence of random frequency changes can be measurable for carrier frequencies lower than 4 kHz.

Another interesting aspect of the studies related to random changes of the signal parameters is associated with some psychophysiological elements of the hearing organ. It would be interesting to find out how the neuron and auditory nerve responses are correlated with random changes in the stimulus parameters and how the mechanism of "phase locking" operates for these signals. Previous papers [7, 10, 14]

have mostly concerned sinusoidal (regular) amplitude changes. The results given in those papers have proved a specific sensitivity of the peripheral auditory neurons to stimuli subjected to amplitude modulation. This sensitivity may additionally affect the ability of the perception system to differentiate particular types of modulation. In this context it is justifiable to put the question whether the responses of the neurons of the auditory system on the level of threshold values are the same for sinusoidal and random changes in the stimulus amplitude. In detection thresholds for sinusoidal and random amplitude changes, the answer to that question seems to be positive. However, REES and PALMER found [14] that the addition of broadband noise to the sinusoidally modulated stimulus increased the neuron's temporal response to low modulation frequencies.

It would suggest that for these frequencies the detection thresholds for random amplitude changes should decrease in comparison with those for regular changes which, however, has not been reported in our study.

7. Acknowledgements

This research was supported by the State Committee for Scientific Research (KBN), grant No 2P302 07204.

The authors wish to thank Dr. R. EWERTOWSKI for preparing the computer program AM RNDA.

Appendix

Annex 1 ("Condition File")

content of the so called condition file constitutes a programmable script of the experiment.

```
COND: 1 5
; Change of the numerical content of position to "*" is
; irrelevant for the experiment
; PLOT: 1200
NUM_TRIALS: 40
INTER_INT_DELAY: 400.0
INTER_TRIAL_DELAY: 1.0
DEFAULT_GATE_TIME: 20.0
GEN_USING: 20.0
; The "track" function concernes the range of variability of modulation index
; 8% 1% 15% (Am/an*100)
TRACK: 1 -20.0 -34.0 -16.0
BIG_STEP: 2.0
SMALL_STEP:1.0
```

```
ENDTRACK
; Signal definition ch.A
SIGNAL: 1 1000.0 −40.00.0
;tone      *c_lev* *c_frq* c_phase rnd_lvr rnd_fqr
TONE: −20.0      1000.0     0.0        0.0        0.0
ENDSIGNAL
SIGNAL: 3  1000.0  −30.0  0.0
;tone  *m_lev* *mod_frq* *m_phase* *rnd_lvr* rnd_fqr*
TONE: TRACK1  4.0     0.0     0.0     0.0
ENDSIGNAL
; Signal definitino ch.B
SIGNAL: 4  1000.0  −40.0  0.0
;tone   *c_lev* *c_frq* c_phase rnd_lvr rnd_fqr
TONE: −20.0     1000.0     0.0        0.0        0.0
ENDSIGNAL
SIGNAL:  6  1000.0  −30.0  0.0
;tone  *m_lev* *mod_frq* *m_phase* *rnd_lvr* *rnd_fqr*
TONE: −6.0          4.0          0.0          0.0          0.0
ENDSIGNAL
; Standard definition ch.A
SIGNAL:  7  1000.0  −40.0  0.0
;tone  *c_lev* *c_frq* c_phase rnd_lvr rnd_fqr
TONE: −20.0  1000.0     0.0        0.0        0.0
ENDSIGNAL
SIGNAL: 9  1000.0  −30.0  0.0
;tone  *m_lev* *mod_frq* *m_phase* *rnd_lvr* *rnd_fqr*
TONE: −6.0        256.0          0.0          0.0          0.0
ENDSIGNAL
; Standard definition ch.B
SIGNAL: 10  1000.0  −40.0  0.0
;tone  *c_lev* *c_frq* c_phase rnd_lvr rnd_fqr
TONE: −20.0  1000.0     0.0        0.0        0.0
ENDSIGNAL
SIGNAL: 12  1000.0  −30.0  0.0
;tone  *m_lev* *mod_frq* *m_phase* *rnd_lvr* *rnd_fqr*
TONE: −6.0       256.0          0.0          0.0          0.0
ENDSIGNAL
; Calibration TONE for Channel-A
SIGNAL: 15  1000.0  −40.0  0.0
TONE: 0.0  1000.0  0.0  0.0  0.0
CALIBRATE_LEVEL: 124.0
ENDSIGNAL
ENDCOND
```

Annex 2

Annex 2 shows an exemplarily final file of the listener's responses:
Experimenter Condition File: CONDHAND.RNA. Cond.001
Run : 001 Thursday, 3/8/1995 start: 13:04:44
stop: 13:07:51

AM_RND : DIF — Values of Parameters (except Track Mag.) used by Subject: MK

SIGNAL	STANDARD
Carrier Frequency ch.A = 4000.0 Hz	Carrier Frequency ch.A = 4000.0 Hz
Carrier Frequency ch.B = 4000.0 Hz	Carrier Frequency ch.B = 4000.0 Hz
Modulation Frequency ch.A = 0.0 Hz	Modulation Frequency ch.A = 256.0 Hz
Modulation Frequency ch.B = 0.0 Hz	Modulation Frequency ch.B = 0.0 Hz
SPL ch.A = 70.0 dB	SPL ch.A = 0.0 dB
SPL ch.B = 70.0 dB	SPL ch.B = 0.0 dB
Modulation depth ch.A = 0.0%	Modulation depth ch.A = 0.0% T
Modulation depth ch.B = 0.0%	Modulation depth ch.B = 0.0% T
Phase of Modulation ch.A = 0.0 deg	Phase of Modulation ch.A = 0.0 deg
Phase of Modulation ch.B = 0.0 deg	Phase of Modulation ch.B = 0.0 deg

Track Number:	(1)dph%
Average:	5.765
Standard Deviation:	0.78111
Final Value:	6.310

Try	SI	RI	AN	AT	Track1 values	sigA dph[%]	sigB dph [%]	stdA dph [%]	stdB dph [%]
1	1	1	T	1	−24.000	6.31	0.00	0.00	0.00
2	1	1	T	1	−24.000	6.31	0.00	0.00	0.00
3	2	1	F	1	−26.000	5.01	0.00	0.00	0.00
4	1	2	F	1	−24.000	6.31	0.00	0.00	0.00
5	1	1	T	1	−22.000	7.94	0.00	0.00	0.00
6	1	1	T	1	−22.000	7.94	0.00	0.00	0.00
7	2	2	T	1	−24.000	6.31	0.00	0.00	0.00
8	2	2	T	1	−24.000	6.31	0.00	0.00	0.00
9	2	2	T	1	−26.000	5.01	0.00	0.00	0.00
10	2	2	T	1	−26.000	5.01	0.00	0.00	0.00
11*	2	1	F	1	−28.000	3.98	0.00	0.00	0.00
12	2	2	T	1	−26.000	5.01	0.00	0.00	0.00
13	1	2	F	1	−26.000	5.01	0.00	0.00	0.00
14	1	2	F	1	−25.000	5.62	0.00	0.00	0.00
15	2	2	T	1	−24.000	6.31	0.00	0.00	0.00
16	2	2	T	1	−24.000	6.31	0.00	0.00	0.00
17	1	1	T	1	−25.000	5.62	0.00	0.00	0.00

18	1	1	T	1	−25.000	5.62	0.00	0.00	0.00
19	1	1	T	1	−26.000	5.01	0.00	0.00	0.00
20	1	1	T	1	−26.000	5.01	0.00	0.00	0.00
21	1	2	F	1	−27.000	4.47	0.00	0.00	0.00
22	1	1	T	1	−26.000	5.01	0.00	0.00	0.00
23	1	2	F	1	−26.000	5.01	0.00	0.00	0.00
24	1	1	T	1	−25.000	5.62	0.00	0.00	0.00
25	1	2	F	1	−25.000	5.62	0.00	0.00	0.00
26	2	1	F	1	−24.000	6.31	0.00	0.00	0.00
27	2	2	T	1	−23.000	7.08	0.00	0.00	0.00
28	2	2	T	1	−23.000	7.08	0.00	0.00	0.00
29	1	2	F	1	−24.000	6.31	0.00	0.00	0.00
30	1	1	T	1	−23.000	7.08	0.00	0.00	0.00
31	2	2	T	1	−23.000	7.08	0.00	0.00	0.00
32	1	1	T	1	−24.000	6.31	0.00	0.00	0.00
33	1	1	T	1	−24.000	6.31	0.00	0.00	0.00
34	2	2	T	1	−25.000	5.62	0.00	0.00	0.00
35	1	1	T	1	−25.000	5.62	0.00	0.00	0.00
36	1	2	F	1	−26.000	5.01	0.00	0.00	0.00
37	2	2	T	1	−25.000	5.62	0.00	0.00	0.00
38	1	2	F	1	−25.000	5.62	0.00	0.00	0.00
39	2	2	T	1	−24.000	6.31	0.00	0.00	0.00
40	2	2	T	1	−24.000	6.31	0.00	0.00	0.00

Annex 3

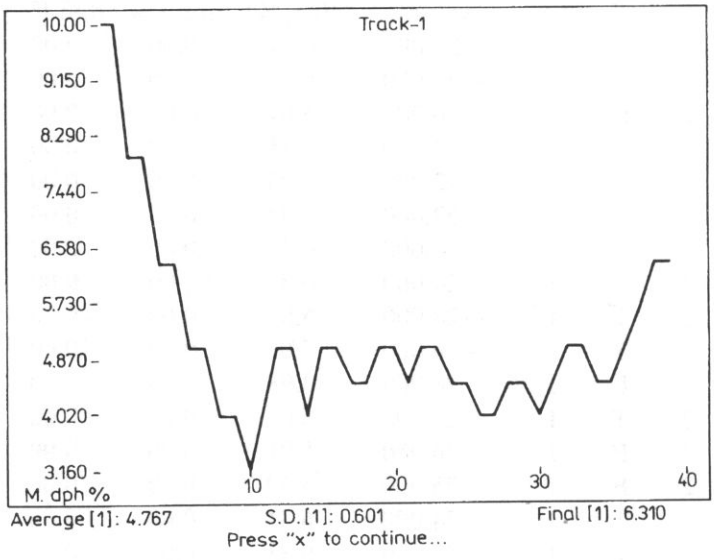

Fig. A. The example of the response curve of a subject.

References

[1] B.W. EDWARDS, N.F. VIEMEISTER, *Frequency modulation versus amplitude modulation discrimination: Evidence for a second frequency modulation encoding mechanism*, J. Acoust. Soc. Am., **96**, 2, 733–730 (1994).

[2] D.D. GREENWOOD, *What is "Synchrony suppression"?*, J. Acoust. Soc. Am., **79**, 6, 1857–1871 (1986).

[3] J.L. GOLDSTEIN, *Auditory spectral filtering and monaural phase persepction*, J. Acoust. Soc. Am., **41**, 2, 458–479 (1967).

[4] W.M. HARTMANN, *Detection of amplitude modulation*, J. Acoust. Soc. Am., Suppl., **65**, 59 (1978).

[5] W.M. HARTMANN and J. PUMPLIN, *Noise power fluctuations and the masking of sine signals*, J. Acoust. Soc. Am., **83**, 6, 2277–2289 (1988).

[6] E. JAVEL, *Coding of AM tones in the chinchilla auditory nerve: implications for the pitch of complex tones*, J. Acoust. Soc. Am., **68**, 1, 133–145 (1980).

[7] P.X. JORIS, T.C.T. YIN, *Responses to amplitude-modulated tones in the auditory nerve of the cat*, J. Acoust. Soc. Am., **91**, 1, 215–231 (1992).

[8] L. MENDOZA, J.W. HALL,, J.H. GROSE, *Modulation detection interference using random and sinusoidal amplitude modulation*, J. Acoust. Soc. Am., **97**, 4, 2487–2491 (1995).

[9] B.C.J. MOORE, A. S-k, M.J. SHAILER, *Modulation discrimination interference for narrow-band noise modulators*, J. Acoust. Soc. Am., **97**, 4, 2493–2497 (1995).

[10] G. LANGNER, *Periodicity coding in the auditory system*, Hear. Res., **60**, 115–142 (1992).

[11] H. LEVITT, *Transformed up-down methods in psychoacoustic*, J. Acoust. Soc. Am., **49**, 2, 467–477 (1971).

[12] E. OZIMEK, A. SĘK, *Perception of irregular frequency changes in sinusoidal signal*, Acustica, **66**, 3, 146–152 (1988).

[13] J. PUMPLIN, *Low-noise noise*, J. Acoust. Soc. Am., **78**, 1, 100–104 (1985).

[14] A. REES, A.R. PALMER, *Neuronal responses to amplitude-modulated and pure-tone stimuli in the guinea pig inferior colliculus, and their modification by broadband noise*, J. Acoust. Soc. Am., **85**, 5, 1978–1993 (1989).

[15] A. SĘK, *Perception of irregular amplitude changes of sinusoidal signals*, Acustica, **77**, 6, 262–269 (1993).

[16] N.F. VIEMEISTER, *Temporal modulation transfer function based upon modulation thresholds*, J. Acoust. Soc. Am., **65**, 1364–1380 (1979).

[17] E. ZWICKER, *Die Grenzen der Hörbarkeit der Amplitudenmodulation und der Frequenzmodulation eines Tones*, Acustica, **1**, 2, AB125–AB133 (1952).

ARCHIVES OF ACOUSTICS
21, 2, 179–194 (1996)

ACOUSTIC WAVE SENSORS

R.M. LEC

Department of Electrical and Computer Engineering
University of Maine,
(Orono, ME04469, USA)

Acoustic waves excited in a piezoelectric medium provide an attractive technology for realizing a variety of sensor that exhibit high sensitivity, small size and portability, fast responses, ruggedness and robustness, high accuracy, compatibility with integrated circuit (IC) technology, excellent aging characteristics and the capability to measure multiple quantities in one sensor package. Sensors based on this technology can be produced using standard photolithography and hence are inexpensive. In this paper acoustic sensing mechanisms and a wide range of bulk and surface acoustic waves used in the sensor development are described. Applications of acoustic sensors in the chemical, environmental, medical, automotive and aeronautic industries are also given.

1. Introduction

There is a need for small, reliable, and inexpensive sensors in a variety of industrial and consumer applications. In the last decade the world sensor market has been growing very fast at an annual rate of about 10%. In 1994 alone sensor sales totaled about 10.5 billion dollars worldwide. The demand for sensor will continue in the foreseeable future due to the fact that further progress in automation and computerization of industrial and consumer products will depend strongly on sensors. As an example one may consider an automobile in which the use of sensor has grown from a few sensors in the twenties to more than 20 in the seventies, and to more than 100 in the nineties. Today's automobile sensor perform such tasks as monitoring engine performance, fuel efficiency, powertrain systems and road conditions which result in improved car performance; driving safety and comfort. Currently, sensor technologies such as silicon, fiber optic, thin and thick film and acoustic are competing for the global sensor market. Acoustic wave technology is emerging as one of the most promising sensor technologies offering several advantages over their competitros.

In the last several years acoustic wave technology has been explored extensively for the development of sensors. Many novel acoustic sensors have been proposed, and extensive research efforts, both theoretical and experimental, have been undertaken

in many academic, government and industrial research centers. As a result, critical fundamental knowledge on acoustic sensors has been accumulated and the market opportunities for acoustics sensors are being explored. In this paper acoustics sensing mechanisms and a wide range of bulk and surface acoustic waves used in the sensor development are described. Applications of acoustic sensors in the chemical, environmental, medical, automotive and aeronautic industries are also given.

2. General features of acoustic sensors

In general, acoustic sensors utilize different types of acoustic waves to obtain information about the entity being measured or what is commonly called a measurand. The range of measurands is wide and include a spectrum of chemical, physical and biochemical phenomena. The acoustic waves can be generated and received by a variety of means including piezoelectric, magnetostrictive, electrostatic, electromagnetic, optical, thermal and other [1, 2]. In this paper a class of acoustic sensors which utilize the piezoelectric effect to generate and receive acoustic waves is discussed.

Acoustic sensors are fabricated with piezoelectric materials in which the electro-mechanical transduction takes place within the material. Therefore, piezoelectric materials are often called smart materials due to the internal material transduction process. This material based transduction process does influence very positively the performance of acoustic sensors in terms of their reliability, size and cost. The piezoelectric materials are also very durable, chemically inert and have excellent mechanical properties and very good aging characteristics. Acoustic sensors made with piezoelectric materials such as quartz or lithium niobiate are robust, and environmentally stable.

Acoustic sensors are versatile and can measure, in principle, any type of measurand. Usually, the sensing acoustic wave is accompanying by both mechanical displacements and electric fields. Thus, both the electrical and mechanical properties of the environment can be sensed directly by piezoelectric sensors. One may increase the number of measurands detected by the acoustic sensor by attaching or connecting a specific sensing element to a piezoelectric transducer/substrate. The measurand causes electrical and mechanial changes in a sensing film. Using such a hybrid configuration, theoretically any measurand can be measured by the acoustic sensors. For example, a thin biofilm placed over a bulk resonator can be used to measure the presence of biospecies, or a magnetic field sensitive nickel film placed over the SAW device can be used for sensing magnetic fields.

Usually, acoustic sensors are designed to operate in resonant type sensors configuration as an oscillator. The output sensor signal is a frequency which is a function of the magnitude of the meaurand. This is important feature, since one can measure frequency easily, and the frequency is quasi-digital signal, which makes simple signal processing operations in acoustic sensors. Therefore, acoustic sensors are relatively sensitive, with good resolution and excellent signal-to-noise ratio.

Acoustic sensors configured in an oscillator configuration can be equipped in an antenna and both remote sensing and control can be achieved.

Finally, another important feature of piezoelectric sensor materials is that the same electro-mechanical transduction mechanism can be used not only for a sensing but also for an actuation as well. Since the ultimate purpose of sensing is to supply an information to an observer or a system in order to perform an action, the same piezoelectric technology platform can perform both the sensing and actuating operations. In the recent years several smart structures using piezoelectric elements for both sensing and actuating have been developed. In summary, the piezoelectric sensing platform offers a very versatile technology base for the development of sensors, actuators and smart structures.

3. Acoustic waves, piezoelectric transducers and sensing mechanisms

There are numerous types of acoustic waves which can be used for sensing. The knowledge of their properties is important for the selection of the optimal acoustic wave for a given measurand. The acoustic waves can be classified in a variety of ways. One way to classify the acoustic waves is by mean of their generation, i.e. into the bulk and surface generated acoustic waves. The bulk generated acoustic waves are usually excited by metalized bulk piezoelectric elements such as plates or rods, whereas the surface generated acoustic waves are excited by the interdigital system of metallic electrodes (IDT) placed on the surface of piezoelectric materials. The electrodes are used to connect the transducer with electronic circuitry for the excitation or reception of acoustic waves. Examples of the two most common configurations of piezoelectric transducers, namely a thin metalized disk used for the excitation of bulk waves, and an interdigital transducer (IDT) for the excitation of surface acoustic waves (SAW) are shown in Figure 1.

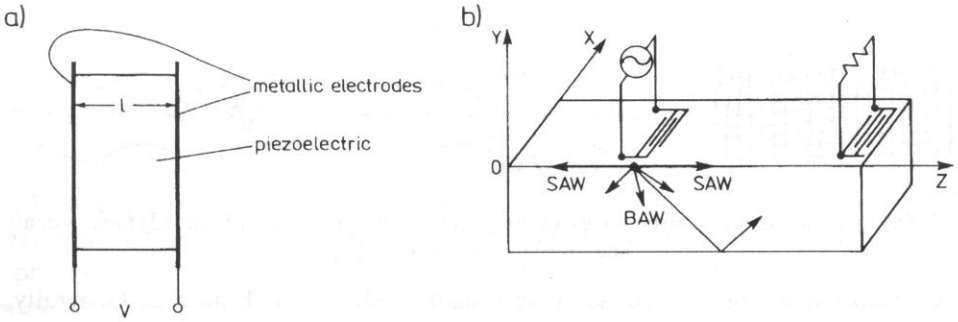

Fig. 1. Typical geometry of piezoelectric transducers used for excitation of the bulk and surface generated acoustic waves.

The different types of acoustic waves which can be excited by a transducer are shown in Figure 2. Some of these waves are schematically illustrated in Figure 3. The acoustic wavs in piezoelectric materials have both the mechanical displacements and

electric fields. These electroacoustic field quantities perform the actual "sensing" in acoustic sensors. Acoustic sensors probe the environment with both displacements and electric fields, hence can detect a wider range of measurands than other sensor technologies.

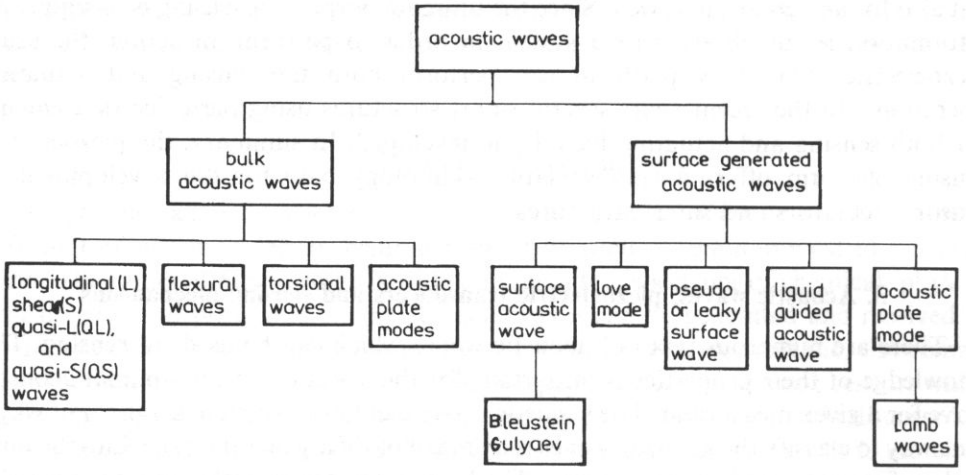

Fig. 2. Classification of acoustic waves

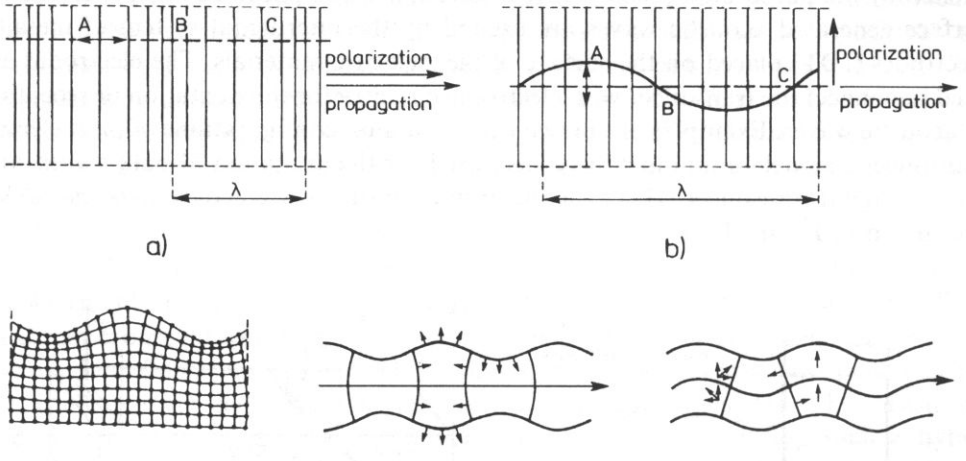

Fig. 3. Examples of various acoustic waves, (a) longitudinal, (b) shear, (c) SAW and (d) Lamb symmetric and antisymmetric mode [1, 2].

Conceptual model for an acoustic sensor is shown in Figure 3. Generally, it consists of a sensing element and an acoustic wave transducer, but also, in some cases, it may consist only of an acoustic wave transducer itself. The **sensing element** is an active substance (for example, a thin biofilm used in an acoustic biosensor) which is selective to the measurand of interest. The **acoustic wave transducers**, which consists of a piezoelectric element with an array of metal electrodes supplies a mean for conversion of usually non-electrical measurands into an output electrical signal.

When a measurand interacts with the sensing element a microscopic physical, chemical and/or biochemical changes are produced. Next, these microscopic changes cause the macroscopic acoustical/mechanical or electrical changes in the sensing element, which in turn modify the acoustic field quantities of the acoustic wave transducer. Subsequently, these acoustic changes are converted/transducted into an output sensor electrical signal by the acoustic wave transducer. For example, in the acoustic immunosensors the antibodies are immobilized in the form of a thin film at the surface of the acoustic wave transducer. When the target antigen is introduced into the sensor environment, the elasticity, density and the viscosity of the film undergoes changes, and these changes modify the acoustic field quantities of the acoustic wave sensor which result in the changes of the output sensor signal. From a sensing point of view, the environment loads the surface, and the surface views the environment as an impedance, either mechanical and electrical, or the both. For most applications, these types of acoustic sensors can be modeled as miniature solid state AC electrical and mechanical impedance meters.

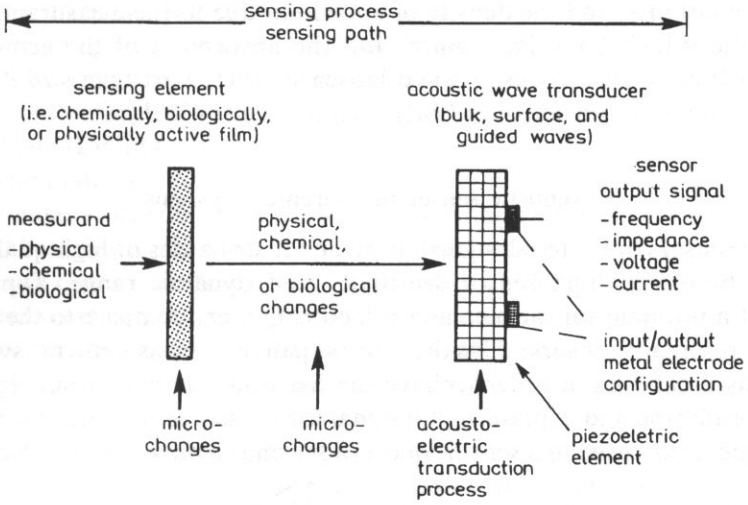

Fig. 4. A conceptual model for an acoustic sensor.

Generally, acoustic sensors can be divided into three groups:

(i) **Homogeneous Acoustic Sensor:** In this case an acoustic sensor consists of the piezoelectric element itself. The measurand does influence directly the electroacoustic properties of the piezoelectric element. The examples are piezoelectric temperature, electric field or viscosity sensors. In principle, any type of a bulk, surface or guided wave acoustic device can be used for this type of sensing. For example, an LST cut quartz bulk resonator has been used as a very sensitive and accurate temperature sensor [3], an ST SAW quart for the determination of acceleration and pressure [4], and a YZ SAW $LiNbO_3$ for the measurement of an electric field [5]. The AT cut quartz is used widely for the measurement of mechanical and electrical properties in liquids [6] and also as a thickness film monitor [7].

(ii) **Hybrid Acoustic Sensor**: In this case a sensor consists of the piezoelectric transducer and a sensing element selective to the measured of interest. The use of sensing element which is usually in form of a thin film allows, in principle, one to detect a wide variety of measurands. The measurand causes changes in the film, which in turn are detected by piezoelectric transducer. The film can be biological, metal, metal oxide and polymer and can be used to probe both gaseous and/or liquid media. For example, a thin tungsten trioxide film is used to detect hydrogen sulfide gas [8], a gold film to detect mercury in water or a polyimide film can detect water vapor [9]. In some application the sensing element could have other form such as a heater structure for flow detection [10]. The probing acoustic wave can be either a bulk wave (S, L, QL, QS), a surface acoustic wave (SAW) or guided bulk acoustic waves (APM, waves on cylinders, rods, etc.).

(iii) **Passive Acoustic Sensor**: The piezoelectric element is not involved in sensing, and is used for transmission and/or reception of acoustic waves into/from the environment. Generally, an acoustic wave is transmitted into a gaseous, liquid or solid medium which undergoes changes due to measurands. The changes in the elastic and viscous constants, and the density of a medium due to the measurand cause the changes in the velocity, the impedance, and the absorption of the acoustic wave. Examples include a bulk acoustic wave biosensor [11], a particle size distribution sensor [12] or an acoustic emission (AE) chemical sensor [13].

5. Acoustic sensor measurement systems

Acoustic sensors are often designed as resonant structures of high quality factor, Q in order to obtain high sensor sensitivity and dynamic range. Typically, the sensitivity of a resonant sensor increases a factor, Q-times compare to the sensitivity of the non-resonant sensors. Usually, accompanying measurement systems are configured as oscillators in order to have the frequency as the output signal which offers high resolution and a quasi-digital signal for further processing. Normally, two acoustic elements are used in a sensor, one as a sensing element, and the second as the

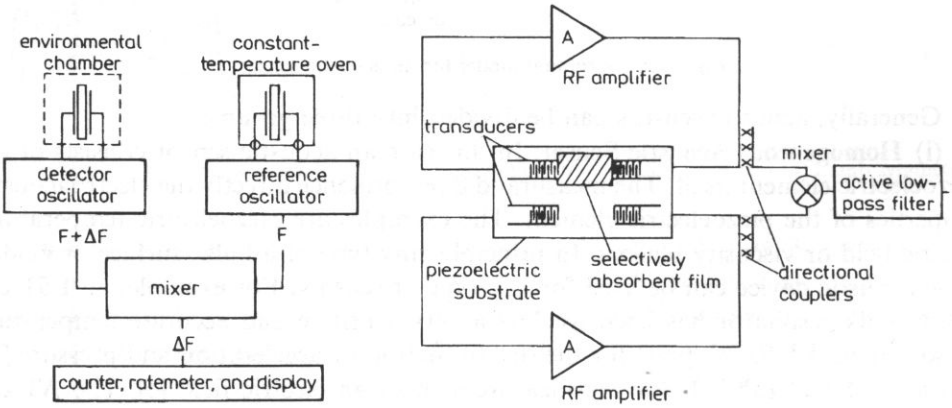

Fig. 5. A typical acoustic dual line measurement system for bulk, (a), [21] and surface waves, (b).

reference in order to eliminate environmental factors such as temperature, mechanical stress or other factors. A typical acoustic measurement system shown is given in Figure 5. The theoretical sensitivity of acoustic sensors can be very high, however, the practical one is much lower due to the loading effect of the measurand causing decrease in the quality factor, Q.

6. Materials and technology

An ideal material for an acoustic sensor is a strong piezoelectric material with good semiconducting, mechanical and temperature properties. Strong piezoelectric properties, good mechanical and thermal properties are necessary for designing wide band, low loss and temperature stable acoustic devices. Such a material will allow the combination of piezoelectric technology with well developed integrated circuit (IC) technology which would result in mass production of inexpensive intelligent acoustic sensors with the signal processing capabilities on a chip. Unfortunately, such a material does not exist at this moment. Currently, some of these desired features are achieved using the hybrid type approach combining zinc oxide (ZnO) and silicon technologies [14, 15]. Gallium arsenide offers a possible single material alternative, however it has a very weak piezoelectric properties [16]. So far, the well known piezoelectric materials such as quartz (SiO_2), lithium niobiate ($LiNbO_3$), and lithium tantalate ($LiTaO_3$) are used to make acoustic sensors. These materials show quite large spectrum of the electro-acoustic properties from being temperature compensated (SiO_2) to haviong a strong piezoelectric properties ($LiNbO_3$). These materials have outstanding mechanical properties, are chemically stable, and can operate at the elevated temperatures . There is a lot research activity towards identifying new cut being temperature or stress compensated cuts in order to have sensors environmentally stable, or just having high value of the temperature or stress coefficients for thermal or mechanical sensors. Recently, the 27°Y-rotated SiO_2 cut was found to be temperature compensated at elevated temperature 200°C which is important in SAW gas sensors applications [17]. Also polymer piezoelectrics are being extensively used for some sensor applications, mostly in the medical area.

Typical acoustic sensors are fabricated with standard photolithography. This technology allows one to fabricate complex sensor electrode patterns and to produce multiple sensor from a single substrate. Recently, micromachining technology has been very popular for the manufacturing of piezoelectric sensors. Micromachining technology, which combines the photolitographic process and either plasma or chemical etching techniques, allows one to create complicated mechanical and electrical sensor structures from a single substrate. An example includes the AT fork resonator technology for watch applications [19] or acoustic force sensor [20].

7. Examples of acoustic sensors

Some recent examples of new acoustic sensor, new sensing mechanisms, new trends in acoustic sensor technology and novel applications are presented below.

A. Acoustic Emission Chemical (AEC) Sensors — a new sensing mechanism

A high frequency piezoelectric microphone can "listen" to the chemical reactions, and identify these reactions. Recently, it was found that many chemical dynamic

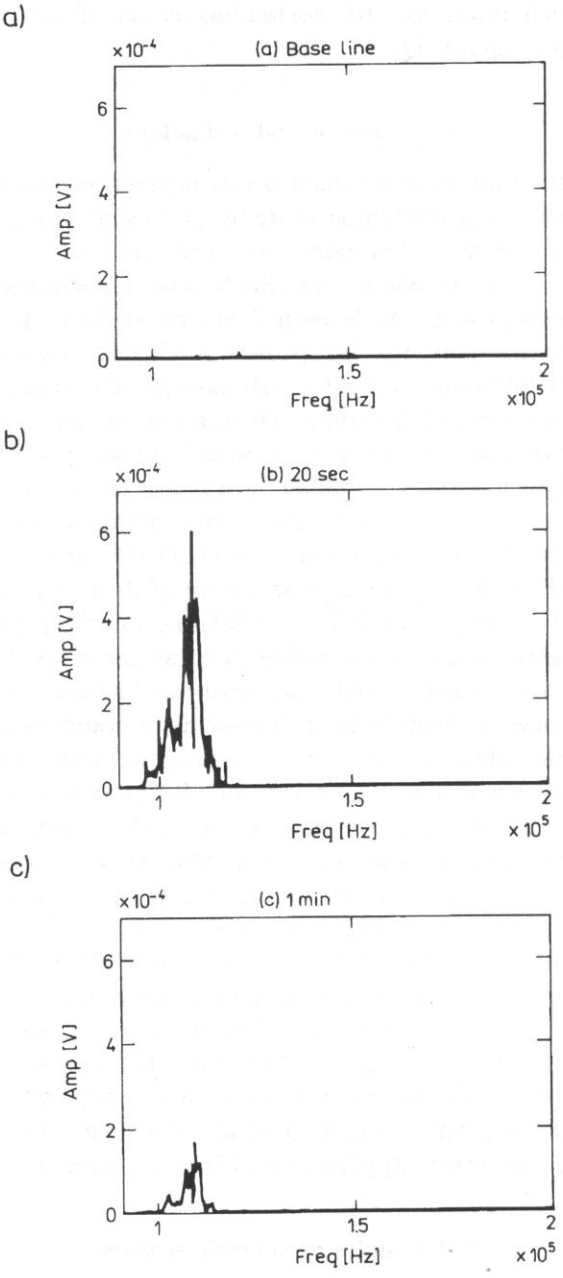

Fig. 6. The AE spectra of dissolution of sodium carbonate taken at different time intervals t = 0, 20 second, 2 and 10 minutes [13].

systems are acoustically active, and during the chemical processes acoustic emission (AE) signals are generated. Based on this phenomena, an AEC sensor was proposed to monitor the caustization process, an important process in paper manufacturing [13]. The caustization process consists of three different reactions. Interestingly, the AE frequency spectra and their time evolution were distinct for these three different reactions. These features of the AE spectra are being used for the identification of chemical reactions and monitoring their kinetics. An example of the time evolution of the AE spectra in the case of the reaction between calcium oxide and sodium carbonate is shown in Figure 6. Potential application of the AEC sensor include process control in the chemical, food and pharmaceutical industries.

B. SAW Gas Sensors — electric impedance change as a sensing mechanism

A change in the electric impedance of thin film due to absorption of hydrogen sulfide (H_2S) gas has been used for the development of a highly sensitive SAW gas sensors. A typical dual oscillator sensor configuration shown in Figure 5 is used. The response to H_2S gas is shown in Figure 7. Here, the changes in the electric conductivity of the thin WO_3 film cause changes in the frequency and the attenuation of the SAW oscillator. Sensitivities of the order parts per billion have been reported

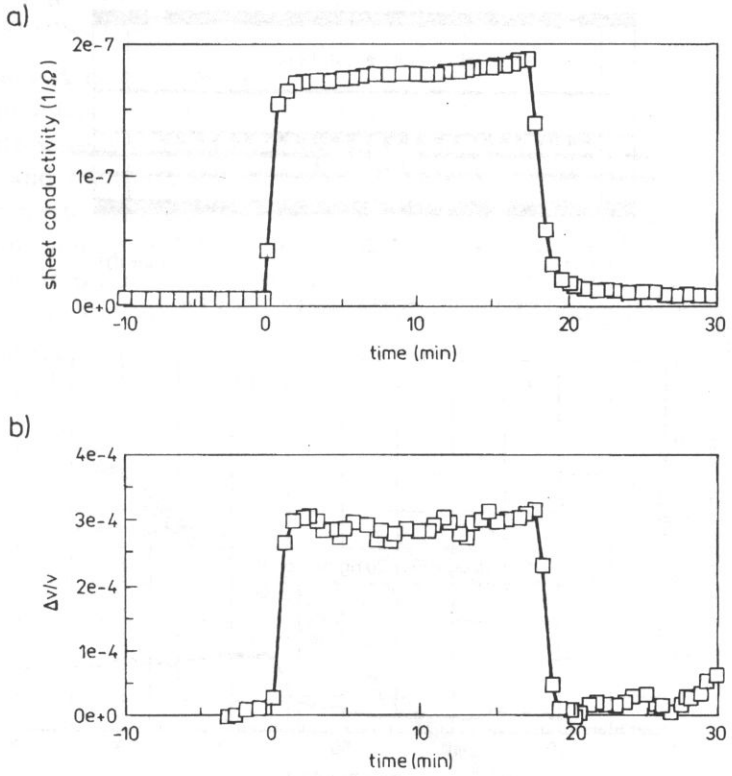

Fig. 7. A typical response of the SAW gas sensor exposed to 20 ppm of H_2S: (a) sheet conductivity of a WO_3 thin film and (b) the fractional SAW velocity change.

for H_2S gas on ST-quartz substrate with 400 A thick WO_3 film [8]. SAW sensors with other metal, metal oxide, polymer and organic films for detection of a variety of gases such as H_2, NO_x, CO have also been reported [21]. In films which do not change their electrical properties when interacting with the measurand, the mechanical impedance of thin film can change. In particular, the changes in the film density (so called mass loading effect) or in the elasticity of the film are responsible for the sensor response. However, the SAW sensor with metal oxide films have shown much better performances in terms of sensitivity, durability, aging and reproducibility.

C. Acoustic Plate Mode (APM) Immunosensor — mechanical impedance as a sensing mechanism

A change in the mass loading and the effective elasticity in the thin immobilized antibody film on a YZ $LiNbO_3$ APM device due to the presence on an antigen has been used for the development of highly sensitive acoustic immunosensors. Here, the transverse guided acoustic wave is utilized for sensing. This wave only penetrates a liquid medium to the depth of an acoustic wavelength which is about a few tens of

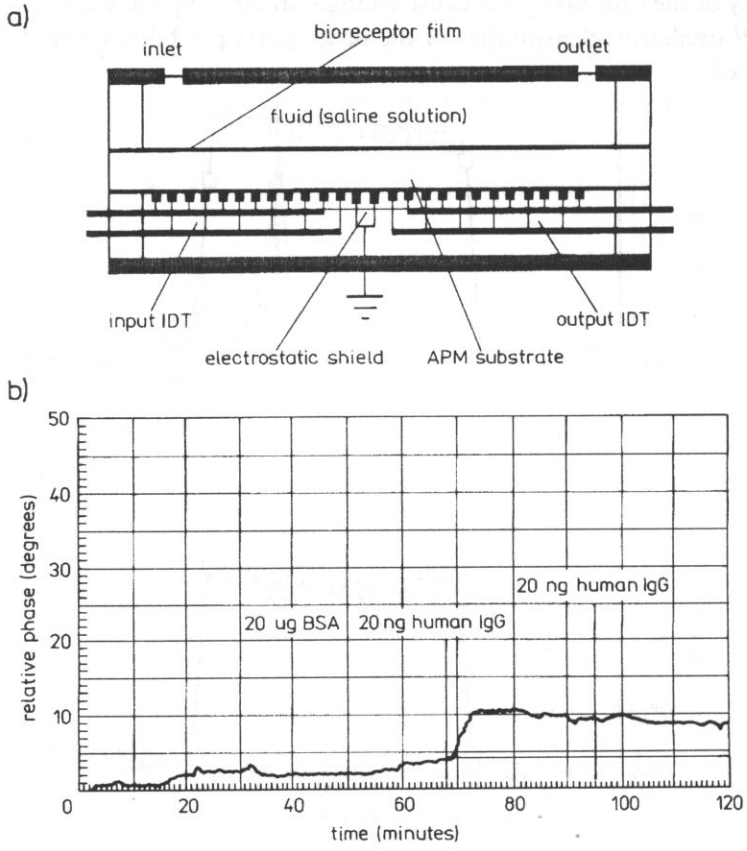

Fig. 8. The APM immunosensor (a) and its response to 20 nanograms of the antigen (b) [23].

microns at the frequency 50 Mhz. Antigen concentrations of the order of nanograms per millimeter were detected [22]. The APM configuration shown in Figure 10 offers a very convenient way to separate the electronics and the biochemical liquid medium. Recently, this configuration has been used to detect the DNA hybridization and to monitor mercury in water with a gold thin film as a sensing medium [23]. Another sensor configuration which is extensively used for monitoring the properties of liquid media a bulk AT cut quartz resonator [6, 18].

D. SAW Adhesion Sensor — monitoring interfacial phenomena

Adhesion strength can be monitored nondestructively with the SAW. In particular, the adhesion of thin polyimide films on ST-cut SAW substrates has been measured. The SAW technique was able to identify the adhesion strength with different adhesion promoters. It can also measure the influence of different environmental conditions such as the level of humidity of the adhesion strength [9].

E. Acoustic Sensors for Other Measurands

Many other chemical, physical and biological quantities or phenomena can be detected with acoustic sensors. Examples include electric and magnetic fields, temperature, gas flow, mechanical quantities as strain, stress and acceleration, viscosity, corrosion etc.

F. Remote Acoustic Sensing

Once an antenna is connected into either a bulk or SAW device it forms a sensor with remote sensing/control capabilities. An antenna supplies a means for remote excitation and reception of the signal from a sensor. Several configurations are possible to create a transmitting and/or receiving antenna. In Figure 9 an example of an configuration is a SAW device with an antenna and a single wide-band input/output transducer with several reflective structures placed on the SAW path is shown. In this case, the SAW is excited by an interrogating RF pulse, and travels along the surface until is reflected from the sequence of reflective structures. Next, the reflected signal is received by the same transducer, and retransmitted as an RF pulse

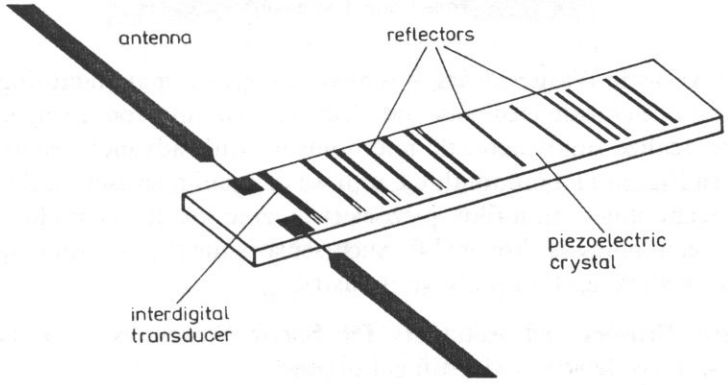

Fig. 9. A SAW remote sensor configuration [28].

into the sender of the interrogating signal. If the measurand is present, than it will change the parameters of the received acoustic wave in the time and frequency domains, and hence the RF pulse parameters. Generally, this type of configurations can be used for the development of remote sensors for a variety of measurands. Recently, this configuration was proposed for the development of a mechanical sensor for the detection of the deformation and stress [24] and a temperature sensor [28].

G. Micromachined Acoustic Sensors — a new manufacturing technology

Inexpensive and high performance acoustic sensors can be manufactured with micromachining technology. This technology uses photolitographic and wet and plasma etching techniques to produce multiple acoustic sensing elements from a single substrate. Examples inlcude a tuning fork quartz resonator used for watch application [19] or a double-ended flexural mode 'string-tension' type resonator force sensor shown in Figure 10 [20].

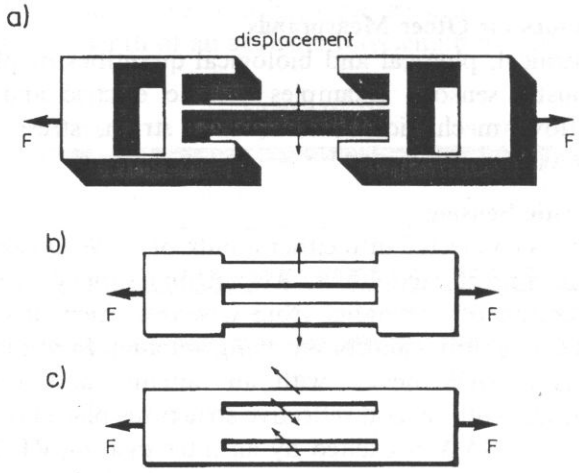

Fig. 10. Micromachined acoustic force sensor: (a) single-beam device, (b) double beam-beam device and (c) triple beam device [20].

H. Smart Acoustic Wave Sensors — a novel integrated manufacturing technology

Integration of acoustic elements and electronic circuitry on a single silicon chip allows one to realize smart acoustic microsensors with advanced signal processing capabilities. In Figure 11 a monolithic Lamb wave liquid microsensor developed with bipolar IC technology, thin-film piezoelectric zinc oxide technology, and micromachining technology is shown [14]. Such sensors may find a wide application in the chemical, medical and automotive industry.

I. Acoustic Sensors and Actuators for Smart Structures — a new class of microsystems, microdevices and artificial organs

Acoustis wave technology is being utilized for the development of smart structures in which the combination of the acoustic actuators and acoustic sensors allows one to

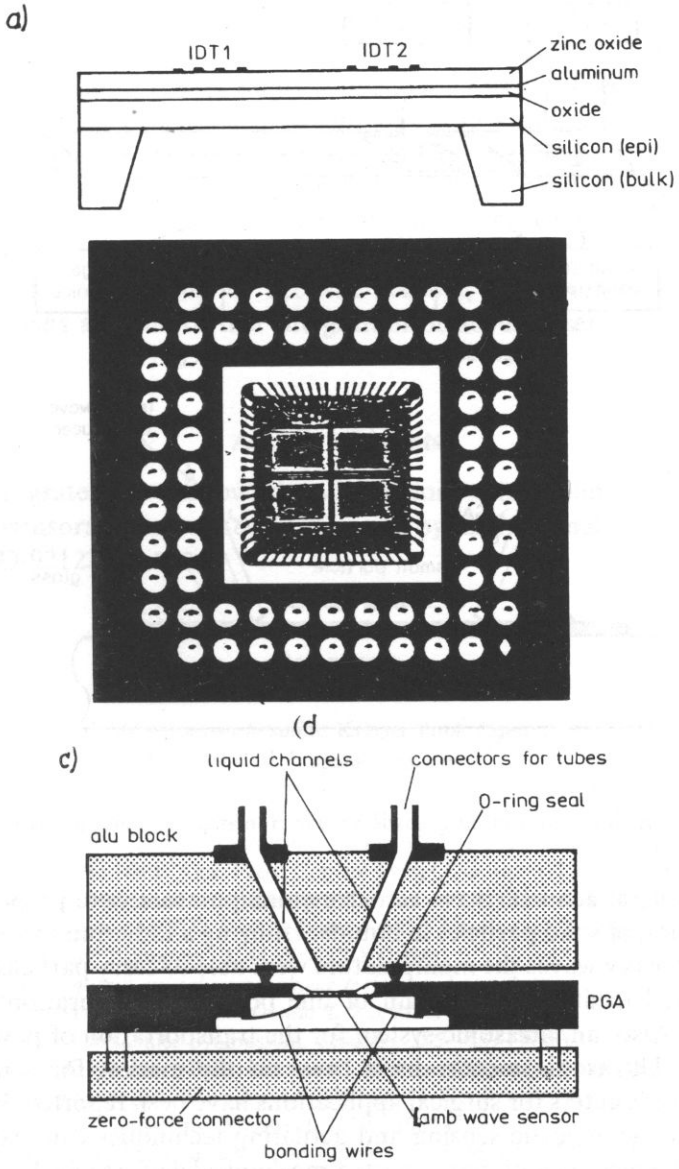

Fig. 11. The monolithic Lamb wave liquid sensor: (a) cross section of a Lamb device, (b) a photograph of a Lamb sensor in a ceramic grid array (PGA) package, chip dimension 10 mm × 10 mm, and (c) PGA-packaged sensor the flow cell [14].

achieve very unique self-control and/or self-adaptive features. An example shown in Figure 12 depicts an active damping system used in the aeronautic industry for controlling the vibration in space vehicles [25]. Here, the piezoelectric element senses the vibrations, and the other generates the out of the phase acoustic vibrations to cancel the initials vibrations.

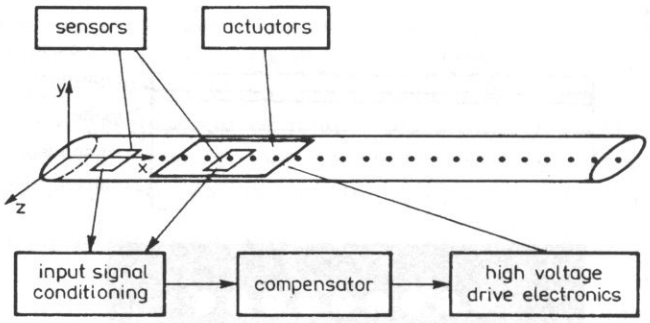

Fig. 12. An active damping system [25]

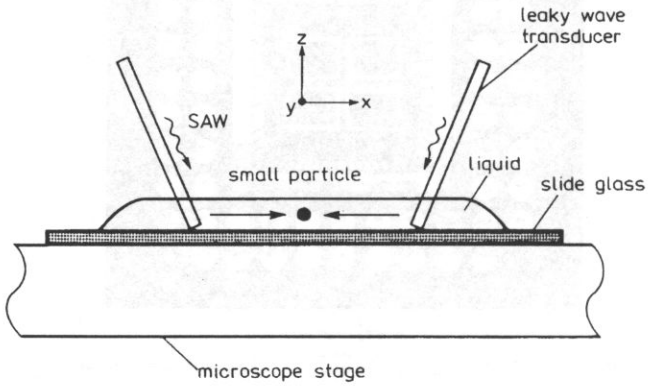

Fig. 13. A schematic representation of the acoustic wave micromanipulator of small particles in liquid [26].

Recently, several acoustic wave actuators/manipulators were proposed for controlling the motion of solid particles in liquids. Utilizing a radiation force generated by either Lamb or leaky waves the manipulators were able to carry particles in the liquid into the required location. A diagram of one possible configurations is shown in Figure 13 [26]. Also, an ultrasonic system for the transportation of powder has been proposed [27]. Ultrasonic motors have been on the market for some time, and recently, ultrasonic cuters for surgical applications have been reported. In general, the combination of the acoustic sensing and actuating techniques can lead toward the development of a new class of micro-electro-mechanical devices which can be used for the development of artificial organs, remote surgery or microrobots.

8. Conclusions

Acoustic waves excited in a piezoelectric medium provide an attractive technology for realizing a variety of sensors that exhibit high sensitivity, small size and portability, fast responses, ruggedness and robustness, high accuracy, compatibility with integrated circuit (IC) technology, and excellent aging characteristics. Sensors

bassed on this technology can be produced using standard photolitography and hence are inexpensive. Integration of acoustic elements and electronic circuitry on a single silicon chip allows one to realize smart acoustic microsensors with advanced signal processing capabilities. Acoustic wave technology is also utilized for the development of smart structures in which the combination of the acoustic actuators and acoustic sensors allows one to achieve very unique self-control and/or self-adaptive features. Acoustic sensors have found wide applications in the chemical, environmental, medical, automotive and aeronautic industries. Future work should focus on the miniaturization and packaging of acoustic sensors, the development of acoustic multisensor systems and the further integration of acoustic sensor technology with silicon technology.

Acknowledgments

The author gratefully acknowledge discussions with John F. Vetelino about resonant microsensors. This work was supported by the National Science Foundation Grant No. EID-921225.

References

[1] B.A. Auld, *Acoustic fields and waves in solids*, Krieger Publ. Comp., 1990.
[2] G.S. Kino, *Acoustic waves*, Prentice-Hall, Inc., 1987.
[3] M. Hoummady, D. Hauden, *Acoustic wave thermal sensitivity: temperature sensors and temperature compensation in microsensors*, Sensors and Actuators, vol. A 44, pp. 177–182 (1994).
[4] D. Hauden, S. Rousseau, and J.J. Gagnepain, *Sensitivities of SAW oscillators to temperature, force and pressure*, Proc. 34th IEEE Ann. Freq. Control Sympl, NJ, pp. 312–316 (1988).
[5] M. Ishido, *Acoustic-wave-based voltage sensors*, Sensors and Actuators, **A 44**, pp. 183–199 (1994).
[6] S.J. Martin, G.C. Free, and K.O. Wassendorf, *Sensing liquid properties with thickness-shear mode resonators*, Sensors and Actuators, **A 44**, 209–218 (1994).
[7] E. Benes, *Improved quartz crystal microbalance technique*, J. Appl. Phys., **56**, 608–626, (1984).
[8] R.M. Lec, J.F. Vetelino, R.S. Falconer and Z. Xu, *Macroscopic theory of surface acoustic wave gas microsensors*, IEEE Ultrasonics Symposium, Chicago, 585–589 (1988).
[9] D.W. Galipeau, J.V. Vetelino, R.M. Lec and C. Freger, *The study of polyimide film properties and adhesion using a surface acoustic wave sensors*, ANTEC'91, Conference Proceedings, Society of Plastic Engineers and Plastic Engineering, Montreal, 1679–1984 (1991).
[10] S.G. Joshi, *Flow sensors based on surface acoustic waves*, **A 44**, 191–197 (1994).
[11] R.M. Lec, W. Lepuschenko and D. McAllister, *The response of the acoustic absorption immunassay to immune and non-immune solutions*, Proc. of the 1994 IEEE International Ultrasonics Symposium, 575–579, Cannes, November, 1–4, (1994).
[12] D. Parker, R.M. Lec, H.P. Pendse and J.F. Vetelino, *Ultrasonic Sensor for the characterization of colloidal slurries*, IEEE Ultrasonic Symposium, Honolulu, HI, 295–299, (1990).
[13] S.W. Bang, R.M. Lec, J.M. Genco and J.C. Randsell, *Acoustic emission sensor for monitoring the kinetics of chemical reactions*, Proc. of the Fifth International Meeting on Chemical Sensors, 39–43, (1994).
[14] M.J. Vellekoop, G.W. Lubking, P.M. Sarro, A. Venema, *Integrated-circuit-compatible design and technology of acoustic-wave-base microsensors*, Sensors and Actuators, **A 44**, 249–263 (1994).

[15] S.W. WENZEL and R.M. WHITE, *A multisensor employing an ultrasonic lamb-wave oscillator*, IEEE Trans. Electron. Dev., **35**, 735–743 (1988).
[16] A. BALLATO, *Piezoelectricity: Old effect, new thrust*, IEEE Trans. Ultrason. Ferroelec., Freq. Contr., vol. **42**, 916–926, (1995).
[17] J.J. CARON, J.F. ANDLE and J.F. VETELINO, *Surface acoustic wave substrate for gas sensing applications*, IEEE Ultrasonic Symposium, Seattle, (1996) (to be published).
[18] F. JOSSE, Z. SHANA, D. RADKE and D. HAWORTH, *Analysis of piezoelectric bulk-acoustic-wave resonators as detectors in viscous conductive liquids*, IEEE Trans. Ulrason., Ferroelec. Freq. Contr., **37**, 359–368 (1990).
[19] E.D. GERBER and A. BALLATO (Ed.), *Precision frequency control*, Academic Press, Inc. (1985).
[20] E. BENES, M. GROSHL, W. BURGER, M. SCHMID, *Sensors based on piezoelectric resonators*, Sensor and Actuators, **A 45**, 1–21 (1995).
[21] A. MANDELIS, C. CHRISTOFIDES, *Solid state gas sensor devices*, John Wiley & Sons, Inc. (1993).
[22] J.C. ANDLE, J.F. VETELINO, R.M. LEC and D.J. MCALLISTER, *An acoustic plate mode immunosensor*, 1990 IEEE Solid state Sensor and Actuator Workshop, Hilton Head, S.C., 82–85, (1990).
[23] J.C. ANDLE and J.F. VETELINO, *Acoustic wave biosensors*, Sensor and Actuators, vol. **A 44**, 165–172 (1994).
[24] B.F. SEIFERT, W. BULST, and C. RUPPEL, *Mechanical sensors based on surface acoustic waves*, Sensors and Actuators, **A 44**, 231–239 (1994).
[25] A.J. BRONOWICKI, T. MANDELLHALL and R.A. MANNING, *Advanced composites with embedded sensors and actuators*, Air Force Report AL-TR-89-086, (April 1990).
[26] M. TAKEUCHI, H. ABE and K. YAMANOUCHI, *Ultrasonic micromanipulation of small particles in liquid using VHF-range leaky wave transducer*, 1994 Ultrasonics Symp., Cannes, 607–611, (1994).
[27] K. YAMADA, T. NAKAGAWA and K. NAKAMURA, *Powder transportation by unidirectional ultrasound radiated from a pair of phase-shifted bending vibrators*, 1993 Ultrasonics Symp., Baltimore MD, 607–610, (1994).
[28] F. SCHMIDT, O. SZCZESNY, L. REINDL and V. MAGORY, *Remote sensing of physical parameters by means of passive surface acoustic waves devices (ID-TAG)*, 1994 Ultrasonics Symp., Cannes, 607–611, (1994).

ARCHIVES OF ACOUSTICS
21, 2, 195–200 (1996)

MICROPROBE TECHNIQUES IN SAW MEASUREMENTS

E. CHILLA, T. HESJEDAL and H.-J. FRÖHLICH

Paul-Drude-Institut für Festkörperelektronik
(D-10117 Berlin, Germany)

Starting from the conventional microprobe techniques, a scanning acoustic tunneling microscope (SATM) and a scanning acoustic force microscope (SAFM) have been developed to detect particle displacements at solid surfaces up to GHz frequencies. Based on the non-linear dependence of the tunneling current in SATM and of the forces in SAFM on the tip to surface distance, respectively, it is demonstrated that wave field parameters of surface acoustic waves can be measured with a lateral resolution in the submicrometer range.

1. Introduction

Many different methods to measure amplitude and phase of surface acoustic waves (SAWs) are available. One of the well established non-contact methods is the laser optical probing. The spatial resolution of this method is given by the minimum achievable spot diameter which is practically of the order of some micrometers [1]. A better resolution, needed for the inspection of high frequency SAWs, can be realised by using the scanning acoustic tunneling microscope (SATM) [2] as well as the scanning acoustic force microscope (SAFM) [3] as a local probe.

Bulk acoustic wave pulses up to several MHz were analysed by an electron tunneling probe [4]. The acoustic amplitude was detected by the contrast variation of a scanning tunneling microscope (STM) image due to acoustic vibration [5]. Amplitude modulated SAWs near 90 MHz were received by a combined boxcar and lock-in technique [6]. First ideas of the phase accurate probing of SAWs using a modified STM were given in 1989 [7]. This SATM utilises an additional rf signal at the tunneling tip leading to a frequency mixing. Amplitude and phase of the ac tunneling current component at the difference frequency were measured at a fixed probe position by an oscilloscope [8]. Strong local variations of the phase were resolved by replacing the oscilloscope by a lock-in amplifier [9, 10]. Measuring at the difference frequency overcomes the limited bandwidth of the STM and reduces the influence of the inevitable displacement current [8, 11]. Nonlinear contributions to the dc and ac components of the tunneling current must be taken into account for SAWs with finite amplitude [11].

Because the SATM is limited to electrically conducting surfaces the SAFM has been developed to measure the amplitude of SAWs on arbitrary surfaces. First results were reported in 1991 [12]. In the so-called contact mode the lever can not follow the surface oscillation at frequencies being sufficiently higher than the lever mechanical resonance frequency. Nevertheless, an output signal is delivered in this case by a shift of the mean lever position [13–15]. The deviation of this position from the position without SAW depends non-linearly on the SAW amplitude.

In this contribution experimental setups for the SATM and the SAFM are described and examples of their application in SAW measurements are demonstrated and discussed.

2. Scanning acoustic tunneling microscope

Figure 1 shows a schematic diagram of the experimental setup. The output voltages of the two rf generators tuned to the SAW frequency f_a and to the modulation frequency f_v of the gap voltage are fed via variable attenuators to the interdigital transducer (IDT) and the tunneling tip, respectively. Additionally, these voltages are fed to a mixing stage. The output signal of this stage which contains the difference frequency supplies the reference channel of a lock-in amplifier. The ac component of the tunneling signal which is generated by the propagating SAW below the tip is fed to the signal input of the lock-in which delivers the amplitude as well as the phase of the SATM signal at the difference frequency. The sample to be

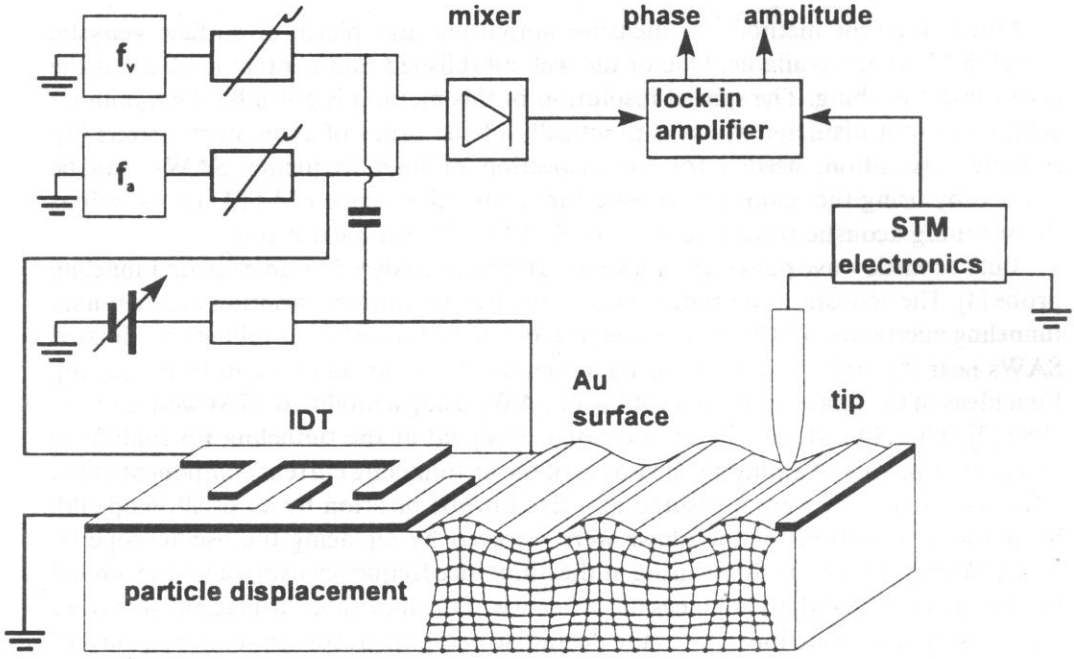

Fig. 1. SATM with gap voltage modulation.

investigated must have an electrically conducting surface to ensure the tunneling current. To avoid disturbing thin oxide coatings the metallization of the SAW propagation path is made by evaporating a thin gold layer.

As an example of a SATM application Fig. 2 displays the phase output signal of the lock-in in dependence on the SAW frequency. The tip of the SATM was positioned at the metallized part of a SAW delay line on $LiNbO_3$. The SAW of

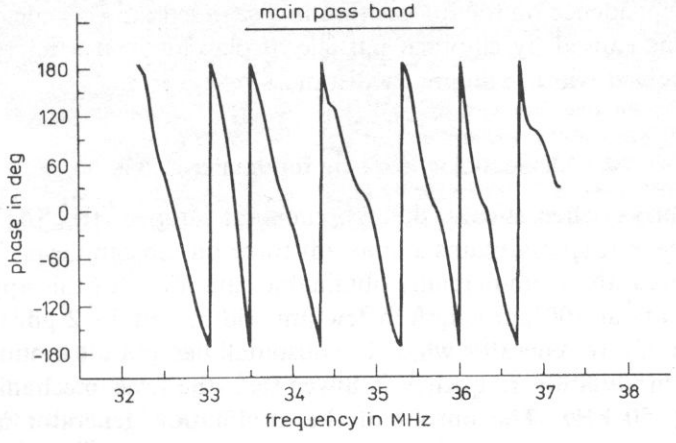

Fig. 2. Phase of a SAW delay line measured by SATM.

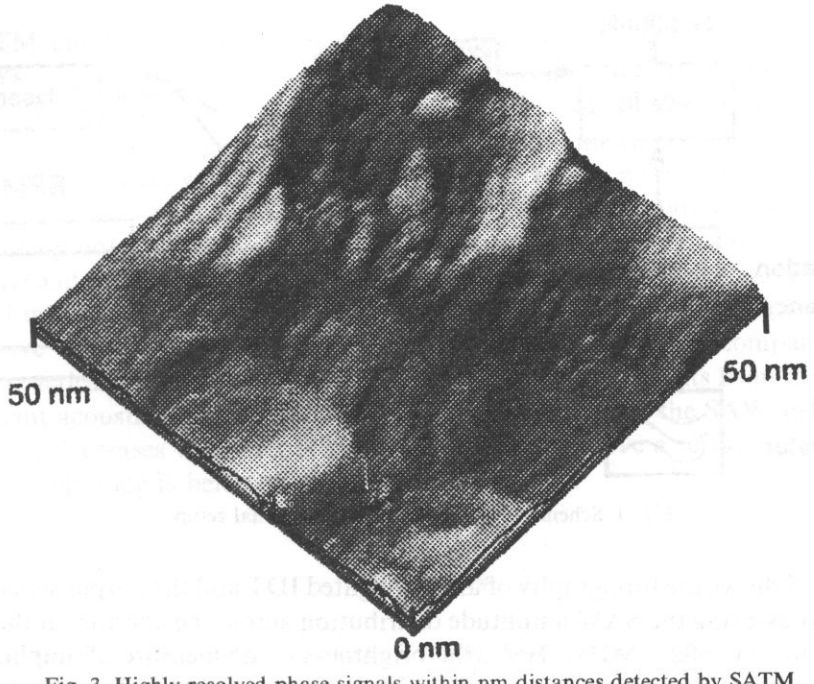

Fig. 3. Highly resolved phase signals within nm distances detected by SATM.

Rayleigh-type was excited by an IDT. The found phase behaviour is typical for delay lines and corresponds also with the estimation of the phase shift as a function of the frequency at known phase velocity and distance between the tip position and the middle of the IDT. It should be noted that the phase is also well imaged outside of the main pass band of IDT which is marked by the arrow. Another SATM application is shown in Fig. 3. There the phase signal of the lock-in is imaged at constant SAW frequency in dependence on the tip position in a scanned area of a delay line. Strong phase variations caused by elliptical particle displacement at a microcsopic rough surface are resolved within nanometer distances.

3. Scanning acoustic force microscope

Figure 4 shows schematically the experimental setup of the SAFM in contact mode. A feedback loop maintains a constant force on the cantilever. Typical forces are some hundred nN. Commercially obtainable cantilever for this application have dimensions of about 100 μm length, a few μm width, and 1–2 μm thickness. The output voltage of a rf generator which is sinusoidally amplitude modulated is fed to the IDT. The modulation frequency is lower than the lever mechanical resonance frequency, e.g. 50 kHz. The output of the modulation generator is additionally connected with the reference input of the lock-in. The output signal of a segmented photo diode which optically measures the deflection of the cantilever is fed to the signal input channel of the lock-in.

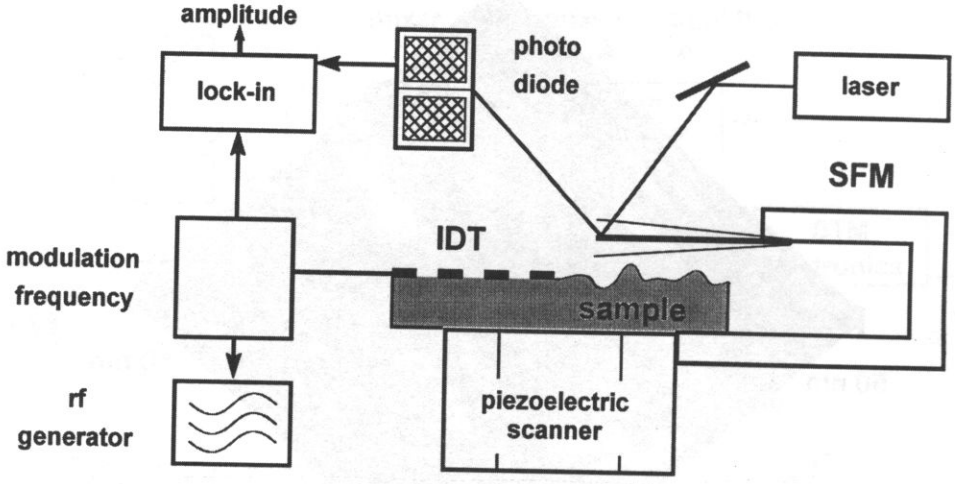

Fig. 4. Schematic of the SAFM experimental setup.

Figure 5 shows the topography of an unweighted IDT and the output signal of the lock-in representing the SAW amplitude distribution across the aperture at the IDT's centre frequency (602.7 MHz). Here, the brightness is the measure of amplitude. In vertical direction the periodic appearance of brightness maxima reflects the standing

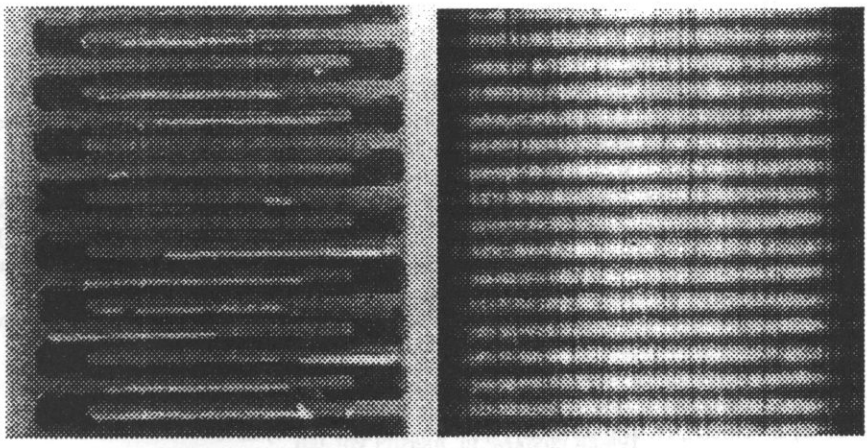

Fig. 5. Amplitude distribution within an IDT measured by SAFM.

wave field within an IDT. Since the lock-in signal depends non-linearly but with a really unknown function on the SAW amplitude the instrument has to be calibrated for quantitative studies. The aperture of the IDT was 26 μm, the scans were formed by 256 points per line. The substrate material was STX quartz.

4. Discussion

SATM and SAFM were demonstrated to be suitable instruments for the detection of SAWs. Applied frequencies were at 35 MHz (SATM) and at 600 MHz (SAFM). An upper frequency limit for the SATM might set in sooner by technical problems of supplying the tunneling gap with a rf signal for the mixing than by the time constant of the tunneling effect which is in the order of 10 fs. Frequencies up to the microwave K band should be applicable. The minimum detectable amplitude with the described setup not optimised in relation to the signal to noise ratio was near 10^{-4} nm. The spatial resolution of amplitude and phase signals is better than 1 nm and is described in detail in [16]. An upper frequency limit for the SAFM does not exist within the microwave range. Nevertheless, the lower amplitude sensitivity compared to the SATM practically limits also the detectable frequency. This results from the fact that at constant acoustic power density in typical SAW structures the SAW amplitude at the surface decreases with $(\text{frequency})^{-1/2}$ and, hence, above a certain frequency the resulting amplitude is below the detectable level.

References

[1] A. Ginter, G. Sölkner, Appl. Phys. Lett., **56** (1990), 2295.
[2] T. Hesjedal, E. Chilla, H.-J. Fröhlich, Thin Solid Films, **264** (1995), 226.

[3] E. CHILLA, T. HESJEDAL, H.-J. FRÖHLICH, in Proc. IEEE Ultrasonics Symposium 1994, 363.
[4] A. MOREAU, J.B. KETTERSON, J. Appl. Phys., **72**, (1992), 861.
[5] J. HEIL, J. WESNER, W. GRILL, J. Appl. Phys., **64** (1988) 1939.
[6] S.E. MCBRIDE, C.G. WETSEL, Jr., in Proc. IEEE Ultrasonics Symposium 1992, 445.
[7] E. CHILLA, H.-J. FRÖHLICH, J. RIEDEL, W. ROHRBECK, in Proc. 8. Tagung Akustik/11. Winterschule Mikroakustik (Phys. Gesellschaft d. DDR), 1989, 212 (in German).
[8] W. ROHRBECK, E. CHILLA, J. RIEDEL, H.-J. FRÖHLICH, Appl. Phys., **A 52** (1991) 344.
[9] E. CHILLA, W. ROHRBECK, H.-J. FRÖHLICH, R. KOCH, K.H. RIEDER, Appl. Phys. Lett. **61** (1992) 3107.
[10] E. CHILLA, W. ROHRBECK, H.-J. FRÖHLICH, R. KOCH, K.H. RIEDER, Annalen der Physik, **3** (1994), 21.
[11] H.-J. FRÖHLICH, E. CHILLA, in Proc. European Workshop on High Frequency Ultrasonic Information Processing, Valenciennes/France, February 17–18, 1994.
[12] W. ROHRBECK, E. CHILLA, H.-J. FRÖHLICH, J. RIEDEL, Abstr. of International Conference on Scanning Tunneling Microscopy, Interlaken/Switzerland, August 12–16, 1991, 52.
[13] W. ROHRBECK, E. CHILLA, Phys. Status Solidi (a), **131** (1992) 69.
[14] O. KOLOSOV, K. YAMANAKA, Jpn. J. Appl. Phys. **32** (1993) L1095.
[15] T. HESJEDAL, E. CHILLA, H.-J. FRÖHLICH, Appl. Phys., **A 61** (1995) 237.
[16] T. HESJEDAL, E. CHILLA, H.-J. FRÖHLICH, submitted to Appl. Phys. Lett.

ARCHIVES OF ACOUSTICS
21, 2, 201–214 (1996)

ROOM RESPONSE TO FREQUENCY CHANGE AND ITS RELATION TO THE PITCH CHANGES

L. RUTKOWSKI

Institute of Acoustics
Adam Mickiewicz University
(60-769 Poznań, ul. Matejki 48/49)

When a signal of constant frequency is sent into a room and its frequency changes to a new value, then, beginning from this moment, in the room there will exist two signals with changing amplitudes (i.e. decreasing one with the old frequency value and an increasing one with a new frequency value). As result of these changes envelope and instantaneous frequency changes appear. These changes have a transient character and exist in a time interval that equals the room reverberation time. Instantaneous frequency and envelope changes are similar to those observed for beating. To describe these changes the modified IWAIF model [1, 2] is used that allows an attempt to evaluate the pitch change in time. It is found that the calculated pitch changes, predicted as an effect of the frequency change in the room, have a monothonical character and appear within the range from the initial frequency to the final one. The rate and character of the calculated predicted pitch changes depends on the amplitude ratio of the two signals, the value of the frequency difference and on the room reverberation time.

1. Introduction

During the superposition of two tones with similar frequencies beating occurs. This phenomenon, elementary from the point of view of physical description, is much more complex from the perceptual point of view. The reason for it are instantaneous frequency (IF) changes which occur simultaneously with the amplitude envelope changes [1, 2, 3, 7]. Moreover, extremal instantaneous frequency changes appear when an amplitude envelope reaches the minimal value [13]. Because of that the perception of instantaneous frequency changes near the envelope minimum is difficult. This problem has already been analysed by Helmholtz. JEFFRESS [7] isolated fragments of beating near the envelope minimum and noticed a considerable difference in pitch for those fragments in comparison with that near the envelope maximum. FETH [3] has studied the pitch for two complementary pair of tones of different frequencies and intensities. The complementarity consisted the fact that the intensity ratios were the same, but for one pair the sound of lower frequency has

a higher amplitude than that of higher frequency while for the other one the amplitude relation was reversed. Owing to this fact, the amplitude envelope for both sounds was the same. Pitch differences for both pairs of signals were perceived by subjects. Feth explains the possibility of pitch discrimination for such complementary pairs of signals by the differences in the calculated envelope weighted averaged of instantaneous frequency (EWAIF). Dai [2], basing on the EWAIF model, defined a new pitch measure that is the squared envelope weighted average of instantaneous frequency (SEWAIF), and pointed out its advantage in comparison with the EWAIF model. On the base of his own and other known results of perceptual studies, he showed this measure to correlate better with the SEWAIF model than with the EWAIF one.

Anantharaman *et al.* [1] applied the IWAIF (intensity weighted average of instantaneous frequency) method for frequency discrimination. The only difference between the SEWAIF and IWAIF models are their names.

The reported studies are closely connected with phenomena observed in rooms for signals of varying frequency. Ozimek and Rutkowski [10] found some differences between instantaneous frequency changes of a signal received from a room and the original frequency changes of the transmitted signal. According to numerical calculations and experimental investigations in rooms, they proved [14] that for linear and jump frequency changes some additional instantaneous frequency changes appear. The extreme values of instantaneous frequency changes correspond to the minimum values of the amplitude envelope.

The analysis of the instantaneous frequency and envelope changes caused by room transmission properties showed that those changes result from the superposition of waves reaching a selected point with different amplitudes and time delay values. The time delays between particular waves for a sound with varying frequency generate some instantaneous frequency differences. The instantaneous frequency and amplitude differences are the reason of phenomena similar to beating. Now, the main question from the view-point of the sound transmission quality evaluation is whether instantaneous frequency changes in rooms are important for the perception.

In this paper the case of simultaneous instantaneous frequency and envelope changes, appearing due to a sudden step frequency change of a sound in the room are discussed. Those changes are interesting because in a finite time interval after a frequency change in the room there appear two signals of constant frequencies and varying amplitudes. Therefore one should expect results similar to those of beating with effects concerning the perception. The purpose of this work is to predict the possibility of the pitch change resulting a step frequency change of the sound in a room on the basis of the IWAIF [1, 2] model. Frequency changes of this kind appear in real sounds, but they concern rather spectral changes than those of the frequency changes of individual tones.

2. The room response to a frequency change

When a sinusoidal signal of constant amplitude A and frequency ω_1 is sent to a room, the steady state room response is

$$x(t)=A|H(j\omega_1)|\exp[j\varphi(\omega_1)]\sin(\omega_1 t). \tag{2.1}$$

Similarly for a signal of frequency ω_2

$$y(t)=A|H(j\omega_2)|\exp[j\varphi(\omega_2)]\sin(\omega_2 t). \tag{2.2}$$

where $|H(j\omega)|$ is the magnitude of a room transmittance of frequency ω and $\varphi(\omega)$ is the phase shift for this frequency. Let us assume that at a moment $t=0$ the frequency value will change from ω_1 to ω_2. The amplitude of signal transmitted from the source remains constant. Beginning from the moment of the frequency change the amplitude of the signal of frequency ω_1 will decrease according to the function

$$x(t)=A|H(j\omega_1)|\exp[j\varphi(\omega_1)]\exp(-kt)\sin(\omega_1 t). \tag{2.3}$$

At the moment of the frequency change a signal of frequency ω_2 with rising amplitude will appear:

$$y(t)=A|H(j\omega_2)|\exp[j\varphi(\omega_2)][1-\exp(-kt)]\sin(\omega_2 t). \tag{2.4}$$

where $k=13.8/T_{60}$, T_{60} is the room reverberation time for a 60 dB decay. We assume that reverberation time changes slowly with the frequency.

From equations (2.3) and (2.4) it follows that in a practically finite time interval there will be two signals in a room: one decreasing with the frequency ω_1 and another one increasing with the frequency ω^2. In a selected point a resultant signal being the sum of signals (2.3) and (2.4) appear:

$$r(t)=X_0\exp(-kt)\sin(\omega_1 t)+Y_0[1-\exp(-kt)]\sin(\omega_2 t), \tag{2.5}$$

where $X_0=A|H(j\omega_1)|$, $Y_0=A|H(j\omega_2)|$.
To find the resultant signal, the analytic signal corresponding to the sum of signals (2.3) and (2.4) must be created see Appendix. The envelope of the calculated analytic signal (A4 — Appendix) equals that of a real signal.

$$e(t)=X_0\sqrt{D^2(t)+\delta^2G^2(t)+2\delta D(t)G(t)\cos(\Delta\omega t)}. \tag{2.6}$$

The following notations were assumed for simplicity

$$D(t)=\exp(-kt),\ G(t)=1-\exp(-kt),\ \Delta\omega=\omega_2-\omega_1 \quad \text{and} \quad \delta=\frac{Y_0}{X_0}.$$

The knowledge of the resultant signal envelope and of the complex instantaneous phase of the signal CI$\Phi(t)$ (A9 — Appendix) allows to calculate the complex instantaneous frequency (A10 — Appendix) after the frequency change in the room

$$\mathrm{CIF}(t)=\frac{1}{2\pi}\frac{dCI\Phi(t)}{dt}=$$

$$=\frac{1}{2\pi}\left\{\frac{-D(t)\{-\delta^2 k+\delta G(t)(k\cos(\Delta\omega t)+\Delta\omega\sin(\Delta\omega t))+kD(t)(1+\delta^2-\delta\cos(\Delta\omega t))\}}{D^2(t)+\delta^2G^2(t)+2\delta D(t)G(t)\cos(\Delta\omega t)}\right\}+$$

$$+j\frac{1}{2\pi}\left\{\omega_1+\left\{\frac{\delta^2\Delta\omega G^2(t)+\delta D(t)[k\sin(\Delta\omega t)+\Delta\omega G(t)\cos(\Delta\omega t)]}{D^2(t)+\delta^2G^2(t)+2\delta D(t)G(t)\cos(\Delta\omega t)}\right\}\right\}. \tag{2.7}$$

The first component of the complex instantaneous frequency (the real part) results from a relative amplitude envelope change. The second component (the imaginary part) equals the sum of the constant value corresponding to the initial frequency and the varying value of the instantaneous frequency IF(t). Using the formula (A11 — Appendix), changes of the complex instantaneous frequency magnitude described by the formula (2.7) as well as the envelope of the resultant signal (2.6) were calculated. The calculations were carried out for an ideal room with an exponential sound decay. Exemplary results of the calculations are shown in the Fig. 1.

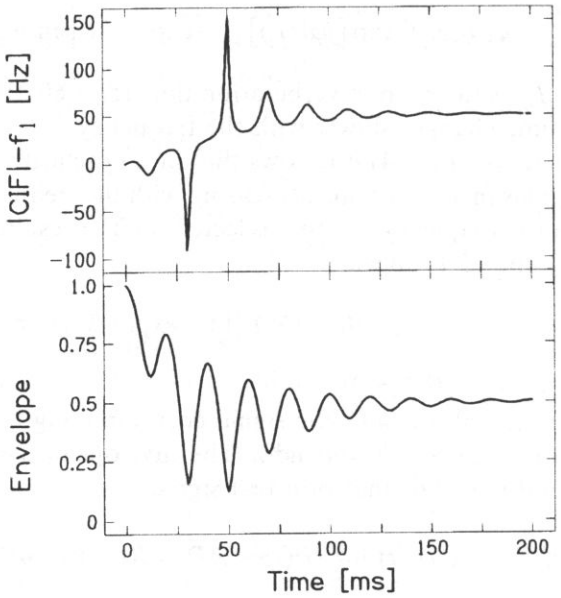

Fig. 1. Exemplary results of the calculated complex instantaneous frequency magnitude and envelope changes after a frequency jump ($\Delta f=50$ Hz, $\delta=0.5$, $T_{60}=0.5$ s).

Figure 1 shows variations in the complex instantaneous frequency magnitude (the top panel) and the relative changes in resultant signal amplitude envelope corresponding to them (bottom panel). The moment of the frequency change corresponds to the zero value on the time axis. At the following moments, specific fluctuations of the complex instantaneous frequency magnitude appear and its steady value corresponds to the frequency ω_2.

For simplicity it was assumed that the initial value of frequency equal zero (which in reality corresponds to the initial frequency ω_1).

An analysis of numerical calculations indicates the following important facts:

The transition from the initial to the final frequency have an oscillating character. These oscillations disappear after the room reverberation time. The frequency of the complex instantaneous frequency magnitude oscillations and of the envelope changes equals (similarly in the case of beating) the value of the frequency difference $\Delta\omega=\omega_2-\omega_1$. The change in the direction of the instantaneous frequency oscillation occurs the moment t_e that is the moment of equilisation of both the signal amplitudes, i.e. it is increasing with the final frequency and decaying with the initial one:

$$t_e=\frac{T_{60}}{13.8}\ln\left(1+\frac{1}{\delta}\right).$$

Around the moment t_e a largest depth of the changes of the amplitude envelope is observed. The value of the instantaneous frequency at t_e equals $f_1+\Delta f/2$.

It is an interesting feature of the complex instantaneous frequency magnitude changes that their extreme values appear at the moments at those the amplitude envelope reaches its minimal values. The observed correlation between instantaneous frequency and envelope changes is similar to that for beating.

Instantaneous frequency changes, very similar to those presented in Fig. 1, can be measured in real rooms. The results of such measurements are presented in [14]. The measured instantaneous frequency changes are more complex because of the approximately exponential sound decay in a real room.

3. Evaluation of the pitch changes as an effect of the frequency change in a room

3.1. The IWAIF model

The expression for the intensity-Weighted Average of Instantaneous Frequency (IWAIF) was defined as a physical measure of the average pitch of complex signals [1, 2]

$$\mathrm{IWAIF}=\frac{\int_0^T e^2(t)f(t)dt}{\int_0^T e^2(t)dt}, \tag{3.1}$$

where $e(t)$ is the amplitude envelope, $f(t)$ is the complex instantaneous frequency magnitude and T is the time interval. When the analytic form of the envelope and instantaneous frequency changes is known from algebraic and trigonometric transformations, the IWAIF calculation is simply. To obtain the envelope and instantaneous frequency changes in the experiments, an appropriate hardware or software, which allows to demodulate the amplitude and frequency is required. The amplitude

envelope demodulation is relatively easy to perform, whereas the frequency demodulation of an acoustic signal produces many problems. One of the possible solutions of frequency demodulation was mentioned in an earlier paper [9]. Avoiding technical details, the method of demodulation presented there consists in the instantaneous frequency evaluation by measuring time intervals corresponding to the following zero crossings of a signal in the same direction. The varying in time zero-crossing frequency ZCF is defined

$$\mathrm{ZCF}(t)=\frac{1}{\Delta\tau(t)}, \tag{3.2}$$

where $\Delta\tau$ is a time interval between the following zero-crossings of a tested signal. The measurements of the instantaneous frequency defined in this way can be performed with high precision.

For a signal having a finite number of spectral components the equation (3.1) takes the form

$$\mathrm{IWAIF}=\frac{\sum_{i=1}^{N} a_i^2 f_i}{\sum_{i=1}^{N} a_i^2}, \tag{3.3}$$

where a_1^2 is the amplitude of the i-th intensity spectrum component, f_i is the frequency, and N is the number of components. The value of IWAIF means the frequency ordinate for the center of gravity of a figure created by the signal intensity spectrum. It is very easy to calculate the value of IWAIF for beating because it concerns only two spectral components.

As reported in papers [2, 4, 7] IWAIF for beating has values lying within the frequency range between the spectral components of the beating tones. If the intensities of both components are the same, IWAIF equals the arithmetic average of their frequencies. When the intensities of both components are different, the value of IWAIF shifts in the direction of the component with higher intensity. FETH *et al.* [4] proved that IWAIF well corresponds to the perceived average pitch if the frequency distance between the spectral components does not exceed a critical band. When the difference in the frequencies of these tones is larger than the critical band [12], we perceive not the average pitch but two separate tones of constant intensities and different pitches characteristic of them. However, when both beating tones have similar frequencies, only one tone of intermediate pitch and varying intensity is perceived. Such a perception of the pitch is determined by resonance properties of a basiliar membrane. When the stimulation of a basiliar membrane is performed by two tones lying relatively far from each other on the frequency scale, the separate (non interlaced) areas on the basiliar membrane corresponding to them are stimulated. For a small frequency difference the stimulated resonance areas on the basiliar membrane overlap each other, so that an intermediate pitch is perceived without the possibility to discriminate the pitches of the particular tones.

3.2. Intensity weighted instantaneous frequency magnitude after a frequency change

In the case of the frequency change in a room, starting from the moment of its appearance there will be two spectral components of constant frequency values f_1 and f_2 but with changing in time amplitudes $a(f_1,t)$ and $a(f_2,t)$. The amplitude variability of both the signals differentiate the considered case from beating. As a result of an amplitude variability the evaluated IWAIF value depends on time and can be described by

$$\mathrm{IWIF}(t)=\frac{a_1^2(t)f_1+a_2^2(t)f_2}{a_1^2(t)+a_2^2(t)}. \tag{3.4}$$

Replacing IWAIF by the IWIF results from the signals parameter variability. Now we are not interested in the averaged but in the momentary changes of the amplitude weighted magnitude of the complex instantaneous frequency. After transformation formula (3.4) can be rewritten in the form

$$\mathrm{IWIF}(t)=f_1+\frac{\delta^2(t)}{1+\delta^2(t)}\Delta f, \tag{3.5}$$

where $\delta(t)$ is the ratio of the varying in time amplitudes, $a_2(t)/a_1(t)$, and Δf is the frequency difference f_2-f_1 (the value of a frequency change). Taking into account the real form of the signal amplitude changes for the frequencies f_1 and f_2 after a frequency change in the room ((2.3),(2.4)) we get finally

$$\mathrm{IWIF}(t)=f_1+\frac{\left(\dfrac{1-\exp(-kt)}{\exp(-kt)}\right)^2}{1+\left(\dfrac{1-\exp(-kt)}{\exp(-kt)}\right)^2}\Delta f. \tag{3.6}$$

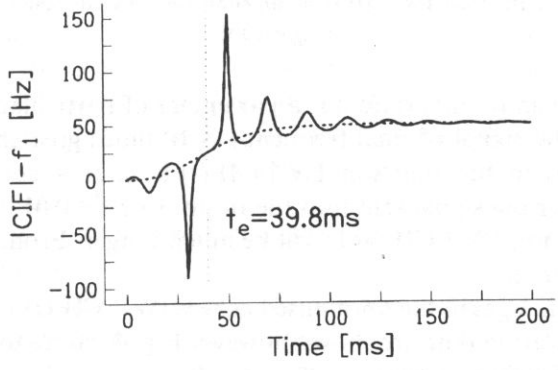

Fig. 2. Comparison of the complex instantaneous frequency magnitude (solid line) and pitch changes IW | CIF(t) | (dashed line) after the frequency change in a room $\Delta f=50$ Hz, $\delta=0.5$, $T_{60}=0.5$ s). Vertical dashed line corresponds to the moment t_e of the equalisation of the amplitude of the decaying and increasing signals.

In Fig. 2 the changes in the complex instantaneous frequency magnitude $|\,\mathrm{CIF}\,| - f_1$ (solid line) are compared with changes in the function IW $|\,\mathrm{CIF}(t)\,| - f_1$ (dashed line). The moment of the amplitude equalisation of both signals is marked by a vertical dotted line.

The function IW $|\,\mathrm{CIF}(t)\,| - f_1$ changes monothonically from the initial value to the final frequency. Similarly as for beating (cf. (3.1)), at the initial moment at that the signal amplitude of the frequency f_1 is maximal, the value IW $|\,\mathrm{CIF}(t)\,| - f_1$ corresponds to the frequency f_1 (0 in the Fig. 2). At the moment of the amplitudes equalisation t_e the value IW $|\,\mathrm{CIF}(t)\,| - f_1$ equals the average of the frequency change. After the time T_{60} measured from the moment of the frequency change, the value of the signal amplitude of frequency f_2 is considerably greater than that of frequency f_1. Then the value IW $|\,\mathrm{CIF}(t)\,| - f_1$, similarly as for beating, equals the final frequency f_2.

The changes in the normalized IW $|\,\mathrm{CIF}(t)\,|$ function, obtained as a result of dividing the second component of the formula (3.6) by the value of the frequency change Δf, are shown in Fig. 3.

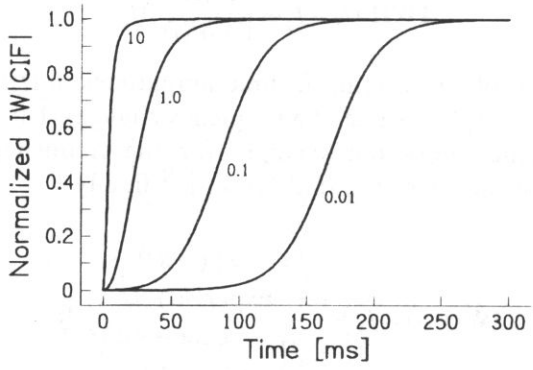

Fig. 3. Changes in the normalised IW $|\,\mathrm{CIF}(t)\,|$ function for selected values of the amplitude ratio δ ($T_{60}=0.5$ s).

The value of the amplitude ratio δ is a parameter of particular curves. For $\delta=10$ (the amplitude of the signal of final frequency is 10 times greater than of the initial frequency), changes in the function IW $|\,\mathrm{CIF}(t)\,|$ have a course similar to the frequency change for the signal sent into the room. For $\delta=0.01$, the time interval of changes in the function IW $|\,\mathrm{CIF}(t)\,|$ will be much longer. From 0 to about 100 ms these changes are small.

In Fig. 4 and 5 changes in the normalised curves IW $|\,\mathrm{CIF}(t)\,|$ for selected values of the room reverberation time are shown however Fig. 4 referes to the constant value $\delta=0.1$ whilst Fig. 5 refers to $\delta=1$.

For small values of the reverberation time $T_{60}=0.1$ s, the IW $|\,\mathrm{CIF}(t)\,|$ changes occur almost immediately. The time interval of the transition from the initial to the final frequency is very short and almost independent from the value of the amplitude

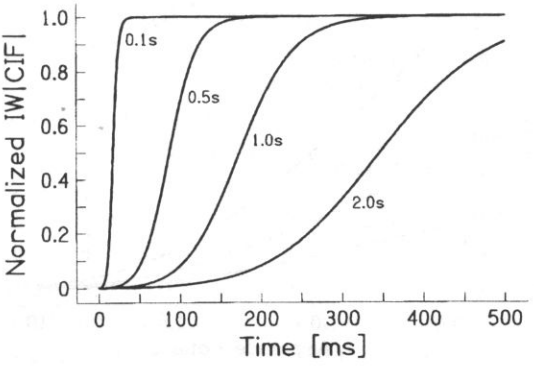

Fig. 4. Changes in the normalised IW | CIF(t) | function for selected reverberatin time values ($\delta=0.1$).

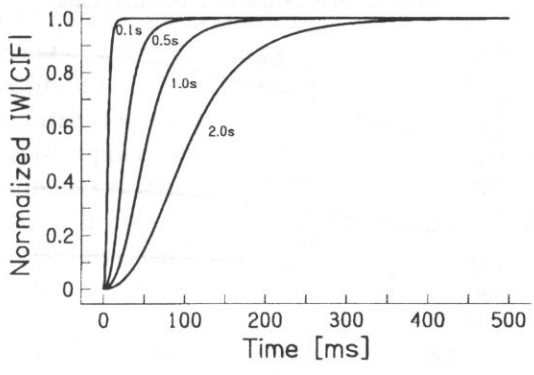

Fig. 5. Changes in the normalised IW | CIF(t) | function for selected reverberation time values ($\delta=1$).

ratio. An increase of the reverberation time causes an increase in that interval. The rate of the IW | CIF(t) | changes is greater for large amplitude ratios δ, but it decreases with the increase in the reverberation time.

As was mentioned earlier, in the initial phase of the magnitude of the instantaneous frequency changes, i.e. up the moment t_e, these changes appear in the proximity of the initial frequency f_1. At moments later than t_e, oscillations appear close to the final frequency f_2. The final frequency is reached after a time equal to the room reverberation time. In Fig. 6 the relation of t_e versus the amplitude ratio δ is shown. A similar relation for the time $T_{60}-t_e$ is shown in the Fig. 7. These relations were calculated from Eq. (2.8). The value of the reverberation time T_{60} is a parameter of the particular curves.

The increase of the amplitude ratio causes a considerable decrease of the time interval of oscillations around the initial frequency Fig. 6. The value of that interval increases proportionally to the room reverberation time. The time interval corresponding to the oscillations around the final frequency almost does not depend on the amplitude ratio δ (Fig. 7) and is much larger than similar values for oscillations around the initial frequency, especially for large values of δ. However, attention

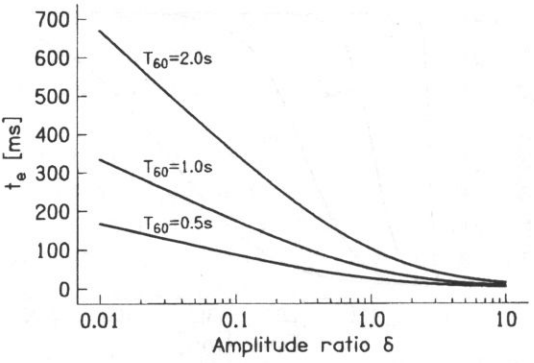

Fig. 6. The relation of the time interval of oscillations around the initial frequency versus amplitude ratio δ for selected value of the reverberation time.

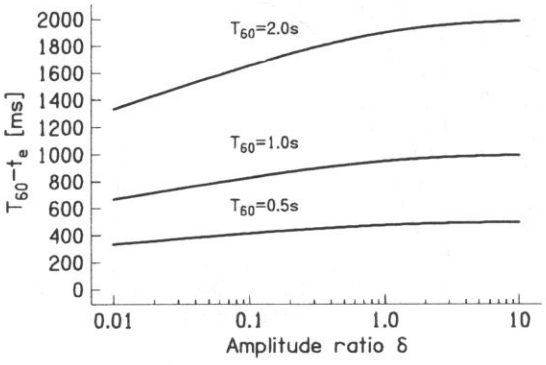

Fig. 7. The relation of the time interval of oscillations around the final frequency versus amplitude ratio for selected value of the reverberation time.

should be paid to the fact that the changes of IW | CIF(t) | in the final phase, i.e. for moments close to the value of the reverberation time, are small (cf. Fig. 3–5).

4. Discussion

The subject of the previous analysis was the physical aspects of the complex instantaneous frequency magnitude and envelope changes accompanying them as a result of the frequency change in a room. Basing on the modified IWAIF model, a measure (function) was found that allows to predict the possibility of pitch changes resulting from frequency change in a room. As opposed to elementary beating of nonsteady envelope and instantaneous frequency changes and settled average pitch (under assumptions described in Sec. 3.1) the calculated changes of pitch after a frequency change in a room have a nonsteady (transient) character. The continuous change of an amplitude ratio of spectral components with different but constant frequencies is the cause of nonsteady pitch changes predicted on the base of IWAIF

model. The calculated predicted continuous pitch change exists in a room in a practically finite time interval. This interval can be very short but, especially in rooms with a large reverberation time, it can reach considerable values (cf. Fig. 6–7). The value of the steady state amplitude ratio of both considered signals also determines the duration of the calculated pitch change. The IWAIF model shows that, as a result of instantaneous frequency envelope weighting the oscillating instantaneous frequency changes are smoothed. Thus, the perceived pitch can be characterised by a number (beating) or by a function describing continuous pitch changes (frequency change in a room). From the point of view of room acoustics it is important to prove that the instantaneous frequency changes, registered in a room, are perceived by a listener. Predicted by the analogy to beating, the pitch changes in a room for the considered nonsteady signal allows to determines a possible sound features change in the room. This is important and useful because changes in the instantaneous frequency and amplitude envelope, similar to those discussed, also exist for a sound with periodic frequency changes.

The predicted possibility of transient pitch changes depends on a few factors such as the duration and course of instantaneous frequency changes. It is also related to the frequency difference of signals sent to the room determining the instantaneous frequency and envelope oscillation frequency. This problem requires separate experiments concerning the perception of predicted pitch changes. Especially the problem of averaging and the possibility to follow pitch changes must be examined in details. It is also important whether and to what extent the model used for beating sinusoids can be useful for the instantaneous pitch analysis. These investigations, exceeding the subject of this paper, have not been done so far.

But it is encouraging that a sudden sound frequency change causes effects perceived in a room, especially in a range of low acoustic frequencies. A frequency change in the range of several Hz gives a sensation similar to vibrato while playing music instruments. For higher acoustic frequencies and large values of the frequency change perceived sensation is similar to a metallic click. Such different sound effects are probably related to the frequency of envelope and instantaneous frequency changes depending on the frequency difference value. For small values of the frequency difference envelope changes are more clearly perceived than instantaneous frequency changes. It is difficult to relate the pitch perception as an envelope-weighted instantaneous frequency for the mentioned assumption. For larger values of the frequency change, the amplitude envelope as well as the instantaneous frequency change at a larger rate. This corresponds to the perception of an averaged or continuously changed pitch.

5. Conclusions

The analysis of instantaneous frequency and envelope changes (2.6), (2.7) occuring in a room as a result of the frequency change shows that those changes have a character of synchronously appearing envelope and instantaneous frequency

changes. Therefore the result of these changes can be treated as a simultaneous amplitude and frequency modulation of finite duration. The synchronous appearing of both kinds of the modulation causes that the possibility of an instantaneous frequency change perception is strongly dependent on the amplitude envelope changes [5, 6]. The IWAIF model described in [1, 2] was used as an attempt to interpret the changes observed in a room from the perceptual point of view. These papers concerned mainly beating and their basic aim was rather the estimation of average pitch changes in time. The use of the IWAIF model for the amplitude ratio of two tones varying in time allowed to calculate "pitch values" in the following time intervals after the frequency change in a room. These calculated values of pitch are changing continuously in a time interval that equals the room reverberation time. One should be aware that proper mathematical calculations of pitch changes do not strictly correspond to the perceived pitch. It results not only from envelope and instantaneous frequency changes more complex than those for beating. Among others it seems to be important that these changes take a finite time interval and their rate depends on the value of the frequency change in the room. The other reason for some ambiguity in the interpretation of the changes perceived in a room is that it has not been clearly known so far what is the mechanism of pitch sensation. But generally it is known that a frequency change influences not only the signal pitch change but also it loudness [11] and an amplitude envelope change influences the change in the loudness and pitch [15].

Independently of the model we use to estimate frequency changes in a room, it can be generally said that simultaneous envelope and instantaneous frequency changes can be perceived as a transient (i.e. of finished duration) change of pitch.

Appendix
Complex instantaneous frequency

Let us consider a real signal resulting from the superposition of two tones with slow envelope changes (narrow band signal)

$$r(t)=x_1(t)\cos\omega_1 t+x_2(t)\cos\omega_2 t\,, \tag{A1}$$

where $x_1(t)$, $x_2(t)$ are functions describing the amplitude envelope change. To create an analytic signal let us calculate the Hilbert transform of the real signal (A1)

$$Hi\{r(t)\}=x_1(t)\sin\omega_1 t+x_2(t)\sin\omega_2 t\,. \tag{A2}$$

Making use of (A1) and (A2), an analytic signal corresponding the real signal $r(t)$ will be equal to

$$r_a(t)=r(t)+jHi\{r(t)\}. \tag{A3}$$

The envelope of the analytic signal is:

$$|r_a(t)| = \sqrt{[r(t)]^2 + [Hi\{r(t)\}]^2}. \tag{A4}$$

The analytic signal envelope is a real function that equals the envelope of the resultant real signal (A1). The phase of the analytic signal is:

$$\varphi_a(t) = \operatorname{arctg}\left[\frac{Hi\{r(t)\}}{r(t)}\right]. \tag{A5}$$

The instantaneous frequency (IF) is calculated as a time derivative of the analytic signal phase (A5)

$$\mathrm{IF}(t) = \frac{d\varphi_a(t)}{dt}. \tag{A6}$$

In practice phase changes are referred to a constant frequency value f_0 for which the phase is a linear function of time $\varphi(f_0) = 2\pi f_0 t$. Thus, the instantaneous frequency changes will be described as follows

$$\mathrm{IF}(t) = \frac{d\tilde{\varphi}_a(t)}{dt} + 2\pi f_0, \tag{A7}$$

where $\frac{d\tilde{\varphi}_a(t)}{dt}$ is a time varying component of the instantaneous frequency.

The resultant signal corresponding to the real signal (A1) is given by

$$r(t) = |r_a(t)| \cos\left[\int \mathrm{IF}(t)dt\right] = \mathrm{Re}\left\{\exp\left[\ln|r_a(t)| + j\int \mathrm{IF}(t)dt\right]\right\}. \tag{A8}$$

The expression

$$\mathrm{CI}\Phi(t) = \ln|r_a(t)| + j\int \mathrm{IF}(t)dt, \tag{A9}$$

is a complex phase of the resultant signal. The complex instantaneous frequency is

$$\mathrm{CIF}(t) = \frac{dCI\Phi(t)}{dt} = \frac{1}{|r_a(t)|}\frac{d|r_a(t)|}{dt} + jIF(t). \tag{A10}$$

The magnitude of the complex instantaneous frequency (the real function describing the frequency change) can be calculated from

$$|\mathrm{CIF}(t)| = \sqrt{\left[\frac{1}{|r_a(t)|}\frac{d|r_a(t)|}{dt}\right]^2 + [IF(t)]^2}. \tag{A11}$$

Let us notice that only for signals with a constant envelope the magnitude of the complex instantaneous frequency equals the instantaneous frequency IF(t).

For signals with simultaneous envelope and instantaneous frequency changes, the value of the complex instantaneous frequency magnitude depends on both the

instantaneous frequency IF(t) and the real part of the complex instantaneous frequency changes.

Acknowledgements

The author wishes to thank Prof. E. OZIMEK for the discussions and critical reading of this manuscript. The reviewer made many interesting and helpful suggestions.

References

[1] J.N. ANANTHARAMAN, A.K. KRISHNAMURTHY, L.L. FETH, *Intensity-weighted average of instantaneous frequency as a model for frequency discrimination*, J. Acoust. Soc. Am., **94** (2), 723–729 (1993).

[2] H. DAI, *On the pitch of two-tone complexes*, J. Acoust. Soc. Am. **94** (2), 730–734, (1993).

[3] L.L. FETH, H. O'MALLEY, *Two-tone auditory spectral resolution*, J. Acoust. Soc. Am., **62** (4), 940–947, (1977).

[4] L.L. FETH, H. O'MALLEY, J.W., RAMSEY, *Pitch of unresolved, two-component complex tones*, J. Acoust. Soc. Am., **72** (5), 1403–1412, (1982).

[5] S. IWAMIYA, K. FUJIWARA, *Perceived principal pitch of FM-AM tones as a function of the phase difference between frequency modulation and amplitude modulation*, J. Acoust. Soc. Jpn (E), **6**, 3, 193–202, (1985).

[6] S. IWAMIYA, S. NISHIKAWA, O. KITAMURA, *Perceived principal pitch of FM-AM tones when the phase difference between frequency modulation and amplitude modulation is in phase and anti-phase*, J. Acoust. Soc. Jpn (E), **5**, 2, (1984).

[7] L.A. JEFFRESS, *Beating sinusoid and pitch changes*, J. Acoust. Soc. Am. **43**, (6), 1464 (1968).

[8] H. KUTTRUFF, *On the audibility of phase distortions in rooms and its significance for sound reproduction and digital simulation in room acoustics*, Acustica **74**, 3–7 (1991).

[9] E. OZIMEK, L. JUGOWAR and L. RUTKOWSKI, *Problem of the instantaneous sound frequency measurement*, Archives of Acoustics, **9**, 325–339 (1984).

[10] E. OZIMEK, L. RUTKOWSKI, *Deformation of frequency modulated signals (FM) propagating in a room*, Applied Acoustics, **26**, 217–230 (1989).

[11] D.W. ROBINSON, R.S. DADSON, *Threshold of hearing and equal-loudness relations for pure tones, and the loudness function*, J. Acoust. Soc. Am. **29**, 1284–1288 (1957).

[12] J.G. ROEDERER, *The physics and psychophysics of music*, 2nd Ed., Springer, Berlin, 1975.

[13] L. RUTKOWSKI, *Zmiany zespolonej częstotliwości chwilowej wynikające z sumowania 2 tonów* (in Polish), (Complex instantaneous frequency changes as a result of superposition of the 2 tones], OSA'94, Wrocław–Szklarska Poręba, 281–284 (1994).

[14] L. RUTKOWSKI, E. OZIMEK, *Linear and jump frequency changes of a signal in a room*, Archives of Acoustics, **20**, 2, 115–138, (1995).

[15] J. VERSHUURE, and A.A. van MEETEREN, *The effect of intensity on pitch*, Acustica, **32**, 33–44, (1975).

ARCHIVES OF ACOUSTICS
21, 2, 215–223 (1996)

EFFECT OF OILING UP ON THE FAILURE OF CONCRETE DETERMINED BY ACOUSTIC EMISSION

J. HOŁA

Institute for Building Engineering
Wrocław Technical University
(Wybrzeże Wyspiańskiego 27, 50-370 Wrocław)

Results showing how the oiling up of concrete series, differing in their aggregate grading, affects their failure are presented. The acoustic emission was used in the test. The determined values of initiating stress, σ_i, and critical one σ_{cr}, in the oiled up concrete and the reference, unoiled up concrete prove that oiling up affects significantly the failure of the concrete. It has been found that the oiling up of concrete results in the reduction of the values of the initiating and critical stress compared to the values of these stresses in the reference unoiled concrete series. The tests have shown this reduction to be practically independent of the concrete's aggregate grading.

1. Introduction

There are frequent cases in industry that the floor and other structural components made of reinforced concrete become oiled up strongly by minearl oil leaking from the installations and production machines. It is commonly believed that mineral oils do not have a corrosive effect on concrete and reinforcing steel but they bring about changes in the physical and mechanical properties of concrete [1, 2, 3]. It has been established, for example, that oiling up has a negative effect on the compressive strength of concrete. A considerable oil-induced reduction in this strength is found when one examines and compares the strength of concrete specimens stored in oil with that of reference concrete specimens [2]. The few papers on this subject that have been published so far do not contain any test results which would allow one to formulate a definite opinion on the contribution of oiling up to the destructive processes that occur in the structure of concrete when it is loaded. This research problem has practically not been taken up yet, especially with respect to the determination of the effect of oiling up on the values of the initiating stress, σ_i, and the critical one σ_{cr}. The above stresses represent certain conventional levels of stress in loaded concrete; when they are reached characteristic phenomena associated with the appearance and the propagation of microcracks occur [4, 5, 6, 7, 8, 9]. According to

[5, 7, 8, 9], the intiating stress reaches values as high as the safe fatigue life of concrete and it can be defined as the lower limit of failure of concrete, whereas the critical stress is identified with the long-lasting strength of concrete [5, 6, 7, 8, 9].

One can expect that the oiling up of concrete should have a negative influence on the value of these stresses, particularly in the case of dynamic loads and shocks and other fatigue loads associated with technological processes or a changed function or purpose of a construction in which some structural components were oiled up in the past. The deep penetration of oil into the structure of concrete is undoubtedly easier when such loads occur. This phenomenon, in turn, contributes to the reduction of the concrete's cohesion and, as a result, to the observed loosening of its structure [1]. This fact seems to have more serious consequences in the case of porous concrete or concrete with a raised or high content of fine aggregate functions.

2. Description of tests

Three series of concrete — designated by the letter A, B and C — possessing similar compressive strength but differing sharply in the grading of the rounded aggregates, were tested. The sand point of the concrete A was 37.5%, that of the concrete B was 60%, whereas the concrete C had no gravel functions at all but 100% of sand. The compositions the same as in 10 of the particular concrete mixes from which the concrete series were made are given in Table 1. The tests were carried out on

Table 1. Compositions of the designed concrete mixes

Concrete mix composition	Designation of the mixes		
	A	B	C
Portland cement 35 from Górażdże Cement Plant [kg/m³]	321	350	469
Natural gravel [kg/m³]	1185	697	–
River sand [kg/m³]	711	1045	1480
Tap water [l]	178	194	257

100 × 100 × 100 mm cube specimens after 360 days. 24 specimens were made from each concrete mix. 12 of them were oiled up, whereas the other 12 ones served reference specimens. All the specimens after preparing were stored for 28 days in a climatic chamber at the air temperature of 18°C ± 1°C and relative humidity of 95% and then for the next 90 days in the laboratory at the air temperature of 18°C ± 3°C and relative humidity of about 65%. After this time, 12 specimens of each concrete batch, A, B, and C, were oiled up and labeled as series AO, BO and CO. The mineral oil Lux 10, having physical and chemical properties specified by the standard

PN-53/C-96085, was used. The specimens were oiled up by the following procedure. First, they were dried to a constant mass and then placed, by means of a cuvette, in a low pressure chamber in that the air temperature was 50°C. The specimens remained in the chamber for a period of about 24 hours under air pressure reduced to 0.006 MPa. Durign this time, the level of oil in the cuvette was raised gradually. Then the oiled up specimens were transferred to the laboratory and placed in a container with oil where they remained till the testing. The described treatment, by removing water and air from the pores and the capillaries of the concrete speeds up considerably the usually long-lasting process of complete oiling up of the concretes structure. The other concrete specimens were stored as reference specimens in the laboratory till the time of testing. They were labeled as series AL, BL and CL. Also $150 \times 150 \times 150$ mm specimens were made to determine the compressive strength of the tested series of concrete. They were stored in the same way as the $100 \times 100 \times 100$ mm specimens.

The acoustic emission was used in conjunction with the quasi-axial compression test. The setup for measuring the acoustic emission was the same as in [8]. The specimens were compressed without friction at the contact with the pressure plates of the testing machine. This was achieved by grinding the surfaces of the specimens and lubricating them with cup grease. During the tests counts sum versus stress increment was recorded.

3. Results and analysis of the tests

The strength tests carried out on the $150 \times 150 \times 150$ mm specimens of the tested concrete series yielded mean compression strength values complied in Table 2. This Table contains also the total porosity values determined for the conrete series. The compressive strength of the oiled concrete series was found to be about 10% lower in comparison with those of the free of oil reference concrete.

Table 2. Mean compressive strength values determined using $150 \times 150 \times 150$ mm specimens after 90 and 360 days of curing and results of the overall porosity tests after 90 days of curing

Designation of concrete series	Mean compression strength R [MPa]		Overall porosity after 90 days P [%]
	90 days	360 days	
AL	42.30	44.30	13.02
BL	41.90	43.90	15.06
CL	38.30	40.10	16.28
AO	–	42.45	–
BO	–	42.00	–
CO	–	38.60	–

The acoustic emission results given in Fig. 1 show that the variation of the counts sum versus the increment in the absolute value of stress is similar for all the tested

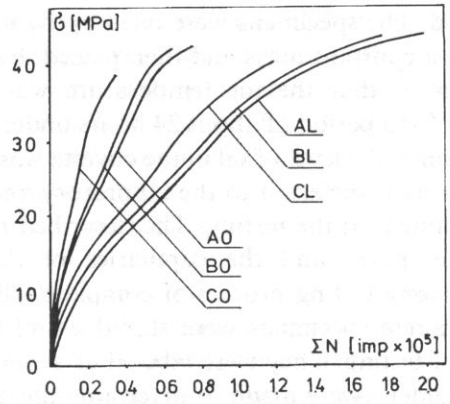

Fig. 1. The variation of the counts sum in the quasi-axially compressed oiled up concrete series AO, BO and CO and the unoiled up series AL, BL and CL as function of the increment in the absolute value of stress.

series of oiled and unoiled concrete. There are, however, marked differences between the values of this total both at the particular stress levels and during the whole process of destruction of the oiled and unoiled concrete. These differences grows the content of the fine aggregate in the concrete increases. For example, the counts sum recorded during the whole process of failure of the oiled concrete the AO series is about 2.65 times smaller than that of the AL ones and 3.60 times smaller for the CO concrete than for the CL one. This manifold reduction in the acoustic "activity" of the oiled concrete in comparison with the reference one can be attributed to the weaker cohesion and the loosening of the structure of the former concrete resulting from the oil penetration, this effect is reflected in the smaller amount of elastic strain energy released during the failure. The results of strength tests compiled in Table 2 corroborate the above statement. Also the damping of elastic waves by the oil filling the pores, capillaries and microcapillaries in the concrete contributes significantly to that reduction. The contribution of this factor certainly grows as the overall porosity of concrete increases. A qualitative analysis of the graphically recorded single acoustic pulses emitted during the destruction of the concrete seems to confirm the above interpretation of the reduced acoustic activity of the oiled concrete in comparison with the unoiled reference concrete. A comparison of such pulses recorded graphically for the concrete series AO and AL at the relative stress levels of 0.15, 0.40 and 0.90 σ/R is presented, as an example, in Fig. 2. It follows from this figure that the amplitude of signals is substantially lower and the duration of the signals is shorter or the oiled concrete than for the unoiled one.

To get a more complete picture of the changes in the failure of the oiled concrete series as compared with the reference concrete, the values of initiating stress σ_i and critical stress σ_{cr} in them were determined on the basis of the counts sum recorded during the destruction process. For this purposes, the intensity of this total versus stress increment was determined using the relation and description given in [11, 12]. Figures 3, 4, and 5 show how the intensity of the counts sum IN changes as a function

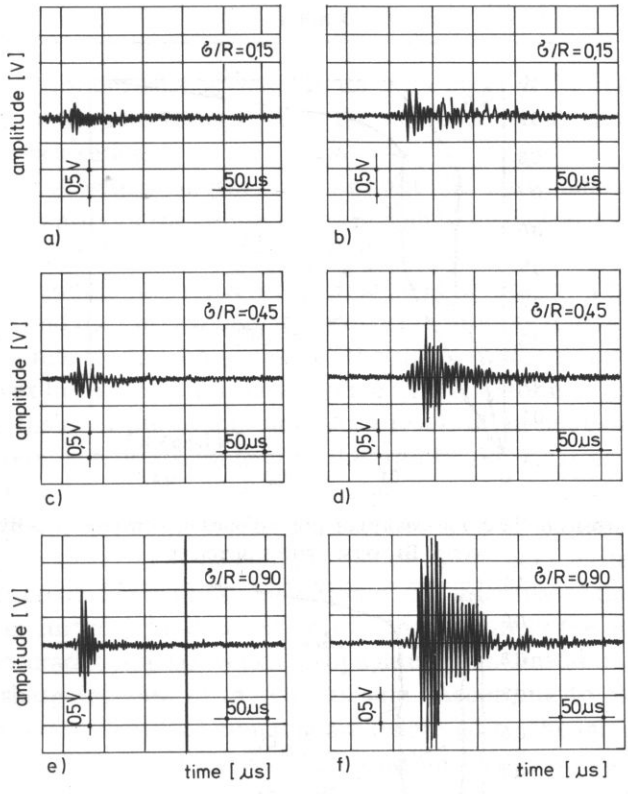

Fig. 2. Graphic recordings of the acoustic emission pulses: a, c, e — in oiled up concrete series AO; b, d, f in the unoiled up concrete series AL.

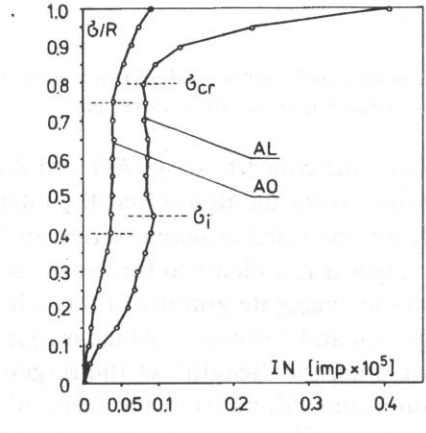

Fig. 3. Counts sum intensity in the quasi-axially compressed oiled up concrete series AO and the unoiled up series AL versus stress increment.

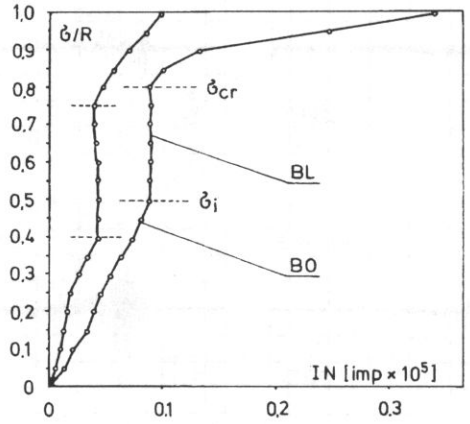

Fig. 4. Counts sum intensity in the quasi-axially compressed oiled up concrete series BO and the unoiled up series BL versus stress increment.

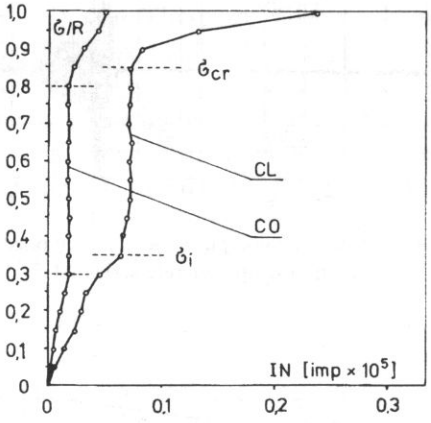

Fig. 5. Counts sum intensity in the quasi-axially compressed oiled up concrete series CO and the unoiled up series CL versus stress increment.

of the stress increment σ/R for the concrete series AO and AL, BO and BL, and CO and CL, respectively. It follows from the figure that the intensity of the counts sum varies in three stages both for the oiled concrete series and the unoiled ones. The "length" of the individual stages is not identical for the tested concrete series and, as shown in [10], it depends on the aggregate grading of the concrete. An analysis of the test results presented in Figs. 3, 4 and 5 shows — which is significant — that for all the tested series of the oiled concrete, the "length" of the stages of constant, stable and rapid increment in the counts sum differs from the "length" of these stages for the unoiled reference concrete series. The stage of the constant increment of acoustic emission in the oiled concrete series is always "shorter" than that in the reference concrete series, no matter what the content of the fine aggregate in the concrete. The greatest difference in the "length" of this stage appear for the concrete series BO and

BL with a 60% content of fine aggregate. In turn, the stage of the abrupt increment in the counts sum is always "longer" for the oiled concrete series than for the comparable reference series.

The stress levels at which the stages of constant and stable and stable and abrupt increment in the intensity of the counts sum are demarcated clearly correspond to the initiating stress σ_i, and the critical one, σ_{cr} in the concrete. The three-stage course of the intensity of the counts sum reflects the three-stage character of the failure of both the oiled concrete and the unoiled one. It is worth mentioning that, according to [6, 9], the failure of concrete starts with a stage of the stable initiation of microcracks that have their origin at the material formation stage. An indication of this is the constant growth in the intensity of the counts sum. As a result of an increase in the load, the failure of concrete enters the stage of the stable propagation of cracks. The microcracks that appeared at the first stage propagate now and new stable microcracks develop, particularly due to the destruction of the adhesion of the aggregate grains to the cement paste and that of the cement paste itself [6, 9]. An indication of this condition is the stabilization of the intensity of the counts sum. As the load increases further, the destruction of concrete enters the stage catastrophic failure, i.e. wide cracks appear which propagate in an unstable manner. This is indicated by a sharp increase in the counts sum. According to [4, 5, 6, 7, 8], the particular stages in the failure of concrete are delimited by the initiating stresses, σ_i, and the critical ones σ_{cr}, respectively. The variation in the values of these stresses determined by the acoustic emission method, for all the tested oiled and unoiled concrete series, versus the percentage of fine aggregate is illustrated in Fig. 6. These values also have been marked in Figs. 3, 4 and 5.

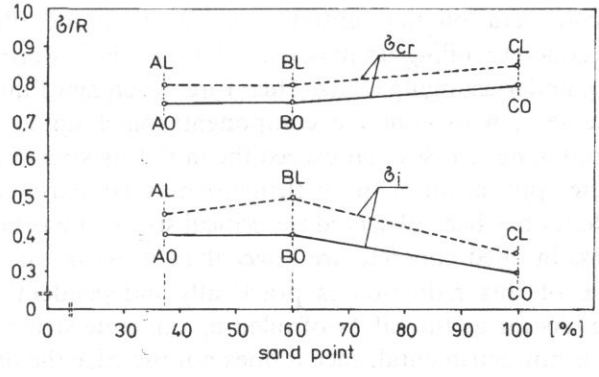

Fig. 6. The variation of the values of the initial stress and the critical stress in the tested oiled up and the unoiled up concrete versus fine aggregate percentage.

It follows from Fig. 6 that the oiling up of concrete affects significantly the values of both the initiating and critical stresses no matter what the fine aggregate content in the concrete. And so, the values of the initiating stress in all the tested series of oiled concrete turned out to be lower than those of this stress in the unoiled reference

concrete series. This means that the $0-\sigma_i$ interval has narrowed in the case of the oiled concrete. It is worth while noting that a similar narrowiong of this interval observed in the case of concrete saturated with water [13, 14]. Thus, the failure of such concrete enters the second stage which is characterized, among other things, by the stable development of microcracks at the smaller effort of the material than in the case of the unoiled concrete. This allows one to conclude that oiled concrete has a shorter safe fatigue life than unoiled concrete, no matter what grading had the aggregate used for its making. A similar tendency has been observed in the case of the critical stresses. The oiling up of concrete also leads to the reduction in the values of these stresses. As afar as the safety of the concrete structures which have become oiled up is concerned, that is not a negative phenomenon. The problem is that when the values of the critical stress are high the cracks appear in the concrete suddenly and they are usually wide as observed by the authors of papers [15, 16]. This means that no warning signs precede the destruction of the concrete. One can conclude that there is no such danger in the case of oiled concrete.

4. Conclusion

By using the method of acoustic emission it has been shown that oiling up affects significantly the course of failure of compressed concrete. This is reflected in the value of the intiating stresss, σ_i, and critical one σ_{cr}, that delimit the particular stages of the destruction of the concrete. Generally, for all the tested series of oiled concrete a reduction in the values of the initiating stress in comparison with the values of the corresponding stress in the unoiled up concrete the reference series has been observed. The largest reduction is observed for the BO series concrete with a 60% fine aggregate content.

Taking into consideration that initiating stress, σ_i, is identified with the safe fatigue life of the concrete, oiling up may contribute to the lowering of the safety of structures working under changing loads. Therefore, when new functions or purposes of a structure element, with concrete components oiled up in the past, involve changing loads producing stresses that exceed the initiating stress value characteristic of the concrete, the application of those elements may be detrimental.

A similar tendency has been observed for critical stress. It has been found that the values of this stress in oiled concrete are lower than those in the reference, unoiled concrete. The size of this reduction is practically independent of the concrete's aggregate grading. As far as the safety of oiled up concrete structures is concerned, this phenomenon is not detrimental since it does not increase the danger of a sudden failure not preceded by any warning signs.

References

[1] K. GRABIEC, *Effect of minearl oils on the strength and deformability of structural concrete* [in Polish], Arch. Inż. Ląd. **19**, 3, 567–572, 1973.

[2] T. BŁASZCZYŃSKI, J. KOZAKIEWICZ, J. NOWAKOWSKI, *On effect of mineral oils on physical strength properties of concrete* [in Polish], XXIXth Scientific conference 9of KILiW PAN, Krynica, **3**, 11–16, 1983.

[3] W. STUPNICKI, W. ZIOBROŃ, *Influence of mineral oil leakage on behaviour of prefabricated rc floor structures* [in Polish], XXXth Scientific Conference of KILiW PAN, Krynica, **2**, 192–196, 1984.

[4] T.C. HSU, F.O. SLATE, G.M. STURMAN and G. WINTER, *Microcracking of plain concrete and the shape of the stress-strain curve*, ACI J., **k60**, 2, 209–224, 1963.

[5] S.P. SHAH and S. CHANDRA, *Critical stress volume change and microcarking of concrete*, ACI J., **65**, 9, 770–781, 1968.

[6] K. NEWMAN and I.B. NEWMAN, *Falure theories and design criteria for plain concrete. Structure, solid mechanics and engineering design*, Proc. Southampton, 1969, Civ. Eng. Mat. conf. 963–995, London, 1971.

[7] K. FLAGA, K. FURTAK, *Influence of aggregate grading on the critical stress levels in the compressed concrete* [in Polish], Arch. Inż. LAd. **27**, 4, 653–666, 1981.

[8] J. HOŁA, *Studies on the effect of heat treatment on stress-produced failure in compressed concrete*, Engineering Transactions, **40**, 1, 25–36, 1992.

[9] K. FLAGA, *The influence of the stresses on the stress destruction and the strength parameters of concrete. Analytical models and new concepts in mechanics of structural concrete*, Published by the Białystok University of Technology, Białystok, 55–77, 1993.

[10] J. HOŁA, *Effects of aggregate grading on the stress degradation of compressed concrete*, Archives of Civil Engineering, **38**, 1–2, 85–101, 1992.

[11] J. HOŁA, *Acoustic emission in concrete, Acoustic Emission-Sources, Application, methods* [in Polish], ed. J. Malecki and J. Ranachowski, Institute of Fundamental Technological Research, Polish Academy of Sciences, Biuro PASCAL Publishers, Warsaw, 223–240, 1994.

[12] T. BRONIEWSKI, J. HOŁA, J. ŚLIWIŃSKI, *Application de la méthode d'émission acoustique aux essais du comportement du béton imprégne de polymére soumis à la compression*, Materials and Structures, **27**, 331–337, 1994.

[13] J. PYSZNIAK, J. HOŁA, *Application of acoustic methods to assessment of concrete humidity influence on the process of concrete destruction*, Archives of Acoustics, **16**, 2, 343–353, 1991.

[14] J. HOŁA, Z. RANACHOWSKI, *Application of AE method to testing of concrete* [in Polish], Trans. Inst. Fund. Techn., Research, No. 26, 1991.

[15] J. RUPPERT, H. LIBURA, W. ZARĘBSKA, *Limit state of cracks reinforced concrete beams with limestone aggregate* [in Polish], IB, **9–10**, 326–327, 1980.

[16] K. FLAGA, K. FURTAK, *Crack propagation in reinforced concrete beams under increasing short-term loading* [in Polish], IB, **3**, 116–118, 1983.